

# Integrative omics and phase IIa clinical trial identify TNF as key node in autoimmune hepatitis

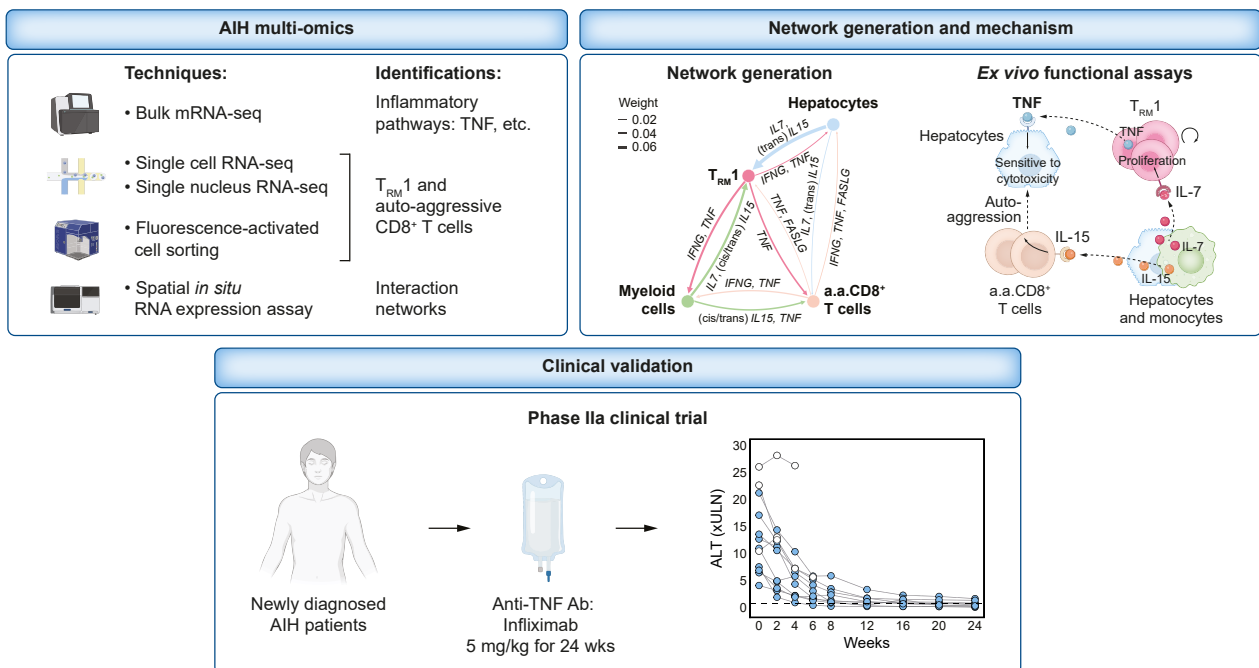
## Authors

Yang Xu, Jan Philipp Weltzsch, Christoph Kilian, ..., Christoph Schramm, Nicola Gagliani, Ansgar Wilhelm Lohse

## Correspondence

n.gagliani@uke.de (N. Gagliani), a.lohse@uke.de (A.W. Lohse).

## Graphical abstract



## Highlights

- Type I cytokines, including TNF and downstream pro-inflammatory signaling, are central to the hepatic immune response in AIH.
- AIH pathology is sustained by a specific network of tissue-resident CD4<sup>+</sup> and CD8<sup>+</sup> memory T cells, myeloid cells, and hepatocytes.
- TNF acts as one of the cytokines linking the cellular nodes of this network.
- IL15-induced cytotoxic auto-aggression by CD8<sup>+</sup> T cells can kill hepatocytes, which is enhanced by CD4<sup>+</sup> T cell-derived TNF.
- Anti-TNF treatment demonstrates efficacy as an alternative to steroid-based induction therapy.

## Impact and implications

These findings have significant implications for the treatment of autoimmune hepatitis (AIH). By mapping the spatial and functional immune network within the AIH liver, this study identifies IL-15 and TNF as central drivers of T cell-mediated cytotoxicity, offering new precision targets for intervention. The successful use of infliximab as a steroid-free therapy in a phase II trial marks a pivotal step toward safer, more specific treatment options for patients with AIH. This research not only advances our understanding of AIH pathogenesis, but also sets the stage for broader application of immune-targeted therapies in autoimmune liver diseases.

# Integrative omics and phase IIa clinical trial identify TNF as key node in autoimmune hepatitis

Yang Xu<sup>1,3,†</sup>, Jan Philipp Weltzsch<sup>1,2,†</sup>, Christoph Kilian<sup>1,2,4,†</sup>, Babett Steglich<sup>1,2,3</sup>, Christina Weiler-Normann<sup>2</sup>, Michael Dudek<sup>5</sup>, Jonas Fackler<sup>5</sup>, Malte H. Wehmeyer<sup>2</sup>, Joseph Tintelnot<sup>1,3,6</sup>, Laura A. Liebig<sup>2,7</sup>, Silja Steinmann<sup>1,2</sup>, Alena Laschtowitz<sup>2</sup>, Ludwig J. Horst<sup>2</sup>, Ida Schregel<sup>2</sup>, Marcial Sebode<sup>1,2</sup>, Johannes Hartl<sup>2</sup>, Christian Casar<sup>1,2</sup>, Jing Lu<sup>1,3</sup>, Gerhard Schön<sup>8</sup>, Antonia Zapf<sup>8</sup>, Maria Rosa Bono<sup>9</sup>, Mariana V. Roseblatt<sup>10</sup>, Sarah Nuñez<sup>11</sup>, Justine Castañeda<sup>12</sup>, Sören Alexander Weidemann<sup>13</sup>, Nico Kaiser<sup>14,15</sup>, Maria Schwerk<sup>15</sup>, Manuela Kolster<sup>1,16</sup>, Guido Rattay<sup>1,3,16</sup>, Hanna Ulrich<sup>1,2,4</sup>, Varshi Sivayoganathan<sup>1,15</sup>, Ning Song<sup>1,15</sup>, Jenny Krause<sup>1,2,3</sup>, Marius Böttcher<sup>1,2</sup>, Adrian Sagebiel<sup>1,3,17</sup>, Jonas Wagner<sup>1,3,17</sup>, Christian F. Krebs<sup>1,15</sup>, Víctor G. Puelles<sup>15,18,19</sup>, Norbert Hübner<sup>7</sup>, Eva Tolosa<sup>1,16</sup>, Stefan Bonn<sup>1,14,20</sup>, Samuel Huber<sup>1,2</sup>, Percy A. Knolle<sup>5</sup>, Johannes Herkel<sup>1,2,†</sup>, Lorenz Adlung<sup>1,2,4,†</sup>, Christoph Schramm<sup>1,2,21,†</sup>, Nicola Gagliani<sup>1,3,\*</sup>, Ansgar Wilhelm Lohse<sup>1,2,\*</sup>

Journal of Hepatology 2026. vol. 85 | 71–90



See Editorial, pages 18–20

**Background & Aims:** Patients with autoimmune hepatitis (AIH) experience increased mortality and severe side effects from non-specific immunosuppressive therapy, highlighting an urgent need for targeted treatment approaches. Here, we aimed to delineate the cellular and molecular network underlying AIH within its spatial context and to validate a key therapeutic target in a clinical trial.

**Methods:** We employed computational modelling, multi-omics analyses, and functional experiments to map the immune landscape of AIH. In addition, we conducted a steroid-free open-label phase IIa clinical trial using infliximab, a TNF-targeting antibody, in patients with AIH.

**Results:** Our studies revealed that myeloid cell and hepatocyte-derived IL-15 promotes cytotoxicity and proliferation of liver auto-aggressive CD8<sup>+</sup> T cells. Full execution of their cytotoxic program is licensed by TNF derived from clonally expanded liver-resident CD4<sup>+</sup> T cells. AIH hepatocytes respond to TNF by increasing expression of adhesion molecules, making them targets for both CD8<sup>+</sup> and CD4<sup>+</sup> T cells. In the clinical trial, targeting TNF with infliximab demonstrated efficacy as an entirely steroid-free AIH treatment.

**Conclusions:** These findings elucidate the immune network in AIH and identify TNF as one of the central network nodes. Accordingly, our findings provide the basis for novel targeted, steroid-free immune therapies, including the use of infliximab.

**Clinical trial number:** European Union Clinical Trials Register (EudraCT No.: 2017-003311-19).

© 2026 The Author(s). Published by Elsevier B.V. on behalf of European Association for the Study of the Liver. This is an open access article under the CC BY license (<http://creativecommons.org/licenses/by/4.0/>).

## Introduction

Autoimmune hepatitis (AIH) is a chronic inflammatory liver disease that can affect all age groups, including young children. AIH is associated with increased mortality in addition to increased morbidity.<sup>1,2</sup> A key histological feature of AIH is lymphocytic infiltrates, extending from the portal fields into the parenchyma of the liver (interface hepatitis).<sup>3</sup> If left untreated, the disease may lead to acute hepatic failure and, in less acute cases, may rapidly progress to liver fibrosis, cirrhosis, and hepatic decompensation with life-threatening complications or the need for liver transplantation. Non-specific immunosuppression

with corticosteroids is the standard treatment for AIH, initially given at high doses as induction therapy, followed by lower doses in combination with maintenance therapies like azathioprine or mycophenolate mofetil. One of the most urgent clinical problems is that these pleiotropic drugs have significant side effects. Most patients strongly disfavor corticosteroid treatment as they experience a drastic and lasting reduction in quality of life due to the frequent occurrence of weight gain, metabolic bone disease, diabetes or depression.<sup>4–6</sup> Indeed, corticosteroid treatment is a major risk factor for major depression (five-fold) or osteoporosis (six-fold) in AIH, compared to the general population.<sup>7,8</sup> Despite the well-known adverse effects of steroids,

\* Corresponding authors. Address: University Medical Center Hamburg-Eppendorf, Martinistraße 52, 20246 Hamburg, Germany; Tel.: +49 7410 52545.

E-mail addresses: [n.gagliani@uke.de](mailto:n.gagliani@uke.de) (N. Gagliani), [a.lohse@uke.de](mailto:a.lohse@uke.de) (A.W. Lohse).

† These authors contributed equally to this work.

‡ These authors jointly supervised this work.

<https://doi.org/10.1016/j.jhep.2026.02.026>



recent registry data from six international centers revealed that only 27% of patients attain steroid-free remission after 1 year of treatment. Accordingly, most patients require long-term corticosteroid treatment to achieve this therapeutic goal.<sup>9</sup> The frequent occurrence of adverse effects may thus explain why more than 55% of patients with AIH worry about their corticosteroid therapy most or all of the time.<sup>6</sup> Therefore, targeted, preferably steroid-free therapeutic approaches for AIH combining efficacy with better tolerability are urgently needed.<sup>10</sup>

The development of targeted treatments for AIH is currently impeded by the lack of a concept that coherently and comprehensively integrates the various components of the liver immune landscape in AIH. AIH is associated with increased activation and numbers of cells of both the innate and adaptive immune response. Accumulation and activation of monocyte-derived macrophages correlate with disease severity.<sup>11–13</sup> The importance of the adaptive immune response, in particular of CD4<sup>+</sup> T cells, is indicated by a strong genetic linkage to the HLA-DRB1\*0301 and HLA-DRB1\*0401 haplotypes.<sup>3,14</sup> In keeping with this, AIH is characterized by increased hepatic infiltration and expansion of CD4<sup>+</sup> T cells.<sup>3</sup> While self-reactive CD4<sup>+</sup> T cells have been detected in the peripheral blood of patients with AIH,<sup>15–17</sup> the role of CD4<sup>+</sup> tissue-resident memory T (T<sub>RM</sub>) cells — identified in healthy livers as CD4<sup>+</sup> CD69<sup>+</sup> CD49a<sup>+</sup> T cells — has only recently begun to be described in AIH.<sup>18</sup> We have previously shown that liver CD4<sup>+</sup> T cells can co-produce IFN- $\gamma$  and TNF in AIH.<sup>19</sup> This analysis was restricted to only a few markers, therefore a systematic and unsupervised characterization of liver CD4<sup>+</sup> T cells, their cellular network and their function in AIH remains to be performed.

Recently it has been shown that the number of liver-resident CD8<sup>+</sup> T<sub>RM</sub> cells, identified as CD8<sup>+</sup> CD69<sup>+</sup> CD103<sup>+</sup> T cells displaying a cytotoxic profile, correlates with the severity of AIH.<sup>20</sup> These cells seem to express CD69 and CD103 in response to IL-15.<sup>20</sup> This cytokine has been shown to promote an auto-aggressive (a.a.) function in mouse and human liver CD8<sup>+</sup> T cells in metabolic dysfunction-associated steatohepatitis (MASH).<sup>21</sup> In the context of MASH, CD8<sup>+</sup> T cells assuming an a.a. state, from here on defined as a.a.CD8<sup>+</sup> T cells, can promote hepatocyte damage.<sup>21</sup> The presence and potential role of a.a.CD8<sup>+</sup> T cells in patients with AIH remain unknown.

In addition, the mechanisms by which innate and adaptive immune cells collectively establish a network that culminates in uncontrolled liver damage and lymphocyte accumulation — the hallmark histopathological feature of AIH — remain unclear.

Here we combine multi-omics and functional experiments to explore the topology of the immune network in AIH and identify its key nodes. We uncover critical cytokines and signaling pathways correlated with the grade of liver inflammation (e.g. TNF, IFNG) and delineate the respective contributions and spatial localization of different immune cell types (e.g. a.a.CD8<sup>+</sup> T cells) and hepatocytes that together cause liver damage in AIH. In parallel, one of the identified cytokines, TNF, was targeted in a phase IIa clinical trial using the anti-TNF antibody infliximab, demonstrating the efficacy of anti-TNF therapy in patients with newly diagnosed active AIH and highlighting an opportunity for steroid-free treatment of patients with AIH. These findings confirm the validity of our integrative omics approach and provide a resource for the identification of additional therapeutic targets in AIH, which might also be used as a blueprint for other autoimmune diseases.

## Materials and methods

### Patient populations and liver samples

For bulk mRNA-sequencing analysis, we included liver biopsies from 16 patients with AIH and 11 patients with primary biliary cholangitis (PBC);<sup>22</sup> samples were stored in liquid nitrogen and sequenced together. For cellular indexing of transcriptomes and epitopes by sequencing (CITE-seq) analysis, we included liver biopsies and paired blood samples from 10 patients with active AIH (eight of the patients were untreated, one received prednisolone for only a few days prior to biopsy, one relapsed on a low dose of budesonide); samples were processed while fresh. For single-nucleus RNA sequencing (snRNA-seq) analysis, we included liver biopsies from six patients with AIH (five of the patients were untreated and distinct from the CITE-seq atlas donors, while one patient was included in the CITE-seq and had been started on emergency prednisolone for a few days as mentioned above); samples were stored in liquid nitrogen and sequenced together. For flow cytometry and *in vitro* functional studies (FACS dataset), we included liver biopsies and paired blood samples from 13 patients with AIH and six controls who underwent bariatric surgery, benign liver lump resection, breast cancer liver metastasis resection, or liver biopsy with unremarkable pathological findings; samples were processed while fresh. For Xenium spatial *in situ* RNA expression assay, formalin-fixed paraffin-embedded liver biopsies from six patients with AIH and three controls (unremarkable pathological findings) were used. The bulk mRNA sequencing, AIH atlas (CITE-seq and snRNA-seq), FACS, and Xenium spatial *in situ* RNA expression assay datasets each represent an independent cohort of patients with AIH.

All samples were collected at the University Medical Centre Hamburg-Eppendorf, and the studies were approved by the Ethics commission Hamburg (Ethikkommission der Ärztekammer Hamburg, Germany). Biopsies were obtained via minilaparoscopy using a TruCut needle, a standard procedure at our center. AIH diagnosis was established according to current guidelines and the 'Simplified Criteria for the Diagnosis of AIH'.<sup>3,23</sup> Histological and laboratory parameters were collected alongside tissue samples for all the patients. For clinical characteristics, see [Table S4–7](#).

### Multi-omics workflow

The multi-omics workflow, including bulk mRNA sequencing, CITE-seq and snRNA-seq, and Xenium spatial *in situ* RNA expression assay, together with their associated bioinformatic analyses (data pre-processing, integration, dimensionality reduction, clustering, and interactome analysis) and sample preparation, is described in the supplementary methods.

### Flow cytometry

Antibodies for flow cytometry are listed in [Table S1](#) (CTAT table). For surface protein staining without cell stimulation, human liver and blood single cell suspensions were first stained with Zombie UV Fixable Viability Kit (BioLegend) on ice for 10 min. In a second step, the single cell suspension was stained with antibodies in PBS containing 1% FCS (PAN Biotech) and 2 mM EDTA on ice for 1 h. For the detection of TNF and IFN- $\gamma$ , cells were thoroughly washed after surface

staining and subsequently stimulated with 50 ng/ml PMA, 1  $\mu$ mol/L Ionomycin (both from Sigma-Aldrich) in the presence of Brefeldin-A solution (1:1,000, BioLegend) in RPMI medium (Gibco) with 10% FCS for 2 h at 37 °C. Dead cells were further labeled using the Zombie UV Fixable Viability Kit following the protocol as described above. Subsequently, cells were fixed and permeabilized using the Fixation/Permeabilization Kit (BD Biosciences) according to the manufacturer's instructions, then stained intracellularly with fluorochrome-labeled antibodies against IFN- $\gamma$  and TNF. For the detection of granzymes, following cell viability and surface staining, cells were fixed and permeabilized as described above without stimulation. Intracellular staining was then performed using fluorochrome-labelled antibodies against granzyme A, B and K. Flow cytometric analysis was conducted using a FACS LSR Fortessa A3 (BD Bioscience), and FACS cell sorting was conducted using a FACS AriaFusion (BD Bioscience). Data analysis was performed using the FlowJo software (v10.4).

### Cell culture

#### *Ex vivo expansion of primary human T cells*

Primary  $T_{RM1}$  and a.a.CD8<sup>+</sup> T cells from AIH livers, CD4<sup>+</sup> and CD8<sup>+</sup>  $T_{EM}$  cells from paired AIH blood, as well as blood regulatory T cells from healthy donors were FACS sorted. The sorted cells were immediately cultured for *ex vivo* expansion in X-VIVO medium (Lonza) by stimulation with 2.5  $\mu$ g/ml PHA (Sigma-Aldrich) and 40 Gy-irradiated peripheral blood mononuclear feeder cells in the presence of recombinant human IL-2 (Miltenyi), 50 U/ml for CD4<sup>+</sup> T cells and 100 U/ml for CD8<sup>+</sup> T cells, respectively. On day 12, the expanded cells were either cryopreserved or subjected to a second round of expansion.<sup>24</sup>

#### *Induction of a.a.CD8<sup>+</sup> T cells in vitro*

CD8<sup>+</sup> T cells were isolated from the blood of healthy, voluntary donors after they gave written and informed consent. This study was approved by a vote from the ethics committee of the University Hospital München rechts der Isar (564/18S). Blood was mixed 1:1 with PBS and loaded on Pancoll (PAN Biotech), followed by centrifugation at 1,400 g for 25 min to isolate peripheral blood mononuclear cells. Cells were washed, counted and subjected to immunomagnetic separation for CD8<sup>+</sup> T cells using human CD8 MicroBeads (Miltenyi Biotec), according to the manufacturer's protocols. To induce a.a.CD8<sup>+</sup> T cells, purified CD8<sup>+</sup> T cells were stimulated with 10 ng/ml IL-15 (PeproTech) for 2 days prior to the analysis.

#### *Impedance-based K562 cytotoxicity assay*

The dynamics of T-cell cytotoxicity against the HLA-deficient cell line K562 (myelogenous leukemia) over time were measured using impedance-based technology on an xCELLigence RTCA MP device (ACEA Biosciences). In brief, cells of the non-adherent cell line K562 were attached to the bottom of a plate (10<sup>4</sup> cells/well) using anti-CD71 (BioLegend) antibodies that were coated on the plate 18 h before. After 48 h (K562 cells reached confluency and maximum cell index), 10<sup>5</sup>  $T_{RM1}$  and a.a.CD8<sup>+</sup> T cells from the liver, and 10<sup>5</sup> paired blood-derived effector memory CD4<sup>+</sup> and CD8<sup>+</sup> T cells from the same patients with AIH were added to the wells. Measured electrical impedance is shown as cell index and normalized to the time point the co-culture of T cells with target cells was

started. The cell index was measured 24 h after co-culture was started to evaluate the efficacy of target cell killing. The percentage of killing was calculated by subtracting the cell index values from controls (target cells alone).

#### *Impedance-based primary hepatocyte cytotoxicity assay*

Primary human hepatocytes were purchased from PELOBio-tech and Lonza. After thawing, cell viability was determined by Trypan blue dye exclusion. 40,000 hepatocytes were seeded and cultivated on plates coated with rat tail collagen R (Advanced Biomatrix) in Williams E medium containing insulin-transferrin-selenium, 1.5% bovine serum albumin, GlutaMAX, non-essential amino acids, 100 U/ml penicillin-streptomycin (all supplements from Gibco) in the presence of 10% FCS for 16 h. Hepatocytes were maintained in medium lacking FCS for 2 days before being subjected to experiments. 100  $\mu$ l supernatants from  $T_{RM1}$  cells from AIH livers activated by anti-CD3/anti-CD28 beads (Gibco) were added to hepatocyte cultures for 24 h. In some conditions, 10  $\mu$ g/ml anti-TNF neutralizing antibody (BioXcell) was added concurrently. Following this pre-treatment, the medium was replaced, and 10<sup>5</sup> autologous or HLA-A-matched blood CD8<sup>+</sup> T cells pre-exposed to IL-15 were added to the hepatocytes. Cell viability was then monitored for an additional 15 h using impedance-based technology by xCELLigence as described above.

#### *Flow cytometry-based K562 cytotoxicity assay*

Cytotoxicity measurement was performed by labelling target cells with CFSE (ThermoFisher) and incubating with effector cells in different effector-to-target ratios for 24 h. In some conditions, K562 cells were treated with 50 ng/ml recombinant human TNF (PeproTech) or with supernatant of  $T_{RM1}$  cells from AIH livers activated with anti-CD3/anti-CD28 beads in the presence of 10  $\mu$ g/ml anti-TNF neutralizing antibody (BioXcell) for 24 h before co-culture with a.a.CD8<sup>+</sup> T cells. Dead K562 cells in co-culture with CD8<sup>+</sup> T cells were detected by flow cytometry.

#### *Stimulation of $T_{RM1}$ and a.a.CD8<sup>+</sup> T cells in vitro*

To assess IL-7 or IL-15 induced proliferation *in vitro*, expanded  $T_{RM1}$  and a.a.CD8<sup>+</sup> T cells from the liver of AIH patients were rested and labelled with CellTrace Violet (Thermo Fisher) according to the manufacturer's protocol. Cells were cultured in X-VIVO medium (LONZA) supplemented with recombinant human IL-15 or IL-7 (both from R&D Systems) at concentrations specified in the figures. Cells were harvested on the indicated days. Their expansion was quantified by measuring CellTrace Violet dye dilution using flow cytometry.

To evaluate the cytokine profile of  $T_{RM1}$  cells at protein level after *ex vivo* expansion, expanded cells were cultured in X-VIVO medium and stimulated with the ImmunoCult Human CD3/CD28 T Cell Activator (STEMCELL Technologies) according to the manufacturer's protocol. Supernatants were collected on the specified days, and cytokine levels were quantified by flow cytometry using the LEGENDplex Human CD8/NK Panel (BioLegend), following the manufacturer's instructions.

#### **Detection of STAT5 phosphorylation**

Frozen  $T_{RM1}$  and a.a.CD8<sup>+</sup> T cells from the liver of AIH patients were thawed, rested in RPMI at 4 °C for 1 h, and stained with

fluorochrome-labelled CD4 and CD8 antibodies (BioLegend), and viability dye AF750 NHS Ester (Thermo Fisher). Cells were stimulated with 10 ng/ml recombinant human IL-15 (R&D Systems or PeproTech as specified) or 100 U/ml recombinant human IL-2 (Miltenyi) in RPMI at 37 °C for 15 min, fixed with 2% PFA at 37 °C for 15 min, permeabilized with 100% methanol on ice for 30 min, and stained with pSTAT5 antibody (Thermo Fisher) for 1 h at room temperature. The readouts were acquired by flow cytometry.

### Clinical trial (AIH-MAB)

In this phase IIa, proof-of-concept clinical trial, we evaluated the effect of intravenous infliximab as the first corticosteroid-free induction treatment for patients with acute and previously untreated AIH. The trial protocol was approved by the local ethics committee (Ethikkommission der Ärztekammer Hamburg, Approval No. PVN5646-3952) and registered within the European Union Clinical Trials Register (EudraCT No.: 2017-003311-19). The study was conducted in accordance with the Declaration of Helsinki.

### Patients

Between October 2018 and February 2023, 13 patients were screened for enrolment in the clinical trial, of whom 12 were consecutively enrolled. Patients aged 18-65 years who were considered to have possible or probable AIH, and who exhibited a treatment requirement as defined by current guidelines (modified hepatic activity index [mHAI]  $\geq 4/18$ ), were eligible for inclusion in the trial. Patients with concomitant liver disease besides AIH, history of decompensation of cirrhosis or liver failure were excluded from participation in the trial. Detailed information on inclusion/exclusion criteria is provided in the trial protocol ([supplementary material](#)). The study results were additionally compared to data from 24 patients included from Hamburg to the prospective R-LIVER registry,<sup>9</sup> who received the current standard of care (SoC) with corticosteroids (prednisolone or budesonide) and azathioprine (or 6-mercaptopurine/mycophenolate in case of intolerance), using propensity score matching (PSM; see “Statistical Analyses” in the supplementary material). All participating patients provided written informed consent before enrolment.

### Experimental treatment

Patients in the trial received a cumulative total of 8 doses of intravenous infliximab (Infliximab<sup>®</sup>, Pfizer) at a dosage of 5 mg/kg over a period of 24 weeks (day 0, weeks 2, 6, 8, 12, 16, 20, and 24). In addition, patients were followed up during additional safety visits in weeks 1 and 4 and were monitored after completion of the infusion therapy at weeks 36 and 48. All patients additionally commenced azathioprine therapy after the week 2 visit at an initial dose of 50 mg daily, which was subsequently titrated in 25-50 mg increments every 7 days to achieve a target dose of 1-2 mg/kg body weight per day. In case of intolerance, patients were switched to 6-mercaptopurine (50 mg/day) or mycophenolate (2,000 mg/day).

### Safety and monitoring

Patients were screened twice within 2 weeks prior to treatment initiation. Physical examinations, as well as assessments of vital signs and body weight, were performed at every visit as

were standard laboratory values. Visits included a safety evaluation regarding clinical and biochemical safety endpoints or (serious) adverse events (AEs). Serious AEs, including their severity and likelihood of a causal relationship to infliximab administration, were documented, followed up, and reported within 24 h, where applicable. Liver stiffness was assessed by transient elastography (Fibroscan<sup>®</sup>) during screening as well at week 12, 24, 36 and 48. Quality of life was assessed using standardized questionnaires (SF-36 [Short Form-36 Health Survey]) at the time of screening, initial administration, as well as at weeks 1, 4, 8, 12, 16, 20, 24, 36, and 48. Patients were withdrawn from infliximab treatment in the event of severe adverse events considered related to the study medication. Participation in the study was also discontinued in case transaminase levels increased more than 20% over the respective patient's individual baseline during the first 4 weeks of treatment or in those who exhibited a decrease of transaminase levels  $< 50\%$  8 weeks after treatment initiation. In this case, patients received standard treatment with corticosteroids in accordance with current guidelines.

### Endpoints

The primary endpoint of the study was defined as biochemical remission at month 6 after treatment initiation. Biochemical remission was specified as normalization of alanine aminotransferase (ALT) and aspartate aminotransferase (AST) ( $\leq 35$  U/L for females and  $\leq 50$  U/L for males) as well as of IgG ( $\leq 16$  g/L). Secondary endpoints were defined as differences in health-related quality of life (HRQoL) as assessed by the questionnaires mentioned above as well as decrease in liver stiffness (measured by transient elastography/FibroScan<sup>®</sup>) and the absence of weight gain (BMI).

### Statistical analyses

Statistical analyses are described in the supplementary materials.

## Results

### Identification of inflammatory pathways associated with the severity of AIH

To characterize the signaling molecules, transcription factors and cytokines constituting the inflammatory process of AIH, and to identify potential drug targets, we profiled the bulk transcriptome of liver biopsies obtained from 16 patients with active AIH. As controls, we included biopsies from 11 patients with another autoimmune liver disease, namely PBC. Standard liver biochemistry and histological grading were used to evaluate disease activity and stage ([Fig. 1A](#)). ALT serum levels and the mHAI were assessed primarily, as they are regarded as the best markers of inflammatory activity in the clinical context of AIH. Considering these features, a principal component analysis showed that the transcriptomes of the liver samples were separated by mHAI rather than by diagnosis or by fibrosis stage ([Fig. 1B](#), multivariate PERMANOVA  $p_{\text{mHAI}} = 0.03$ ,  $p_{\text{diagnosis}} = 0.25$ ,  $p_{\text{fibrosis}} = 0.19$ ). Next, to further evaluate how the clinical markers represent inflammatory activity at the gene expression level, we used the MSigDB gene set “Hallmark Inflammatory Response” (M5932) to calculate a patient-wise inflammation score. As expected, patients with PBC

exhibited relatively low scores compared to AIH. Furthermore, we found that biopsies showing severe histologic activity (*i.e.* mHAI  $\geq 10$ ) showed a markedly increased expression of pro-inflammatory genes (Fig. 1C). In addition, there was a strong association between the inflammation score and serum ALT levels in patients with AIH, which was not observed in the PBC cohort (Fig. 1C). These results showed that the clinical signs of inflammation were reflected at the transcriptome level.

Next, we analyzed the expression of key cytokines. To this end, we determined the association between gene expression and clinical features in patients with AIH by applying Spearman's rank correlation ( $r_s$ ) (Fig. S1A). Subsequently, we performed a KEGG enrichment analysis on genes ranked by  $r_s$ . We found that in terms of signal transduction, the TNF-, NFKB- and JAK-STAT signaling pathways in particular were positively associated with histologic and laboratory features of inflammation (Fig. 1D). Consistently, when we inferred the transcription factor activity by applying a univariate linear model between the gene correlation and the gene regulatory network CollecTRI,<sup>25</sup> transcription factors annotated to the previously identified pathways (*e.g.* STAT1, RELA, NFKB1) were among the top hits (Fig. 1E).

In accordance with the identified pathways, several ligands (*e.g.* TNF, IL12A, IFNG, IL15) exhibited a strong correlation to both features of inflammation, mHAI and ALT (Fig. 1F and S1B). To validate our findings, we examined the expression of selected cytokine genes by real-time PCR in samples from the AIH and PBC cohorts (Fig. 1G). In line with the bulk mRNA-sequencing data, an association between mRNA levels and both mHAI and ALT was confirmed.

These analyses suggested that the type I cytokines TNF, IL-12, IFN- $\gamma$  and the corresponding pro-inflammatory downstream signaling in the liver are central players in the inflammatory pathophysiology of AIH, and thus might be promising therapeutic targets. However, the specific cellular network encompassing these inflammatory pathways remained unclear.

### Development of an AIH atlas integrating liver immune and non-immune cell transcriptomes

To reveal the cellular network related to the AIH-specific pro-inflammatory pathways identified above, we assembled a comprehensive single-cell RNA sequencing atlas of the immune and non-immune cells found in AIH livers, using a patient cohort distinct from the one shown in Fig. 1. To this end, we analyzed fresh liver biopsies from 10 patients with AIH. Moreover, to discriminate between systemic and tissue-specific immune mechanisms, we also analyzed paired peripheral blood samples collected from 3 of those patients taken at the same time as the respective fresh liver biopsies (Fig. 2a). CD45<sup>+</sup> immune cells from the liver biopsies and CD3<sup>+</sup> T cells from paired blood samples were FACS-sorted and subjected to CITE-seq and single-cell T-cell receptor sequencing (scTCR-seq). The capture of non-immune cells, particularly hepatocytes, was technically challenging. To overcome this, we isolated nuclei from cryopreserved liver biopsies of six patients with AIH (one of whom also contributed a sample to the CITE-seq/scTCR-seq dataset introduced above) and performed snRNA-seq (Fig. 2A).

To simultaneously depict the immune and non-immune profiles in the liver of patients with AIH and achieve robust

clustering, we integrated our CITE-seq dataset with the snRNA-seq dataset. Cells recovered from fresh CITE-seq predominantly comprised immune cells, while cells recovered from cryopreserved snRNA-seq encompassed both immune and non-immune cell types (Fig. 2B). Although CITE-seq and snRNA-seq show different sequencing depths (Fig. S2A), by integrating the CITE-seq and snRNA-seq datasets, we identified similar populations to those derived from the analysis of the two datasets independently (Fig. S2B–D). This showed the validity of the integration approach used here.

Next, we annotated the identified major clusters from both immune and non-immune cells in the liver based on a combination of differentially expressed genes (DEGs) in a semi-supervised approach. Immune cell clusters encompassed CD4<sup>+</sup> T cells, CD8<sup>+</sup> T cells, B cells, plasma cells, innate-like T cells, and myeloid cells (including monocytes, macrophages and dendritic cells), while non-immune cells included hepatocytes, endothelial cells, cholangiocytes, and stellate cells/fibroblasts (Fig. 2c and S2E,F). Considering that the strong association of AIH with specific HLA-DR haplotypes suggests a T cell-driven immune response,<sup>3,14</sup> and the recent description of CD8<sup>+</sup> T<sub>RM</sub> cells in AIH,<sup>20</sup> we further investigated liver-derived T cells. We annotated nine major CD4<sup>+</sup> T-cell clusters, including naïve-like T cells, central memory T cells (T<sub>CM</sub>), five effector memory T-cell clusters (T<sub>EM</sub>-a, -b, -c, -d, -e) and two FOXP3<sup>+</sup> regulatory T-cell clusters (T<sub>REG</sub>-a, -b) (Fig. 2D and S3A,B). Following the same approach, we annotated 12 major CD8<sup>+</sup> T-cell clusters including a naïve-like cell cluster, two T<sub>CM</sub> (T<sub>CM</sub>-a, -b) and seven effector memory T-cell clusters (T<sub>EM</sub>-a, -b, -c, -d, -e, -f, -g) (Fig. 2E and S3C,D).

Hepatocytes have distinct functions based on their location in the hepatic lobule, a concept known as zonation.<sup>26</sup> Zone 1 consists of periportal hepatocytes surrounding the portal triad, zone 2 comprises the mid hepatocytes, and zone 3 includes central hepatocytes located near the central vein. We annotated ten distinct hepatocyte clusters (Fig. 2F and S3E,F), three of which expressed gene signatures representing the three zonation populations, periportal, midzone, and central hepatocytes. Moreover, we found an inflammatory cluster with high expression of immune regulation-related genes, such as *IL32*, *ICAM1* and *STAT1*, reflecting the involvement of hepatocytes in the inflammatory process in AIH. Additionally, two proliferative clusters and one *BICC1*-high cluster were annotated, which probably reflect disease-related damage and subsequent regenerative responses of hepatocytes.<sup>27,28</sup> We also annotated two clusters with unclear biological relevance as *PTPRB*-hi and *PTPRC*-hi, which co-express hepatocyte genes with endothelial (*PTPRB*) or immune cell-related (*PTPRC*) genes, respectively. Their functional relevance requires further investigation.

In conclusion, we generated a comprehensive single-cell AIH atlas which enables the study of immune and non-immune cells and their potential interactions in the liver.

### Identification of CD4<sup>+</sup> T<sub>RM</sub>1 cells in AIH liver

Based on the DEGs and signature genes, we refined the annotation of the liver CD4<sup>+</sup> T<sub>EM</sub> clusters and within them identified T<sub>FH</sub> cells (former T<sub>EM</sub>-d) and T<sub>R</sub>1 cells (former T<sub>EM</sub>-e). In our effort to identify clusters relevant to AIH, we found that



the cluster  $T_{EM-C}$  was enriched for *TNF* and *IFNG*, two of the cytokines which we found to be associated with AIH and correlated with disease states, as shown above (Fig. 1). Accordingly, this cluster was also enriched for the type 1 master transcription factor *TBX21* and molecules associated with cytotoxicity, such as *TNFSF10* and *FASLG* (Fig. 3A). In addition, although not the only one, this cluster was clonally expanded (Fig. 3B and S4A). Using the TCR sequences (Fig. S4B and C), we found that 80% (8 out of 10) of the most highly expanded clonotypes ( $n \geq 6$  clones) within the  $T_{EM-C}$  cluster were present in the liver, but not in the blood (Fig. 3C). In contrast, clonotypes that were expanded at lower levels ( $n \leq 5$  clones) could be detected both in the liver and in the blood of the same patients (Fig. S4D). As these findings suggested a possible residency of the highly expanded clones within the  $T_{EM-C}$  cluster, we tested for the expression of a literature-based residency and migratory score<sup>29</sup> and observed that the  $T_{EM-C}$  cluster was enriched for genes associated with residency but not with migration, particularly in comparison with  $T_{EM-a}$  cells, which were *S1PR1*-positive, thus favoring egress from the tissue (Fig. 3D). Considering the type 1 cytokine profile, residency signature and in particular the expression of two widely accepted prototypical residency markers, *CD69* and *CXCR6* (Fig. S4E), we propose referring to  $T_{EM-C}$  as tissue resident-like type 1 memory ( $T_{RM1}$ ) cells.

To confirm the presence and the features of  $T_{RM1}$  cells, we validated the AIH atlas findings at the protein level using multiparametric flow cytometry on a new set of AIH tissue samples. We first selected potential  $T_{RM1}$  surface markers from the CITE-seq data accepted in the field, *i.e.* *CD69*, *CXCR6*, *ITGA1* and *TIGIT* (Fig. S4E). *CD69* and *CXCR6* were expressed in  $T_{RM1}$  cells but not in migratory  $T_{EM-a}$  cells. *ITGA1*, which is commonly used to identify type I cytokine-producing and resident cells,<sup>30</sup> appeared to be expressed, albeit by few cells, mainly in the  $T_{RM1}$  cluster. Finally, *TIGIT* was selectively expressed in  $T_{FH}$  and regulatory cells,<sup>31</sup> as expected, but not in  $T_{RM1}$  cells. Once these markers were selected, we tested them on cells isolated from fresh liver biopsies of patients with AIH. We hereby identified a distinct population of memory  $CD4^+$  T cells co-expressing *CD69*, *CXCR6*, *CD49a* (encoded by the *ITGA1* gene) but negative for *TIGIT*, and thus probably reflecting  $T_{RM1}$  cells (Fig. 3E and S4F). Considering that one of the key features of  $T_{RM1}$  cells is the expression of *TNF* and *IFNG*, we restimulated liver  $CD4^+$  T cells *in vitro* and found that the majority of the  $CD69^+ CD49a^+ CD45RO^+ CD4^+$  T cells co-produced *TNF* and *IFN- $\gamma$*  (Fig. 3F left, and S4G). Using a complementary analysis, we found that the majority of *TNF* and *IFN- $\gamma$*  co-producing  $CD4^+$  T cells were  $CD69^+ CD49a^+ CD45RO^+ CD4^+$  T cells (Fig. S4H). Finally, we found that  $T_{RM1}$  cells showed the highest average expression of both *TNF* and *IFN- $\gamma$* , as indicated by mean fluorescence intensity, followed by  $CD69^+$  cells in the liver-infiltrate and

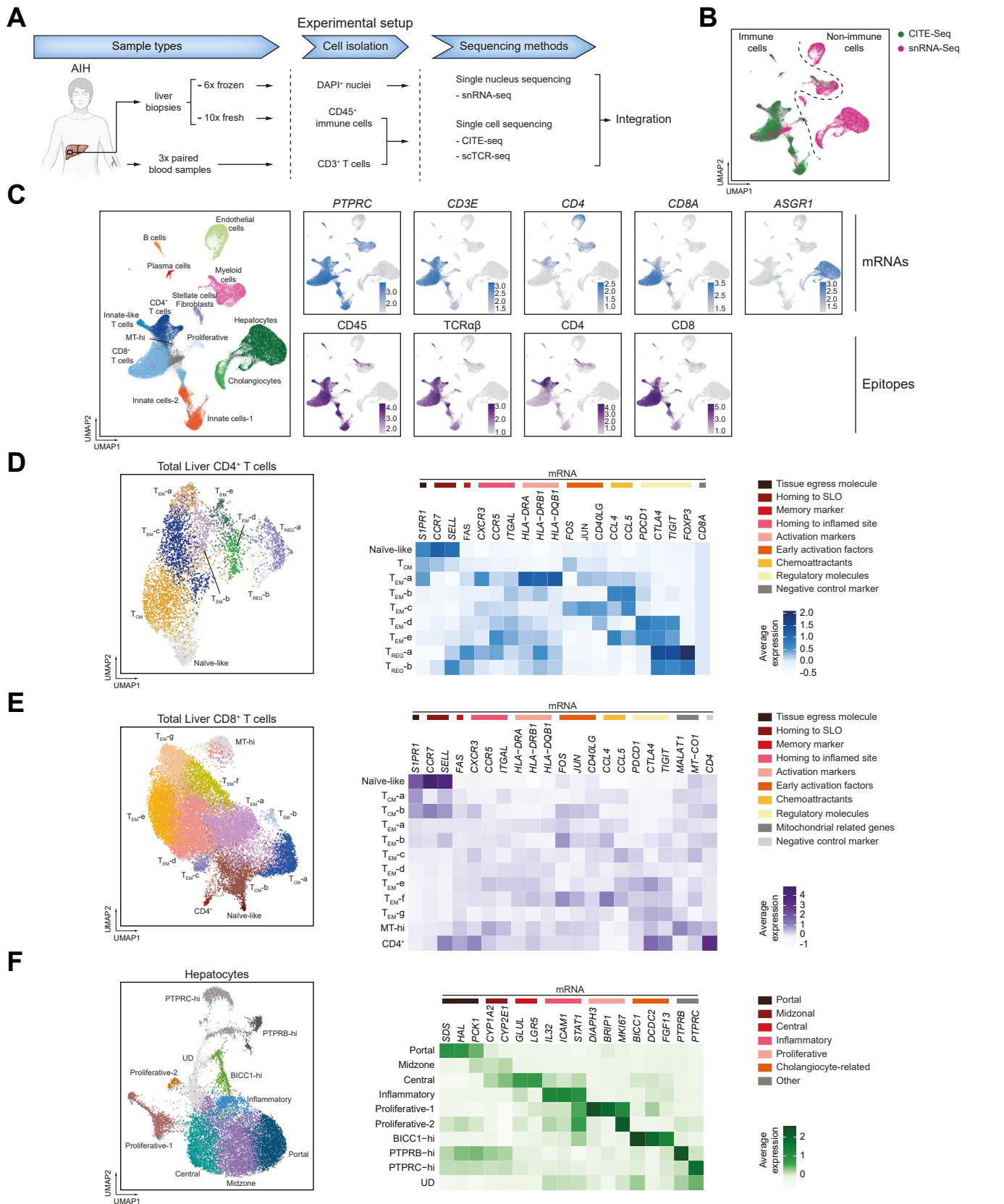
blood  $T_{EM}$  cells (Fig. 3F, middle and right). Further confirmation of the phenotype of  $T_{RM1}$  cells in the liver of patients with AIH was obtained by the capacity of  $CD69^+ CD49a^+ CD45RO^+ CD62L^- CD4^+$  T cells to produce granzyme A, B, and K, as was also indicated in the AIH atlas dataset (Fig. S4I). Finally, we tested whether  $T_{RM1}$  cells were more abundant in AIH livers compared to mildly inflamed livers in various other conditions. We found a higher abundance of  $T_{RM1}$  cells per milligram of liver in patients with AIH compared to controls (Fig. S4J).

### Identification of a.a. $CD8^+$ T cells in AIH liver

Following a similar approach to that used for  $CD4^+$  T cells, we also characterized liver  $CD8^+$  T cells. In the livers of patients with MASH, Dudek *et al.* reported a population of a.a. $CD8^+$  T cells expressing the chemokine receptor *CXCR6*, along with key cytokines, including *TNF* and *IFN- $\gamma$* ,<sup>21</sup> which we also observed in AIH livers. a.a. $CD8^+$  T cells represent a state of  $CD8^+$  T cells characterized by transient MHC I-independent cytotoxic capacity under conditions of IL-15 exposure.<sup>21</sup> We therefore wondered whether  $CD8^+$  T cells, present in AIH livers, were characterized by the a.a. state. To address this, we first analyzed *CXCR6* and *CD69* expression in our sequencing data (Fig. S5A). Although *CXCR6* was expressed by fewer cells within the  $T_{EM-a}$  cluster, it was broadly expressed at the RNA level across  $T_{EM-b}$  to  $-g$ . Similarly, the tissue residence marker *CD69* was widely expressed at the protein level from  $T_{EM-a}$  to  $-g$ . We further assessed the presence of an a.a. gene signature, assigning a.a. scores to each cluster.<sup>21</sup> We found that  $CD8^+ T_{EM-a}$  to  $-g$  exhibited elevated a.a. scores compared to the other clusters, namely naïve-like and  $T_{CM}$  cell clusters (Fig. 3G and S5B). Consistent with the a.a. potential,  $T_{EM-f}$  and  $-g$  were enriched for AIH-associated pro-inflammatory genes, such as *TNF* and *IFNG* (Fig. S5A). In addition,  $T_{EM-d}$  and  $-e$  were enriched for cytotoxicity-related genes, such as *FASLG*, *PRF1* and *GZMB* (Fig. S5A). All  $CD8^+$  T-cell clusters except for the naïve-like cluster exhibited large clonal expansion (Fig. 3H and S5C). By analyzing TCR sequences from the three paired blood and liver samples, we identified 16 highly expanded clonotypes ( $n \geq 31$  clones). Notably, 50% (8 out of 16) of these clonotypes were exclusively present in the liver but not in the blood, and were found within  $T_{EM-e}$ ,  $-g$ , as well as partially within  $T_{EM-c}$ ,  $-d$  and  $-f$ . In contrast, the other 50% of highly expanded clonotypes were detectable both in the liver and blood and were primarily associated with clusters  $T_{EM-a}$ ,  $-b$ ,  $-c$  and partially  $T_{EM-d}$  and  $-f$  (Fig. 3I). Clonotypes with lower expansion ( $n \leq 30$  clones) exhibited a similar pattern (Fig. S5D). Collectively, these findings suggest longer dwell times of the cells of the  $T_{EM-e}$  and  $T_{EM-g}$  clusters in the liver, whereas the cells of the  $T_{EM-a}$  cluster appear more circulatory. Meanwhile, the  $T_{EM-b}$ ,  $-c$ ,  $-d$  and  $-f$  clusters might represent an

Significant differences are indicated by Wilcoxon Rank Sum test, FDR adjusted. Right: Linear regression plot for patients with AIH (black regression line, black dots) and PBC (green regression line; dots omitted). (D) Enrichment of KEGG terms in the "signal transduction" category for genes using the Spearman correlation to mHAI, ALT, or fibrosis scores in patients with AIH. Only terms significant for at least one feature are shown. Statistical significance is indicated as follows: \* $p < 0.05$ , \*\* $p < 0.01$ , \*\*\* $p < 0.001$  and \*\*\*\* $p < 0.0001$ . (E) Bar plots of the top six transcription factors per feature with the highest activity scores, calculated using the t-statistic of a univariate linear model on the CollecTRI Database and strongly correlating genes. (F) Heatmap of strongly correlating tumor necrosis factor superfamily members, interleukins and interferon.  $r_s$  values are labelled. Fields with  $r_s > 0.6$  are emphasized by black border. (G) Boxplots and regression plots comparing normalized expression by mRNA sequencing with relative expression by qPCR for selected cytokines. AIH, autoimmune hepatitis; ALT, alanine aminotransferase; FDR, false discovery rate; mHAI, modified hepatic activity index; PBC, primary biliary cholangitis.

## TNF as key target in autoimmune hepatitis



intermediate state, consisting of some cells with a residency path and others adopting a circulatory pattern. Using residency and migratory scores as described above,  $T_{EM-e}$ , -f, and -g exhibited a higher residency score and a lower migratory score, albeit with some heterogeneity, compared to the other clusters.  $T_{EM-a}$  to -d exhibited an intermediate residency score (Fig. 3J). In short, these  $CD8^+$   $T_{EM}$  sub-clusters consist of cells with a potential migratory progression, transitioning from infiltrating to resident or vice versa. Nevertheless, based on the similar expression of the a.a. score, suggesting a potential common cytotoxicity function and the expression of the key markers CD69 and CXCR6, we simplified the potential heterogeneity of the  $T_{EM-a}$  to -g cell clusters by referring to them as  $CD8^+$  T cells with a potential a.a. function (i.e. a.a. $CD8^+$  T cells).

As for  $CD4^+$   $T_{RM1}$  cells, we confirmed the presence and characteristics of a.a. $CD8^+$  T cells at the protein level using multiparameter flow cytometry. We identified a distinct population co-expressing CD69 and CXCR6, which have been used to identify a.a. T cells (Fig. 3K and S4F). Additionally, this population also co-expressed PD-1 and TIGIT, which are additional surface markers identified in the a.a. gene set, reflecting their status as highly activated cells.<sup>32</sup> In contrast, the CXCR6 and CD69 double-negative population exhibited relatively low expression of PD-1 and TIGIT. Notably, CD49a, although not yet associated with auto-aggression, was also expressed by  $CD69^+$   $CXCR6^+$  a.a. $CD8^+$  T cells (Fig. 3K). Upon *in vitro* restimulation, a large fraction of liver  $CD69^+$   $CD49a^+$   $CD45RO^+$   $CD8^+$  T cells co-produced TNF and IFN- $\gamma$ , further lending support to the notion that these cells represent a.a. $CD8^+$  T cells in accordance with our CITE-seq analysis (Fig. 3I and S5E). Unlike the  $CD4^+$  populations, a.a. $CD8^+$  T cells showed a similar expression of TNF as liver-infiltrating  $CD69^-$   $CD49a^-$   $CD45RO^+$   $CD8^+$  T cells. IFN- $\gamma$  expression tended to be higher in the a.a. $CD8^+$  T cells. Moreover, granzyme A, B, and K were also detected in this population without *in vitro* stimulation (Fig. S5F). Finally, we investigated whether a.a. $CD8^+$  T cells were more prevalent in the livers of patients with AIH. Analysis of  $CD8^+$  T cells from the same group of patients used for the  $CD4^+$  T-cell study revealed that the  $CD8^+$  T cells in the livers of patients with AIH showed significantly higher abundance of cells per mg of liver with the a.a. phenotype compared to controls (Fig. S5G).

Overall, we identified and validated  $CD4^+$   $T_{RM1}$  cells and a.a. $CD8^+$  T cells in AIH livers as a potential source of TNF and IFN- $\gamma$ , two of the proinflammatory cytokines we found to be associated with AIH.

### AIH molecular-cellular network and its spatial distribution

Following the identification of the key AIH-related pathways and their cellular sources, we then aimed to integrate their relationships into a coherent interactome that enables the

generation of hypotheses explaining the pathological immune network of AIH. To this end, we used CellChat<sup>33</sup> to infer intercellular communication probabilities by analyzing the expression of the preselected set of cytokine ligand-receptor pairs from the above analyses. *IL12*, which exhibited a positive correlation with disease severity in Fig. 1, was not included in this analysis due to low RNA counts. We differentiated between conventional IL-15 signaling (referred to as '*IL15 - (IL15RA+IL2RB+IL2RG)*') and the trans-presentation of IL-15 (*(IL15RA+IL15) - (IL2RB+IL2RG)*).<sup>34</sup> The inferred interactions suggested that both  $T_{RM1}$  cells and a.a. $CD8^+$  T cells can potentially respond to IL-15 and IL-7, which are produced by myeloid cells. In turn,  $T_{RM1}$  and a.a. $CD8^+$  T cells could interact with myeloid cells by secreting TNF and IFN- $\gamma$  and thus promote the pro-inflammatory phenotype of these innate cells. In addition, we found that TNF and its receptors can connect  $T_{RM1}$  cells with a.a. $CD8^+$  T cells, suggesting potential support of  $CD8^+$  T-cell survival by  $CD4^+$  T cells. Next,  $T_{RM1}$  and a.a. $CD8^+$  T cells were shown to potentially interact with hepatocytes through TNF, IFN- $\gamma$  and FASLG, thus potentially contributing to tissue damage. Finally, hepatocytes secreting IL-7 and IL-15 could target the corresponding cytokine receptors on both  $T_{RM1}$  and a.a. $CD8^+$  T cells, closing a potential vicious cycle, which may lead to chronic inflammation typical of AIH (Fig. 4A). A cell type-focused overview of these findings is provided in Fig. 4B.

To further support this AIH molecular-cellular network, we investigated cell neighborhoods within the spatial context using an independent cohort of patients with AIH. Specifically, we profiled the spatial distribution of 477 selected genes across six AIH liver biopsies and three control liver biopsies with unremarkable histopathological findings using the Xenium *In Situ* platform (10x Genomics) (spatial *in situ* RNA expression assay) (Fig. 4C). Dimensionality reduction of these data yielded 21 well-segregated clusters for AIH samples and 17 clusters for control samples, with a median of 50 genes detected per cell (Fig. S6A-C). We used the DEGs identified from our AIH atlas as a reference to annotate clusters and map cell types to their spatial localization (Fig. 4C and S6B,C). Compared to control livers, which exhibited clear zonation and minimal immune cell infiltration, AIH biopsies demonstrated disrupted zonation patterns and a marked increase in immune cell infiltration, including T cells, B cells, and myeloid cells (Fig. 4C). We next quantified the proportions of different immune and non-immune cell populations.  $T_{RM1}$  and a.a. $CD8^+$  T cells were more abundant in AIH compared to control livers, while hepatocytes appeared to be diminished in AIH livers, as expected (Fig. S6D). Focusing on the different types of hepatocytes, their proportions varied between AIH and controls with a relative increase in hepatocytes with inflammatory features in AIH (Fig. S6E). In addition, more immune cells, including  $T_{RM1}$  and a.a. $CD8^+$  T cells, were found adjacent to hepatocytes in AIH compared to control livers (Fig. S6F). At the hepatic-immune

donors excluded due to <80  $CD4^+$  T cells) (CITE-seq: n = 9; snRNA-seq: n = 5). Right: Heatmaps of selected canonical marker genes across all  $CD4^+$  T-cell sub-clusters. (E) Left: Sub-clustering analysis of  $CD8^+$  T cells including all 16 donors (CITE-seq: n = 10; snRNA-seq: n = 6). Right: Heatmaps of selected canonical marker genes across all  $CD8^+$  T-cell sub-clusters. (F) Left: Sub-clustering analysis of hepatocytes based solely on snRNA-seq (n = 6), excluding hepatocytes from CITE-seq due to low recovery. Right: Heatmap of selected markers associated with zonation, inflammation, proliferation and regeneration. AIH, autoimmune hepatitis; CITE-seq, cellular indexing of transcriptomes and epitopes by sequencing; SLO, secondary lymphoid organ; snRNA-seq, single-nucleus RNA sequencing; UD, undefined; UMAP, uniform manifold approximation and projection.

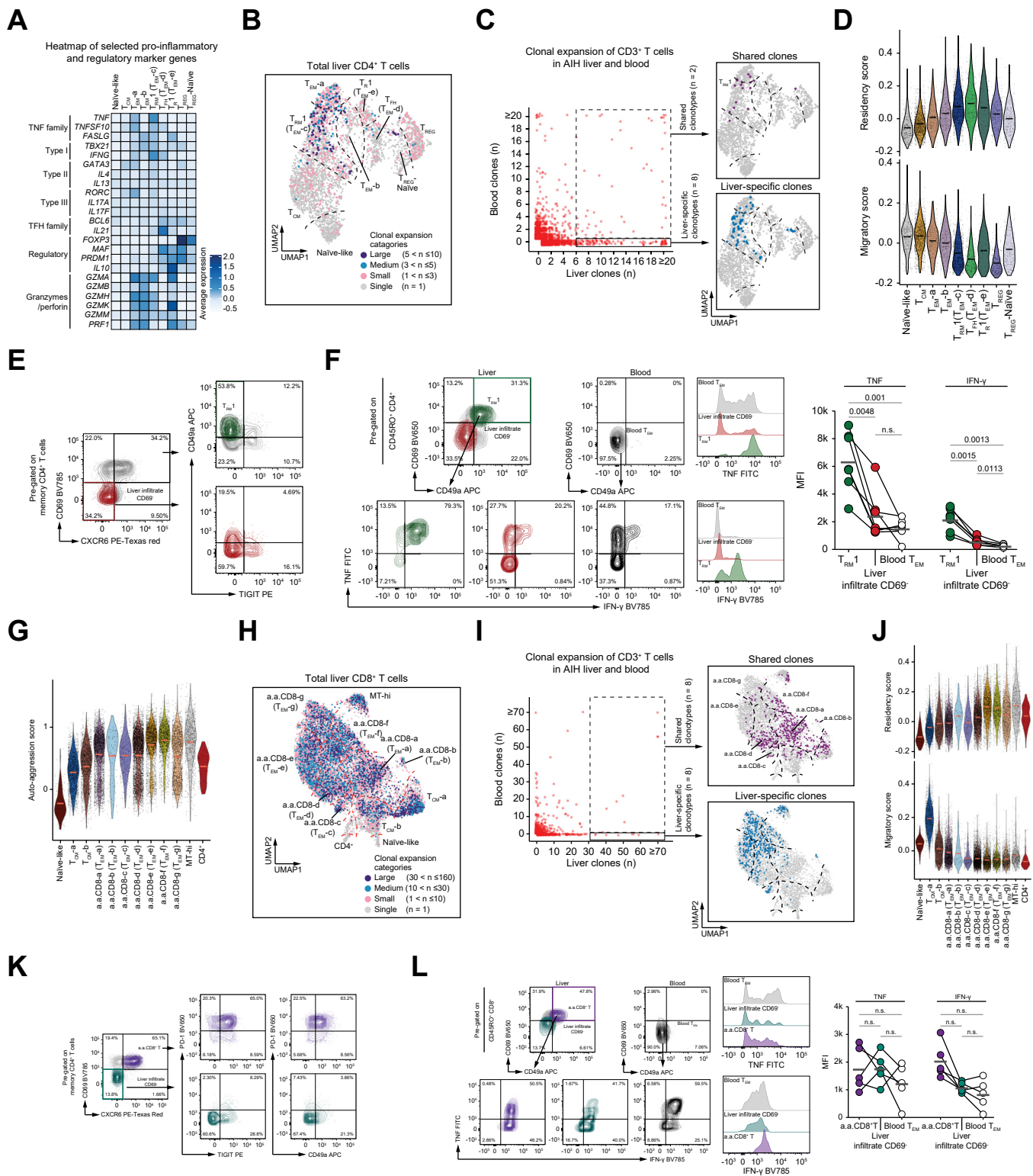


**Fig. 3. Characterization of intrahepatic conventional T cells in AIH.** (A) Heatmap of selected pro-inflammatory and regulatory marker genes across CD4<sup>+</sup> sub-clusters corresponding to those defined in Fig. 2D. Re-annotation of T<sub>EM</sub>-c, T<sub>EM</sub>-d, and T<sub>EM</sub>-e as T<sub>RM</sub>1, T<sub>FH</sub>, and T<sub>R</sub>1, respectively, based on their features. (B) UMAP showing the clonal expansion of CD4<sup>+</sup> T cells from CITE-seq data. Clonal expansion is determined by the total number of cells sharing the same clonotype. (C) Left: Clonal expansion of CD3<sup>+</sup> T cells, in livers and paired blood (liver CITE-seq: n = 3; paired blood CITE-seq: n = 3). The X-axis and Y-axis represent liver and blood clones, respectively, with clone counts ≥ 20 truncated to 20 for visualization. Right: UMAP of CD4<sup>+</sup> T cells highlighting highly abundant clones (frequencies of n ≥ 6) shared between the liver and blood (top), and liver-specific clones (bottom). (D) Migration and residency scores for all CD4<sup>+</sup> T-cell subclusters (CITE-seq: n = 9; snRNA-seq: n = 5). (E) Representative flow cytometry plots showing the expression of CD69 and CXCR6 on memory CD4<sup>+</sup> T cells in AIH livers. Distinct expression pattern of CD49a and TIGIT are used to identify T<sub>RM</sub>1 cells. The gating strategy for memory CD4<sup>+</sup> T cells is shown in Fig. S4F. (F) Left: Representative flow cytometry plots showing TNF and IFN-γ expression patterns following *in vitro* stimulation in the indicated CD4<sup>+</sup> populations. CD45RO<sup>+</sup> CD4<sup>+</sup> T cells were pre-gated on TCRαβ<sup>+</sup>

interface, we observed close adjacency between *TNF*-expressing  $T_{RM1}$  cells and hepatocytes or  $CD8^+$  T cells expressing *TNFRSF1A* or *TNFRSF1B* (Fig. 4D). Additionally, *IL7*- or *IL15*-expressing myeloid cells or hepatocytes were found in close proximity to  $T_{RM1}$  and a.a. $CD8^+$  T cells expressing *IL7R* or *IL15R* (Fig. 4A). Targeting the same key players as indicated in Fig. 4A, namely  $T_{RM1}$ , a.a. $CD8^+$  T cells, myeloid cells and hepatocytes, we further analyzed the interaction probabilities of the selected ligand-receptor pairs, incorporating their spatial distances to calculate interaction probabilities (Fig. 4E). The resultant heatmap revealed various probable interactions similar to those shown in Fig. 4A; the majority of these interaction potentials were observed in AIH livers, but not in control livers (Fig. 4E). These findings provide further evidence of the potential interactions we proposed in AIH livers.

### Functional validation of identified cellular interactions

Subsequently, we aimed to functionally validate some of the above-mentioned findings (Fig. 4). Based on the AIH cellular-molecular network and the cellular abundance of  $T_{RM1}$  and a.a. $CD8^+$  T cells in AIH, we hypothesized that *IL-7* and *IL-15* play a role in inducing the proliferation of these cells. To functionally test this, we isolated and expanded both types of T cells from AIH liver biopsies and then exposed them to recombinant human *IL-7* or recombinant human *IL-15*. *IL-7* could induce the proliferation of  $T_{RM1}$  cells in a dose-dependent manner, and *IL-15* promoted the proliferation of both  $T_{RM1}$  and a.a. $CD8^+$  T cells, also in a dose-dependent manner (Fig. 5A and S7A-F).

Next, we wondered whether the transcriptomic profile of a.a. $CD8^+$  T cells found in AIH livers translates into an a.a. function, *i.e.* MHC I-independent killing. To address this, we utilized a validated *in vitro* approach by co-culturing indicated populations with K562 target cells that lack MHC-I molecules without additional stimulation to test for auto-aggression,<sup>21</sup> and found that AIH liver-derived a.a. $CD8^+$  T cells displayed an MHC I-independent killing capacity (Fig. 5B). In contrast, we did not observe a reproducible a.a. function from liver  $T_{RM1}$  cells nor from  $CD8^+$  and  $CD4^+$  T cells isolated from blood (Fig. 5B).

Although  $T_{RM1}$  did not display direct a.a. properties, our interactome analysis identified both hepatocytes and a.a. $CD8^+$

T cells as targets of  $T_{RM1}$  and of *TNF*, raising the possibility that  $T_{RM1}$  may indirectly contribute to hepatocyte damage, potentially through *TNF* secretion. To explore this, we designed experiments to evaluate the impact of *TNF* pre-treatment on either the target cells or a.a. $CD8^+$  T cells, which, for the purpose of standardization, were generated by *in vitro* stimulation of blood-derived  $CD8^+$  T cells with *IL-15* as described.<sup>21</sup> Pre-treating *IL-15*-induced a.a. $CD8^+$  T cells with soluble *TNF* did not augment their a.a. function (Fig. 5C); however, pre-treating the target cells did enhance auto-aggression by a.a. $CD8^+$  T cells (Fig. 5D). Since  $T_{RM1}$  cells can secrete *TNF*, we next pre-treated target cells with the culture supernatant of anti-*CD3*/anti-*CD28*-activated  $T_{RM1}$  cells. We observed that this pre-treatment enhanced the a.a. effect exerted by blood-induced a.a. $CD8^+$  T cells. Of note, this increase in cytotoxicity was partially reversed by *TNF* blockade (Fig. 5E and S7G).

We next aimed to confirm some of these findings using primary human hepatocytes. We found that the pre-treatment of hepatocytes with the supernatant of activated  $T_{RM1}$  cells increased the killing capacity of a.a. $CD8^+$  T cells, which was inhibited by *TNF* blockade (Fig. 5F and S7H).

Finally, we aimed to investigate the potential pathological effects of *TNF* on hepatocytes. *TNF* has been shown to upregulate *ICAM1* in human epithelial cells.<sup>35</sup> Additionally, hepatocytes exposed to *TNF* upregulate *ICAM1*, facilitating close interactions with cytotoxic T cells in a MASH mouse model.<sup>21</sup> Therefore, we proposed that *TNF* exerts a similar effect in AIH. To assess this, we quantified *TNF* signaling activity in hepatocytes exploiting data from our atlas. Based on our AIH atlas dataset, using  $CD8^+$  T cells as a positive control for *TNF* signaling, we classified hepatocytes into high and low *TNF* response groups (Fig. S7I). Differential gene analysis between the *TNF*-high and -low response groups revealed that several adhesion molecules, which facilitate physical interactions between hepatocytes and T cells, were upregulated in the *TNF*-high response group (Fig. S7J). Furthermore, a regression model revealed a significant positive association between *TNF* signaling pathway activity and the expression of adhesion molecules, including *ICAM1* (Fig. 5G). To further validate our findings in a spatial approach reflecting the *in vivo* conditions, we analyzed the spatial *in situ* RNA expression dataset with a particular focus on *TNF* receptor-positive hepatocytes in close proximity to *TNF*-producing cells (within 20  $\mu$ m), including  $T_{RM1}$ ,

TCRV $\alpha$ 24-J $\alpha$ 18<sup>-</sup> live, singlet lymphocytes. Middle: Representative histograms showing the mean fluorescence intensity (MFI distribution) of *TNF* and *IFN- $\gamma$*  across the indicated  $CD4^+$  populations. Right: MFI quantification in 7 AIH donors. Each dot represents a single donor, with MFI levels of different populations from the same donor connected by lines. Grey lines represent mean values. Significant differences are determined by RM one-way ANOVA, Tukey's multiple comparisons test. (G) a.a. score for all  $CD8^+$  T-cell subclusters (CITE-seq: n = 10; snRNA-seq: n = 6). Re-annotation of  $T_{EM-a}$  to -g as a.a. $CD8^+$  -a to -g respectively, based on their a.a. features. (H) UMAP showing the clonal expansion of  $CD8^+$  T cells from CITE-seq data (n = 10). Clonal expansion is determined by the total number of cells sharing the same clonotype. (I) Left: Clonal expansion of  $CD3^+$  T cells, in livers and paired blood (liver CITE-seq: n = 3; paired blood CITE-seq: n = 3). The X-axis and Y-axis represent liver and blood clones, respectively, with clone counts  $\geq 70$  truncated to 70 for visualization. Right: UMAP of  $CD8^+$  T cells highlighting highly abundant clones (frequency  $\geq 31$ ) shared between liver and blood (top), and liver-specific clones (bottom). (J) Migration and residency scores for all  $CD8^+$  T-cell subclusters (CITE-seq: n = 10; snRNA-seq: n = 6). (K) Representative flow cytometry plots showing the expression of indicated markers on memory  $CD8^+$  T cells in AIH liver. The gating strategy for memory  $CD8^+$  T cells is shown in Fig. S4F. (L) Left: Representative flow cytometry plots showing *TNF* and *IFN- $\gamma$*  expression patterns in the indicated  $CD8^+$  T-cell populations.  $CD45RO^+$   $CD8^+$  T cells were pre-gated on TCR $\alpha\beta^+$  TCRV $\alpha$ 24-J $\alpha$ 18<sup>-</sup> live, singlet lymphocytes. *TNF* and *IFN- $\gamma$*  detection were performed after *in vitro* stimulation. Middle: Representative histogram showing the MFI distribution of *TNF* and *IFN- $\gamma$*  across the indicated  $CD8^+$  T-cell populations. Left and middle panels represent images from the same donor. Right: MFI quantification across five AIH donors. Each dot represents a single donor, with MFI levels of different populations from the same donor connected by lines. Grey lines represent mean values. Statistical differences are determined by repeated measures one-way ANOVA, Tukey's multiple comparisons test. Panels (A-D) and (G-J) were based on the AIH atlas, whereas panels (E,F,K,L) were based on the FACS dataset. Donors included in the FACS dataset represent an independent cohort. AIH, autoimmune hepatitis; CITE-seq, cellular indexing of transcriptomes and epitopes by sequencing; MFI, mean fluorescence intensity; snRNA-seq, single-nucleus RNA sequencing;  $T_{EM}$ , effector memory T cell;  $T_{FH}$ , T follicular helper cell;  $T_{R1}$ , type 1 regulatory T cell;  $T_{RM}$ , tissue-resident memory T cell; UMAP, uniform manifold approximation and projection.

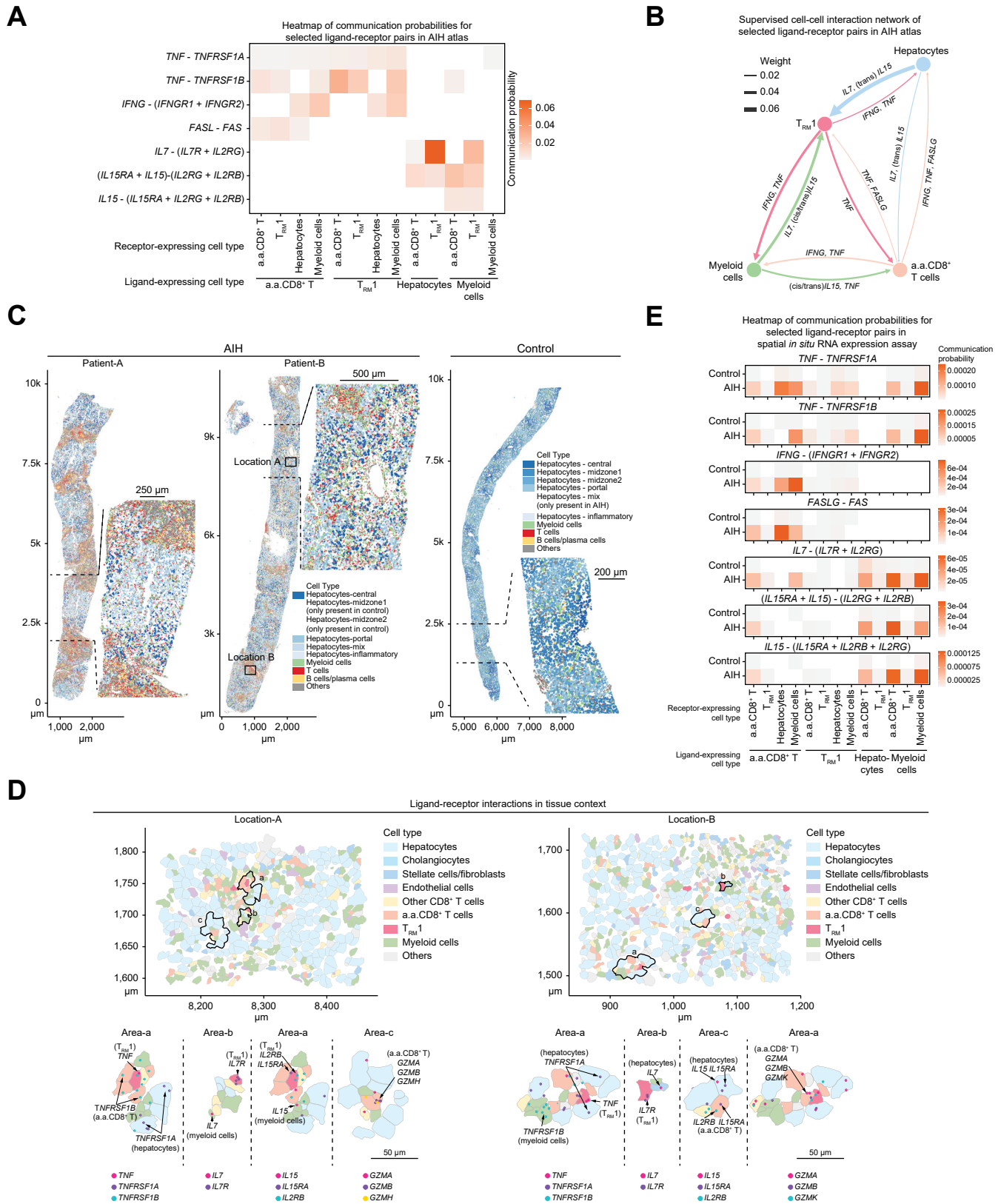


**Fig. 4.** Single cell-resolution spatially resolved interactome depicting interactions among T<sub>RM1</sub>, a.a.CD8<sup>+</sup> T cells, myeloid cells, and hepatocytes in the livers of patients with AIH. (A) Heatmap showing the significant (*p* adjusted <0.05, one-sided permutation test) communication probability values by CellChat of selected ligand-receptor pairs and the interacting cell types, based on gene expression from the AIH atlas. (B) Supervised interaction network of indicated players and selected ligands, based on data from (A). Cytokines of source cell type (line color) are labeled. Weight equals the sum of communication probability. (C) Representative spatial

a.a.CD8<sup>+</sup> T cells and myeloid cells. As controls, we included hepatocytes without TNF receptor expression in close proximity to TNF-secreting cells. Consistent with the AIH atlas analysis, both *ICAM1* and *CDH1* mRNA were highly expressed in hepatocytes, presumably reflecting their response to TNF (Fig. 5H and S8A). Our findings suggest a potential mechanism of TNF action on hepatocytes, involving the upregulation of adhesion molecules, including ICAM1, to induce a.a.CD8<sup>+</sup> T cell/T<sub>RM</sub>1-mediated cytotoxicity in the AIH liver.

In summary, our data revealed a molecular and cellular network that could contribute to the pathogenesis of AIH. While myeloid and hepatocyte-derived IL-7 and IL-15 may have accounted for the accumulation of T cells in the liver, the cytokine TNF, which can derive from liver T<sub>RM</sub>1 cells, enhanced the cytotoxic activity of a.a.CD8<sup>+</sup> T cells by upregulating adhesion molecules on hepatocyte targets.

### Anti-TNF treatment with infliximab in patients with newly diagnosed AIH

In parallel, we investigated one of the suspected key nodes of AIH pathogenesis, TNF, as a therapeutic target in a phase IIa, proof-of-concept trial testing infliximab (IFX) as an alternative to conventional corticosteroid induction therapy for a distinct cohort of patients with newly diagnosed AIH (Trial Registration: EudraCT No. 2017-003311-19). In total, 12 patients were enrolled in the trial, nine of whom could be analyzed (Fig. 6B). The primary endpoint – defined as complete biochemical remission (*i.e.* normalization of ALT, AST and IgG) after 24 weeks (6 months) of treatment with IFX was reached by 2/12 patients (17%, Fig. 6A). Nine patients were included in the final analysis cohort ( $n = 8$  who completed all scheduled infusions and  $n = 1$  who received 6/8 doses). 9/9 patients (100%) exhibited transaminases  $\leq 2x$  the upper limit of normal after 6 months of treatment. IFX significantly decreased ALT and AST levels by 92.7% and 65.5%, respectively, after six months (Fig. 6C,D, percentages/ $p$  values based on the linear mixed-effects model analyses [ $n = 12$ ],  $p < 0.0001$  for reductions of ALT and AST; see Table S2 for observed relative reductions of the final analysis cohort [ $n = 9$ ]). Complete normalization of AST and ALT was achieved in 6/9 and 5/9 patients (67% and 56%), respectively.

Trial outcomes were compared with standard-of-care corticosteroid induction therapy for AIH using prospectively collected data from 24 patients in the R-LIVER registry,<sup>9</sup> treated at the same center. Propensity score matching was applied to the baseline covariates age, ALT, mHAI, IgG and bilirubin, with sex and histologically confirmed advanced fibrosis or cirrhosis (F3-4) specified as exact-matching variables. Detailed baseline characteristics are outlined in Table 1. Further analysis revealed no significant differences regarding ALT reduction between the treatment groups ( $p$  for interaction group  $\times$  time point [ $p_{\text{group}\times\text{time}}$ ] = 0.68, Fig. 6E). The rate of

complete normalization of serum transaminases was similar in both cohorts (12/24 patients [50%] in the SoC cohort vs. 5/9 patients [56%] in the IFX cohort,  $p = 1.0$ , Fig. 6E and S9A). IgG normalization was observed more frequently in the SoC cohort (18/24 patients [75%] vs. 3/9 patients [30%] receiving IFX in the clinical trial,  $p = 0.04$ , Fig. 6F), though IgG reduction did not differ significantly between groups ( $[p_{\text{group}\times\text{time}}] = 0.051$ ). The composite endpoint of normalized AST, ALT and IgG after 6 months was achieved in 10/24 patients (41.7%) in the SoC cohort and 2/12 patients (17%) in the cohort receiving IFX ( $p = 0.26$ ).

Liver stiffness measurement by transient elastography reflects inflammation and fibrosis in AIH.<sup>36</sup> The impact of IFX treatment on liver stiffness was hence evaluated as a secondary endpoint (Fig. 6G). After 6 months, IFX led to a significant reduction of liver stiffness by 7.1 kPa on average in the linear mixed-effects model ( $p = 0.002$ ). In the control cohort receiving SoC, available data from 13 patients with measurements at both time points revealed a mean reduction of 5.2 kPa ( $p = 0.005$ ). The linear mixed-effects model revealed no significant differences between groups with regard to liver stiffness ( $p_{\text{group}\times\text{time}} = 0.46$ ).

Given the considerable known side effects associated with the current steroid-based standard induction therapy,<sup>4–7</sup> the clinical trial assessed both weight/BMI, as well as reports of the patients' HRQoL. Changes in BMI did not differ significantly between groups ( $p_{\text{group}\times\text{time}} = 0.52$ , Fig. 6H). Detailed information on primary and secondary outcome measures, as well as on further laboratory findings, is provided in Table S2. At month 6, minor improvements in the mean difference from baseline were observed in the majority of subcategories of the SF-36 health survey (see Fig. S9B and Table S3 for detailed information on HRQoL collected within the clinical trial).

During the 6-month treatment phase with IFX (Fig. 6A), a total of 37 AEs of any kind were reported. All AEs were classified as mild or moderate. All AEs for which a possible relationship to study participation could not be excluded had resolved by the end of the observation period. With 9 out of 37 AEs (24%), gastrointestinal symptoms (such as heartburn/abdominal pain, nausea, vomiting) were the most frequently observed events. Two patients experienced serious AEs, both assessed as of questionable relation to the trial treatment: one patient was admitted to the emergency room for symptoms of marked arthralgia 24 h after their second dose of IFX associated with a mild acute upper respiratory tract viral infection not requiring hospitalization. This patient, whose ALT levels had already fallen by >60% compared to baseline, subsequently withdrew study consent. The second patient developed two consecutive episodes of febrile pyelonephritis after 6 out of 8 planned IFX doses and received inpatient antibiotic treatment. The patient had already achieved complete biochemical remission at the onset of the SAE, so further administration of the study drug was deemed inappropriate in this

distribution of cells from two active AIH livers and one control liver, color-coded by cell type (myeloid cells: macrophages, monocytes, Kupffer cells, granulocytes and dendritic cells; T cells: CD4<sup>+</sup> and CD8<sup>+</sup> T cells). Magnified views provide detailed depictions of cellular distributions. (D) Zoomed-in views of the spatial distribution of cells from the two areas indicated in (C). Below: magnified spatial distribution of cells, with selected ligand and receptor RNA expression overlaid. (E) Heatmap showing the significant ( $p$  adjusted  $< 0.05$ , one-sided permutation test) communication probability values by CellChat of selected ligand-receptor pairs and the interacting cell types at distances up to 50  $\mu\text{m}$ , based on *spatial in situ* RNA expression dataset. Donors included in the *spatial in situ* RNA expression dataset represent an independent cohort. AIH, autoimmune hepatitis; a.a.CD8<sup>+</sup>, auto-aggressive CD8<sup>+</sup> T cell; T<sub>RM</sub>1, tissue resident-like type 1 memory cell.

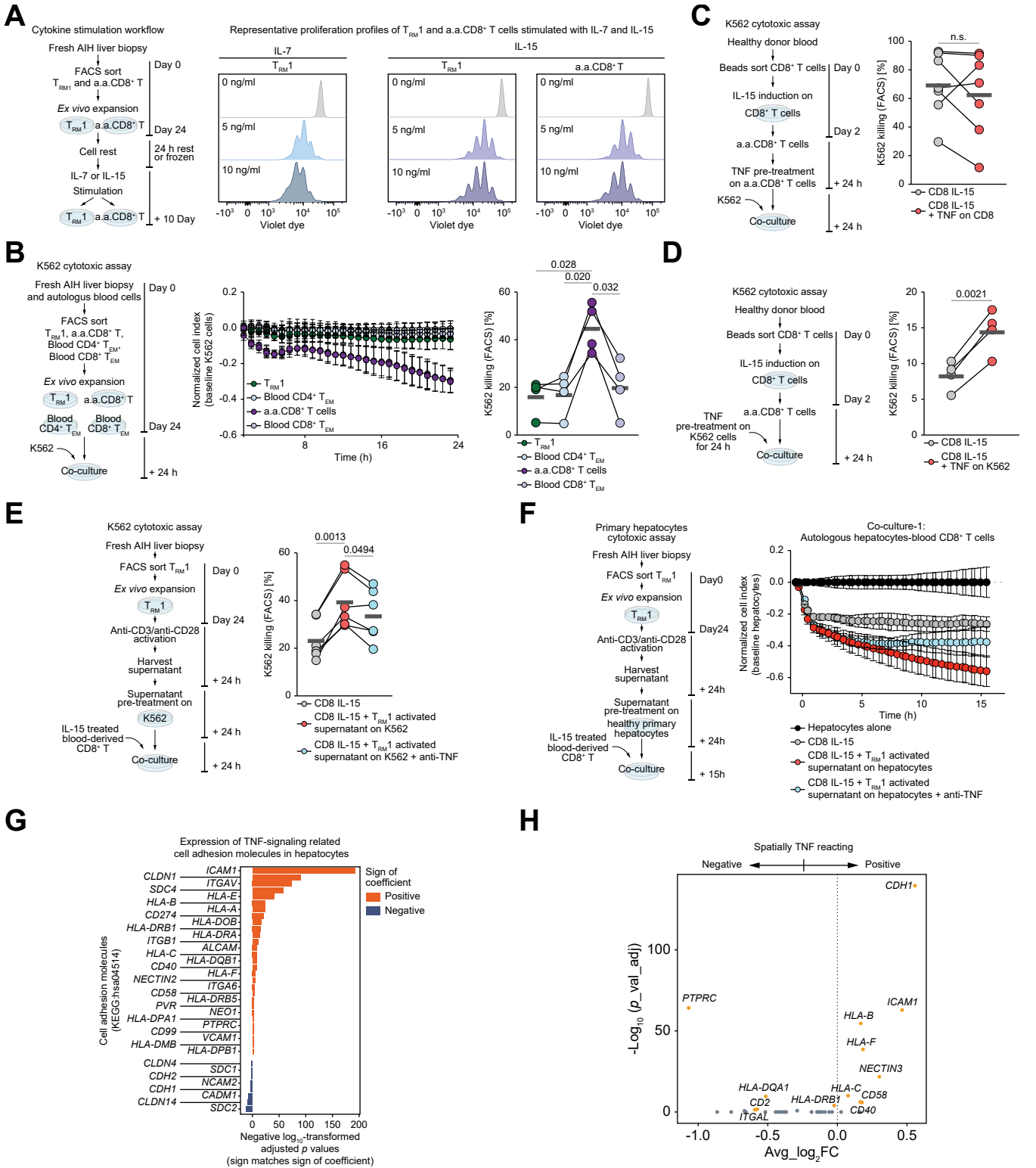


**Fig. 5.  $T_{RM1}$ -derived TNF licenses the killing capacity of a.a.CD8<sup>+</sup> T cells.** (A) Left: Schematic representation of the cytokine stimulation workflow. Right: Representative CellTrace Violet histograms showing proliferation of AIH liver-derived  $T_{RM1}$  and a.a.CD8<sup>+</sup> T cells in response to IL-7 and IL-15 stimulation. (B) Left: Schematic representation of the K562 cytotoxicity assay. Middle: Real-time cell impedance analyses performed over 24 h showing auto-aggressive activity of AIH liver-derived a.a.CD8<sup>+</sup> T cells,  $T_{RM1}$  cells, and paired blood CD4<sup>+</sup>  $T_{EM}$  and CD8<sup>+</sup>  $T_{EM}$  cells against K562 target cells (AIH patient, n = 1). Cytotoxicity was assessed in the absence of external stimulation and quantified using xCELLigence. Each dot represents the mean of triplicates for the indicated condition at the specified time point, with bars indicating the standard deviation. Right: Auto-aggressive activity of AIH liver-derived a.a.CD8<sup>+</sup> T cells,  $T_{RM1}$  cells, and paired blood CD4<sup>+</sup>  $T_{EM}$  and CD8<sup>+</sup>  $T_{EM}$  cells against K562 target cells (AIH patients, n = 4). Cytotoxicity was quantified using flow cytometry. Each dot represents a single donor. Grey lines represent mean values. Significant differences are determined by repeated measures one-way ANOVA, Tukey's multiple comparisons test. (C) Left: Schematic

circumstance. Having already received 75% of the planned doses, the patient was included in the endpoint analyses. Two patients were prematurely excluded from further study participation after one and two doses, respectively, as they fulfilled the definition of insufficient response by the very strict safety rules of the phase IIa trial protocol (requiring premature study discontinuation in case of an increase in transaminases >20% over baseline within the first 4 weeks of treatment). They also received steroid-based rescue therapy.

In summary, this trial demonstrates the efficacy of the anti-TNF antibody infliximab as a steroid-free therapy in newly diagnosed AIH, confirming TNF as a key node of the pathogenic AIH immune network.

## Discussion

We provide a description of a comprehensive and cohesive cellular and molecular network which might be responsible for the thus far elusive pathogenesis of AIH. In addition, this data set can be used as a resource for the identification of new targets for immunotherapeutic interventions in AIH. To obtain this resource, we integrated several mutually corroborating omics techniques, computational modelling, and functional assays from distinct cohorts of patients with AIH. Unsupervised analysis identified several cytokines associated with type I immune responses, particularly TNF, IL-12, and IFN- $\gamma$ , and their downstream signaling pathways (RELA, NF- $\kappa$ B, JAK-STAT), correlating with the degree of liver inflammation and damage (Fig. 1). This finding is in line with previous reports of elevated plasma levels of cytokines in patients with AIH,<sup>37,38</sup> in particular of TNF, IL-12, and IFN- $\gamma$ , which decline in disease remission.<sup>37</sup> We generated a comprehensive single-cell atlas (Fig. 2), profiling immune and non-immune cell populations, *i.e.* CD4<sup>+</sup> T cells, CD8<sup>+</sup> T cells, myeloid cells, hepatocytes and cholangiocytes. This AIH atlas is in alignment with published reports of healthy and diseased human livers in representing the major cell types and typical organ features like zonation,<sup>26,39,40</sup> but in addition, it

establishes a unique representation of AIH-specific liver cell characteristics.

The AIH atlas confirmed our previous observation of an abundance of TNF-producing Th1 cells in AIH livers,<sup>19</sup> but also suggested a critical role of liver-resident CD4<sup>+</sup> T<sub>RM</sub>1 cells as producers of TNF (Fig. 3). These hepatic T<sub>RM</sub>1 cells matched a previously described phenotype.<sup>18</sup> The presence of T<sub>RM</sub>1 cells is not unique to AIH, as these cells have also been detected in livers with less inflammatory activity, albeit at lower abundance. The TNF-producing T<sub>RM</sub>1 cells were clonally expanded in the livers of patients with AIH. However, the identification of the specific activating antigens requires further investigation. Autoreactive CD4<sup>+</sup> T cells have previously been identified in the blood of anti-SLA/LP auto-antibody-positive patients with AIH.<sup>16,17,41</sup> These autoreactive T cells mainly seemed to represent IL21-positive T<sub>FH</sub> cells. Our study did not assess TCR specificity, limiting direct comparison with these findings. However, liver T<sub>FH</sub> cells in our dataset are characterized by *PDCD1*, *CTLA4*, *TIGIT*, and *ICOS*, as well as by *TOX2*, *NR3C1*, and *MAF* genes, markers that were previously described for autoreactive CD4<sup>+</sup> T cells.<sup>16,17</sup> This suggests a potential link between what we identified here as liver T<sub>FH</sub> and blood autoreactive CD4<sup>+</sup> T cells and calls for further investigation in this regard.

Our AIH atlas also revealed a substantial clonal expansion of CD8<sup>+</sup> T cells in AIH livers. This cell population appears to be heterogeneous, with some of the clusters exhibiting a T<sub>RM</sub> signature and partially exclusive clonal representation in the liver (Fig. 3). Note that a CD8<sup>+</sup> T-cell population with similar memory and residency markers was found to be significantly increased in the livers of patients with AIH, strongly correlating with disease severity.<sup>20</sup> Intriguingly, our atlas revealed that this population displays an a.a. state (Fig. 3) and function, including cytotoxicity independent of TCR-stimulation (Fig. 5). This is consistent with the recent report indicating a pathogenic role of a.a.CD8<sup>+</sup> T cells in MASH,<sup>21</sup> suggesting that a.a.CD8<sup>+</sup> T cells might be of pathogenic relevance in different liver diseases.

representation of the K562 cytotoxicity assay. Right: Auto-aggressive activity of IL-15-treated blood CD8<sup>+</sup> T cells (*i.e.* CD8 IL-15) pre-treated without or with TNF, against K562 target cells. Cytotoxicity was quantified by flow cytometry. Blood CD8<sup>+</sup> T cells were derived from healthy donors (n = 7). Each dot represents a single donor. Grey lines represent mean values. Statistical difference is determined by paired t-test. (D) Left: Schematic representation of the K562 cytotoxicity assay. Right: Auto-aggressive activity of IL-15-treated blood CD8<sup>+</sup> T cells against K562 cells pre-treated without or with TNF. Cytotoxicity was quantified by flow cytometry. Blood CD8<sup>+</sup> T cells were derived from healthy donors (n = 4). Each dot represents a single donor. Grey lines represent mean values. Significant difference is determined by paired t-test. (E) Left: Schematic representation of the K562 cytotoxicity assay. Right: Auto-aggressive activity of IL-15-treated blood CD8<sup>+</sup> T cells against K562 target cells (grey), K562 cells pre-treated with supernatant from anti-CD3/anti-CD28 activated T<sub>RM</sub>1 cells, in the absence (red) or presence (blue) of anti-TNF. Cytotoxicity was quantified by flow cytometry. Blood CD8<sup>+</sup> T cells were derived from healthy donors (n = 6) and T<sub>RM</sub>1 cells were derived from AIH livers (n = 4). Supernatant from T<sub>RM</sub>1 cells from two AIH donors was cultured with CD8<sup>+</sup> T cells from one healthy donor each. Supernatant from T<sub>RM</sub>1 cells from two additional AIH donors was cultured with CD8<sup>+</sup> T cells from two healthy donors each, resulting in a total of six independent measurements. Each dot represents a co-culture condition. Grey lines represent mean values. Significant differences are determined by repeated measures one-way ANOVA, Tukey's multiple comparisons test. (F) Left: Schematic representation of human primary hepatocyte cytotoxicity assay. Right: Real-time cell impedance analysis over 15 h showing auto-aggressive activity of autologous blood CD8<sup>+</sup> T cells against primary human hepatocytes under the indicated conditions. Hepatocytes were co-cultured with CD8<sup>+</sup> T cells (grey), or pre-treated with supernatant from anti-CD3/anti-CD28-activated T<sub>RM</sub>1 cells in the absence (red) or presence of anti-TNF (blue). Baseline hepatocytes are shown in black. Auto-aggression was assessed by hepatocyte viability and quantified using xCELLigence. Primary hepatocytes and autologous blood CD8<sup>+</sup> T cells were obtained from one healthy donor, and T<sub>RM</sub>1 cells were isolated from the liver of one AIH donor. Each dot represents the mean of triplicates for the indicated condition at the specified time point, with bars indicating the standard deviation. (G) TNF signaling pathway score (see Fig. S7I), based on the AIH atlas, indicating the expression of cell adhesion molecules (KEGG:hsa04514) in hepatocytes using a hurdle regression model. Depicted are significant ( $p < 0.05$ ) negative  $\log_{10}$ -transformed  $p$  values multiplied by the sign of the coefficient. (H) Volcano plot of spatial *in situ* RNA expression data showing differentially expressed cell adhesion genes between TNF receptor positive and negative cells within 20  $\mu$ m of TNF-producing cells. TNF receptor-positive cells are defined by the expression of either *TNFRSF1A* or *TNFRSF1B*. Cells used in panels (A-E) derived from the same donors as the FACS dataset in Fig. 3. The gating strategies for T<sub>RM</sub>1 and a.a.CD8<sup>+</sup> T cells are described in Fig. S4F followed by Fig. 3E and K, respectively. Paired blood CD4<sup>+</sup> and CD8<sup>+</sup> T<sub>EM</sub> cells were identified using the same gating strategies described in Fig. S4F for CD4<sup>+</sup> and CD8<sup>+</sup> memory subsets, respectively. AIH, autoimmune hepatitis; a.a.CD8<sup>+</sup>, auto-aggressive CD8<sup>+</sup>; MFI, mean fluorescence intensity; T<sub>EM</sub>, effector memory T cell; T<sub>RM</sub>1, tissue resident-like type 1 memory cell.

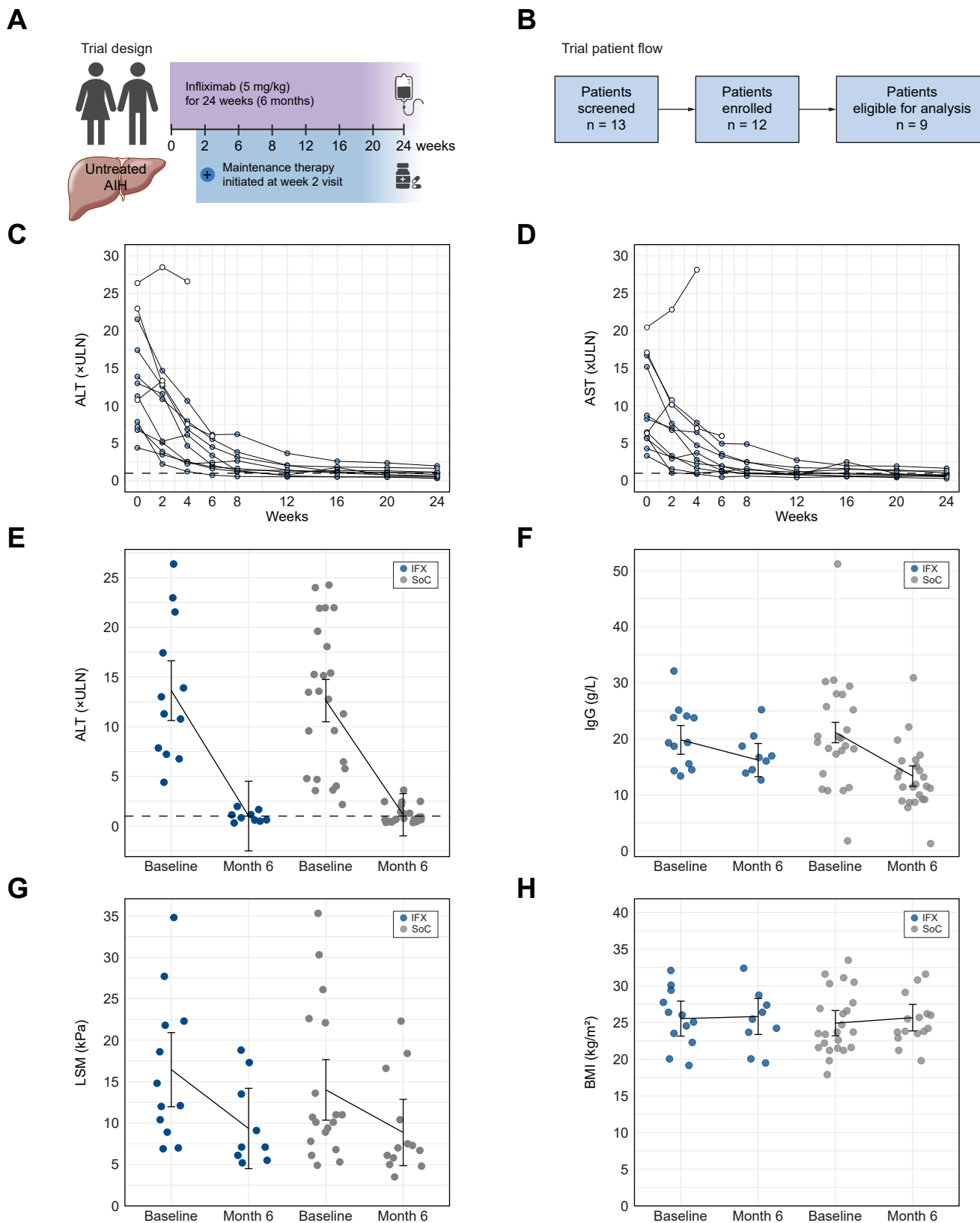


**Fig. 6. Steroid-free treatment with infliximab ameliorates hepatic inflammation in patients with previously untreated AIH.** (A) Trial design (AIH-MAB): n = 12 patients were enrolled to receive infliximab (5 mg/kg) for 24 weeks and were started on maintenance therapy commencing after the week 2 visit. (B) Patient flow within AIH-MAB. (C,D) Individual ALT (C) and AST (D) levels (xULN) over the course of the 24-week experimental treatment. Light circles depict patients who were excluded from the primary analysis (n = 3). (E,F) Comparison of ALT (xULN, (E)) and IgG (g/L, (F)) between baseline and month 6 in patients receiving IFX (individual values shown as purple dots, n = 12) or standard care (n = 24, orange dots). (G,H) Comparison of liver stiffness (kPa, (G)) and BMI (kg/m<sup>2</sup>, (H)) between baseline and month 6,

**Table 1. Baseline patient characteristics of the AIH-MAB cohort receiving IFX (n = 12) and the matched prospective control cohort receiving SoC (n = 24).**

	IFX (n = 12)	SoC (n = 24)	SMD
Female, n (%)	9 (75)	18 (75)	0
Age at diagnosis, years	36 (18-63)	41 (22-62)	-0.205
mHAI	9 (5-15)	10 (4-14)	-0.124
Simplified AIH score	7 (5-8)	7 (4-7)	0.383
Advanced fibrosis/cirrhosis, n (%)	3 (25)	6 (25)	0
Liver stiffness (kPa)	13.5 (6.9-34.8)	10.4 (4.9-35.3) <sup>1</sup>	0.271
BMI (kg/m <sup>2</sup> )	25.6 (19.2-32.1)	23.7 (17.9-33.5) <sup>2</sup>	0.150
ALT xULN	12.15 (4.40-26.37)	13.11 (2.16-24.26)	-0.140
AST xULN	7.36 (3.32-20.46)	16.49 (4.26-28.46)	-0.961
IgG (g/L)	19.3 (13.4-32.1)	19.8 (1.81-51.2)	-0.059
GGT (U/L)	120 (41-331)	146 (50-422)	-0.287
ALP (U/L)	131 (67-343)	130 (59-396)	0.026
Total bilirubin (mg/dl)	1.1 (0.5-4.7)	1.2 (0.4-3.0)	-0.025
Albumin (g/dl)	36.6 (32.2-41.7) <sup>3</sup>	37.0 (25.6-46.1) <sup>4</sup>	-0.119
INR	1.1 (1.0-1.1) <sup>5</sup>	1.1 (0.9-1.5)	-0.576
ANA, n (%) <sup>6</sup>	12 (100)	21 (88)	0.534
SMA, n (%) <sup>6</sup>	7 (58)	10 (42)	0.338
LKM, n (%)	1 (8)	0	0.426
SLA/LP, n (%)	0 (0)	1 (4)	-0.295

Continuous variables = medians (range).

Group comparisons = SMD.

AIH, autoimmune hepatitis; ALP, alkaline phosphatase; ALT, alanine aminotransferase; ANA, antinuclear antibodies; AST, aspartate aminotransferase; GGT, gamma-glutamyl transferase; IFT, immunofluorescence testing; IFX, infliximab; INR, international normalized ratio; LKM, liver kidney microsomal antibodies; mHAI, modified histology activity index; SLA/LP, soluble liver antigen/liver pancreas antibodies; SMA, smooth muscle antibodies; SMD, standardized mean difference; SoC, standard of care; ULN, upper limit of normal.

<sup>1</sup>Data available for 18 patients.

<sup>2</sup>Data available for 23 patients.

<sup>3</sup>Data available for 9 patients.

<sup>4</sup>Data available for 22 patients.

<sup>5</sup>Data available for 10 patients.

<sup>6</sup>Considered positive if IFT  $\geq 1:160$ .

Our data do not exclude a role for antigen-specific CD4<sup>+</sup> and CD8<sup>+</sup> T cells. Notably, we observed upregulation of MHC I and II molecules in hepatocytes, potentially in response to TNF stimulation. Thus, a conceivable hypothesis is that self-reactive T cells represent the initial triggers and effectors of the inflammatory reaction in AIH, and that, once the immune response is established, MHC-independent CD8<sup>+</sup> T-cell-mediated killing could further escalate the response. Further efforts are needed to dissect the relationship between self-reactive, non-self-reactive and a.a. T cells in the pathogenesis of AIH.

Having found clonal expansion of both T<sub>RM</sub>1 and a.a.CD8<sup>+</sup> T cells in the liver of patients with AIH, we searched for potential drivers of this expansion. IL-7 has been shown to promote the proliferation of naive and T<sub>EM</sub> cells.<sup>42</sup> Consistent with this, our computational modelling identified interactions between hepatocytes and myeloid cells with T<sub>RM</sub>1 cells via IL-7 and IL-7R. Furthermore, *in vitro* functional validation demonstrated that AIH liver-derived T<sub>RM</sub>1 cells can proliferate in response to IL-7 in a dose-dependent manner (Fig. 5). Similarly, IL-15, also mainly produced by myeloid cells and hepatocytes, could drive the proliferation of AIH liver-derived T<sub>RM</sub>1 and a.a.CD8<sup>+</sup> T cells in a dose-dependent manner (Fig. 5). However, proliferation occurs only after 4 days of *in vitro* stimulation, consistent with the observation that short-term IL-15 stimulation induces an a.a. phenotype, while long-term

stimulation promotes proliferation.<sup>21,43,44</sup> Hepatocytes seemed to actively participate in AIH pathogenesis, not only by producing IL-7 and IL-15, but also by upregulating *IL32* expression, which has been shown to induce TNF expression in human monocytic cells,<sup>45</sup> suggesting that hepatocytes are not just passive victims in AIH.

At least to a certain extent, the inflammatory and activated phenotype of hepatocytes seemed to be induced by TNF derived from expanded CD4<sup>+</sup> T<sub>RM</sub>1 cells in livers of patients with AIH, as inferred from interactome analysis and confirmed by spatial Xenium analysis (Fig. 4). While TNF signaling is linked to both hepatocyte proliferation and apoptosis,<sup>46,47</sup> we also observed upregulation of integrins, such as *ICAM1*, *ITGAV* and *ITGB1*, in hepatocytes that appeared to exhibit active TNF signaling (Fig. 5). This observation correlates well with data showing that TNF exposure upregulates *ICAM1* in mouse hepatocytes and human vascular epithelial cells.<sup>21,35</sup> Moreover, our *in vitro* study showed that pre-treatment of target cells with TNF enhanced the killing capacity of a.a.CD8<sup>+</sup> T cells. Considering this and previous published data in mouse models,<sup>21</sup> we speculate that this effect was due to the enhanced expression of *ICAM1*, which increased the contact between hepatocytes and a.a.CD8<sup>+</sup> T cells, resulting in increased hepatocyte killing. These data also affirm the idea that hepatocytes not only serve as the primary targets of the immune-mediated damage, but also play an active role in

separated by treatment (IFX vs. SoC). Black lines and error bars indicate respective EMMs and their respective 95% CIs of the linear mixed-effects model analyses. AIH, autoimmune hepatitis; ALT, alanine aminotransferase; AST, aspartate aminotransferase; EMMs, estimated marginal means; IFX, infliximab; SoC, standard of care; xULN, times the upper limit of normal.

sustaining the immune response by responding to immunological insults. Accordingly, hepatocytes upregulated the expression of MHC II molecules enabling them to interact with CD4<sup>+</sup> T cells, in particular with TNF-producing T<sub>RM</sub>1 cells.

In addition to identifying TNF as a central node in the AIH inflammatory network, we conducted a phase IIa clinical study targeting TNF with the anti-TNF antibody IFX, which proved effective in ameliorating hepatic injury (Fig. 6), further adding to the validity of our analysis. More significantly, this trial marks the first demonstration that steroid-free induction therapy for acute AIH is both viable and achievable. While not all patients responded rapidly to IFX, the overall response rate was high, as indicated by the clear reduction of transaminases and the similar rate of transaminase normalization at month 6, compared to the SoC control group. This proof-of-concept clinical trial naturally has limitations. Firstly, it was performed in a small number of patients. To address that limitation, we have applied the linear mixed-effects model, which provides a conservative and statistically appropriate framework for small, incomplete longitudinal datasets such as ours. Secondly, despite thorough matching for various parameters that might have influenced the therapeutic response,<sup>48</sup> this was not a randomized blinded trial and thus its efficacy as an alternative standard therapy requires further validation. As this trial was not focused on safety outcomes, the cohort size was not sufficient to detect rare AEs such as IFX-induced liver injury. However, existing data indicate that IFX-associated hepatotoxicity is uncommon, usually mild and reversible after treatment discontinuation,<sup>49</sup> and safety concerns regarding IFX in the context of AIH have not been reported so far.<sup>50,51</sup> Nevertheless, larger controlled studies will be required to confirm the safety profile of IFX in AIH. In large cohort studies on the treatment of chronic inflammatory bowel disease, long-term comparisons of corticosteroids with anti-TNF therapies

revealed an increased mortality rate and reduced quality of life in the steroid group.<sup>52,53</sup> These findings underscore the need to further explore corticosteroid-free treatment strategies for AIH.

This very cautiously designed trial protocol may even have underestimated the strength of the treatment effect. Firstly, the two patients excluded early in the trial who did not respond rapidly to the treatment may have required more time for the immune intervention to take effect. To handle delayed responses, adding a short-term steroid treatment in combination with IFX (as is routine in other applications like inflammatory bowel disease) might be a feasible solution in respective cases without lasting untoward effects. Secondly, in line with the current consensus on a complete biochemical remission, the primary endpoint was complete normalization of both transaminases and IgG after six months. However, this definition of remission is controversial, and it remains unclear whether normalization of IgG is of any prognostic significance. Indeed, recent studies indicated that only elevated aminotransferases, but not IgG, were associated with impaired prognosis,<sup>48,54</sup> which further underscores the relevance of the transaminase reduction observed in the present trial. Our results are an encouraging signal for patients affected by AIH, particularly for those with relative contraindications (such as diabetes or established osteoporosis) to corticosteroid therapy.

Overall, these computational, experimental and clinical data reveal the pathogenic AIH network at a hitherto unprecedented depth, providing a resource for the identification of therapeutic targets in AIH. Although we focused on TNF here, which we identified as a major node in the AIH network, additional potential drug targets may be derived from this dataset. After decades of solely steroid-based induction therapy, these data may usher in a new era of immunotherapy in AIH.

### Affiliations

<sup>1</sup>Hamburg Center for Translational Immunology (HCTI), University Medical Center Hamburg-Eppendorf (UKE), Hamburg, Germany; <sup>2</sup>I. Department of Medicine, University Medical Center Hamburg-Eppendorf (UKE), Hamburg, Germany; <sup>3</sup>Institute for Inflammation and Carcinogenesis, University Medical Center Hamburg-Eppendorf (UKE), Hamburg, Germany; <sup>4</sup>Center for Biomedical AI (bAlome), University Medical Center Hamburg-Eppendorf (UKE), Hamburg, Germany; <sup>5</sup>Institute of Molecular Immunology and Experimental Oncology, School of Medicine, Technical University of Munich (TUM), Munich, Germany; <sup>6</sup>II. Department of Medicine, University Medical Center Hamburg-Eppendorf (UKE), Hamburg, Germany; <sup>7</sup>Max Delbrück Center for Molecular Medicine in the Helmholtz Association (MDC), Berlin, Germany; <sup>8</sup>Institute of Medical Biometry and Epidemiology, University Medical Center Hamburg-Eppendorf (UKE), Hamburg, Germany; <sup>9</sup>Departamento de Biología, Facultad de Ciencias, Universidad de Chile, Santiago, Chile; <sup>10</sup>Faculty of Medicine, Universidad de los Andes, Chile; <sup>11</sup>Centro Científico y Tecnológico de Excelencia Ciencia & Vida, Fundación Ciencia & Vida, Santiago, Chile; <sup>12</sup>Facultad de Medicina, Universidad de Chile, Santiago, Chile; <sup>13</sup>Institute of Pathology, University Medical Center Hamburg-Eppendorf (UKE), Hamburg, Germany; <sup>14</sup>Institute of Medical Systems Bioinformatics, Center for Molecular Neurobiology (ZMNH), University Medical Center Hamburg-Eppendorf (UKE), Hamburg, Germany; <sup>15</sup>III. Department of Medicine, University Medical Center Hamburg-Eppendorf (UKE), Hamburg, Germany; <sup>16</sup>Institute for Immunology, University Medical Center Hamburg-Eppendorf (UKE), Hamburg, Germany; <sup>17</sup>Department of General, Visceral and Thoracic Surgery, University Medical Center Hamburg-Eppendorf (UKE), Hamburg, Germany; <sup>18</sup>Department of Clinical Medicine, Aarhus University, Denmark; <sup>19</sup>Department of Pathology, Aarhus University Hospital, Denmark; <sup>20</sup>German Center for Child and Adolescent Health (DZKJ), Partner Site Hamburg, University Medical Center Hamburg-Eppendorf (UKE), Hamburg, Germany; <sup>21</sup>Martin Zeitz Center for Rare Diseases, University Medical Center Hamburg-Eppendorf (UKE), Hamburg, Germany

### Abbreviations

AE, adverse events; AIH, autoimmune hepatitis; ALT, alanine aminotransferase; AST, aspartate aminotransferase; a.a., auto-aggressive; CITE-seq, cellular indexing of transcriptomes and epitopes by sequencing; DEGs, differentially expressed genes; HRQoL, health-related quality of life; IFX, infliximab; MASH, metabolic dysfunction-associated steatohepatitis; mHAL, modified hepatic activity index; PBC, primary biliary cholangitis; scTCR-seq, single-cell T-cell receptor sequencing; snRNA-seq, single-nucleus RNA sequencing; SoC, standard of care; T<sub>CM</sub>, central memory T cell; T<sub>EM</sub>, effector memory T cell; T<sub>REG</sub>, FOXP3<sup>+</sup> regulatory T cell; T<sub>RM</sub>, tissue-resident memory T cell; T<sub>RM</sub>1, tissue resident-like type 1 memory cell.

### Financial support

This study was supported by the German Research Foundation (“Deutsche Forschungsgemeinschaft”) through funding of the collaborative research centers (“Sonderforschungsbereiche”/SFB) CRC 841 and CRC 1700 (project number 530990199). J.P.W. was supported by the German Liver Foundation (“Deutsche Leberstiftung”, project number S0163/10182/2023) and the “iDfellows Hamburg Clinician Scientist Programme” in Infectious Diseases (German Research Foundation, funding code 493624519). C.Ki. was supported by the “iDfellows Hamburg Clinician Scientist Programme” in Infectious Diseases (German Research Foundation, funding code: 493624519). J.Ha. was supported by the German Federal Ministry of Education and Research (project number 01EO2106)

and German Research Foundation (project funding HA 8440/3-1). N.K. and S.B. were funded by CDL FLIGHT of the University of Hamburg and SFBs 1700 and 1192. M.R.B. and S.N. were funded by Centro Ciencia & Vida FB210008 from ANID and Grant from ANID FONDECYT 1230183, and CONICYT/FONDEQUIP EQM220027. C.S. was supported by the Helmut and Hannelore Greve Foundation and the YAEL Foundation.

### Conflicts of interest

Authors declare that they have no conflict of interests. NG reports financial support from F. Hoffmann-La Roche and GSK via UKE. These are outside the submitted work.

Please refer to the accompanying ICMJE disclosure forms for further details.

### Authors' contributions

Yang Xu, Jan Philipp Weltzsch and Christoph Kilian collaboratively conceived, designed and carried out the experiments and clinical trial, analyzed the data, provided critical intellectual input, prepared the figures and wrote the manuscript. Babett Steglich analyzed the Xenium data and supported sequencing data analyses. Alena Laschtowitz and Christian Casar performed bulk sequencing alignment. Hanna Ulrich and Ning Song supported the sequencing data analyses. Gerhard Schön and Antonia Zapf supported statistical analyses. Christina Weiler-Normann, Christoph Schramm and Ansgar Wilhelm Lohse designed and initiated the clinical trial and recruited patients. Malte Wehmeyer recruited patients and assisted in conducting the clinical trial. Ida Schregel provided the matched clinical registry data. Ludwig J. Horst, Silja Steinmann, Johannes Hartl, Marcial Sebode, Adrian Sagebiel and Jonas Wagner recruited participating patients. Michael Dudek and Jonas Fackler performed *in vitro* cytotoxic assays. Joseph Tintelnot performed single-cell sequencing. Laura A. Liebig performed single-nucleus sequencing. Varshi Sivayoganathan and Christian F. Krebs performed and supervised the Xenium spatial *in situ* RNA expression assay. Sören Alexander Weidemann and Jenny Krause collected and provided formalin-fixed paraffin-embedded tissue for analyses. Manuela Kolster performed pSTAT5 detection and supported T-cell *ex vivo* expansion experiments. Jing Lu provided additional support for *ex vivo* expansion experiments. Guido Rattay performed cytokine characterization in the T-cell activation experiments. Mariana V. Roseblatt, Sarah Nuñez, Justine Castañeda, María Rosa Bono, Nico Kaiser, Maria Schwerk, Victor Puelles, Stefan Bonn, Marius Böttcher, Norbert Hübner, Eva Tolosa, Samuel Huber, and Percy A. Knolle provided critical intellectual input for experimental design and manuscript preparation. Johannes Herkel, Lorenz Adlung, Christoph Schramm, Nicola Gagliani and Ansgar Wilhelm Lohse provided critical intellectual input for the experimental design, conceived and designed experiments, acquired funding, supervised the study and wrote the manuscript. All co-authors critically revised the manuscript.

### Data and code availability

The processed Seurat objects will be available on the Research Data Repository of the University of Hamburg (<https://www.fdr.uni-hamburg.de/under the DOI 10.25592/uhhfdm.18135>). Individual-level transcriptomic data and code are available upon reasonable request to the corresponding author.

### Declaration of generative AI and AI-assisted technologies in the writing process

During the writing of the manuscript, the authors used openAI GPT4/4o to proofread some of the sentences.

### Acknowledgements

We thank Madeleine Hamely for performing the final proofreading of the text.

### Supplementary data

Supplementary data to this article can be found online at <https://doi.org/10.1016/j.jhep.2026.02.026>.

### References

Author names in bold designate shared co-first authorship

- [1] Slooter CD, van den Brand FF, Lleo A, et al. Lack of complete biochemical response in autoimmune hepatitis leads to adverse outcome: first report of the IAIGH retrospective registry. *Hepatology* 2024;79:538–550.
- [2] Grønbaek L, Vilstrup H, Jepsen P. Autoimmune hepatitis in Denmark: incidence, prevalence, prognosis, and causes of death. A nationwide registry-based cohort study. *J Hepatol* 2014;60:612–617.
- [3] European Association for the Study of the Liver. EASL Clinical Practice Guidelines on the management of autoimmune hepatitis. *J Hepatol* 2025;83:453–501.
- [4] van den Brand FF, van der Veen KS, Lissenberg-Witte BI, et al. Adverse events related to low dose corticosteroids in autoimmune hepatitis. *Aliment Pharmacol Ther* 2019;50:1120–1126.
- [5] Schmidt C, Stürznickel J, Strahl A, et al. Bone microarchitecture in patients with autoimmune hepatitis. *J Bone Miner Res* 2021;36:1316–1325.
- [6] Lloyd C, Leighton J, Wong LL, et al. Patient priorities in autoimmune hepatitis: the need for better treatments, more education and challenging stigma. *Dig Dis Sci* 2023;68:87–97.
- [7] Schramm C, Wahl I, Weiler-Normann C, et al. Health-related quality of life, depression, and anxiety in patients with autoimmune hepatitis. *J Hepatol* 2014;60:618–624.
- [8] Schmidt T, Schmidt C, Strahl A, et al. A system to determine risk of osteoporosis in patients with autoimmune hepatitis. *Clin Gastroenterol Hepatol* 2020;18:226–233.e3.
- [9] Schregel I, Papp M, Sipeki N, et al. Unmet needs in autoimmune hepatitis: results of the prospective multicentre European Reference Network Registry (R-LIVER). *Liver Int* 2024;44:2687–2699.
- [10] Heneghan MA, Lohse AW. Update in clinical science: autoimmune hepatitis. *J Hepatol* 2025;82:926–937.
- [11] Zhang J, Guo L, Liu M, et al. Receptor-interacting protein kinase 3 mediates macrophage/monocyte activation in autoimmune hepatitis and regulates interleukin-6 production. *United Eur Gastroenterol J* 2018;6:719–728.
- [12] Tsirikoni A, Kyriakou DS, Rigopoulou EI, et al. Markers of cell activation and apoptosis in bone marrow mononuclear cells of patients with autoimmune hepatitis type 1 and primary biliary cirrhosis. *J Hepatol* 2005;42:393–399.
- [13] Zachou K, Rigopoulou EI, Tsirikoni A, et al. Autoimmune hepatitis type 1 and primary biliary cirrhosis have distinct bone marrow cytokine production. *J Autoimmun* 2005;25:283–288.
- [14] de Boer YS, van Gerven NM, Zwiers A, et al. Genome-wide association study identifies variants associated with autoimmune hepatitis type 1. *Gastroenterology* 2014;147:443. 52.e5.
- [15] Kramer M, Mele F, Jovic S, et al. Clonal analysis of SepSecS-specific B and T cells in autoimmune hepatitis. *J Clin Invest* 2025;135:e183776.
- [16] Cardon A, Guinebretière T, Dong C, et al. Single cell profiling of circulating autoreactive CD4 T cells from patients with autoimmune liver diseases suggests tissue imprinting. *Nat Commun* 2025;16:1161.
- [17] Renand A, Cervera-Marzal I, Gil L, et al. Integrative molecular profiling of autoreactive CD4 T cells in autoimmune hepatitis. *J Hepatol* 2020;73:1379–1390.
- [18] Wiggins BG, Pallett LJ, Li X, et al. The human liver microenvironment shapes the homing and function of CD4+ T-cell populations. *Gut* 2022;71:1399–1411.
- [19] Bovensiepen CS, Schakat M, Sebode M, et al. TNF-producing Th1 cells are selectively expanded in liver infiltrates of patients with autoimmune hepatitis. *J Immunol* 2019;203:3148–3156.
- [20] You Z, Li Y, Wang Q, et al. The clinical significance of hepatic CD69+ CD103+ CD8+ resident-memory T cells in autoimmune hepatitis. *Hepatology* 2021;74:847–863.
- [21] Dudek M, Pfister D, Donakonda S, et al. Auto-aggressive CXCR6+ CD8 T cells cause liver immune pathology in NASH. *Nature* 2021;592:444–449.
- [22] Laschtowitz A, Lindberg EL, Liebhoff AM, et al. Liver transcriptome analysis reveals PSC-attributed gene set associated with fibrosis progression. *JHEP Rep* 2024;7:101267.
- [23] Hennes EM, Zeniya M, Czaja AJ, et al. Simplified criteria for the diagnosis of autoimmune hepatitis. *Hepatology* 2008;48:169–176.
- [24] Brucklacher-Waldert V, Steinbach K, Lioznov M, et al. Phenotypical characterization of human Th17 cells unambiguously identified by surface IL-17A expression. *J Immunol* 2009;183:5494–5501.
- [25] Müller-Dott S, Tsvirvoui E, Vazquez M, et al. Expanding the coverage of regulons from high-confidence prior knowledge for accurate estimation of transcription factor activities. *Nucleic Acids Res* 2023;51:10934–10949.
- [26] Aizarani N, Saviano A, Sagar, et al. A human liver cell atlas reveals heterogeneity and epithelial progenitors. *Nature* 2019;572:199–204.
- [27] Andrews TS, Nakib D, Perciani CT, et al. Single-cell, single-nucleus, and spatial transcriptomics characterization of the immunological landscape in the healthy and PSC human liver. *J Hepatol* 2024;80:730–743.
- [28] Segal JM, Kent D, Wesche DJ, et al. Single cell analysis of human foetal liver captures the transcriptional profile of hepatobiliary hybrid progenitors. *Nat Commun* 2019;10:3350.

- [29] Kumar BV, Ma W, Miron M, et al. Human tissue-resident memory T cells are defined by core transcriptional and functional signatures in lymphoid and mucosal sites. *Cell Rep* 2017;20:2921–2934.
- [30] Cheuk S, Schlums H, Gallais S  r  zal I, et al. CD49a expression defines tissue-resident CD8+ T cells poised for cytotoxic function in human skin. *Immunity* 2017;46:287–300.
- [31] Brockmann L, Soukou S, Steglich B, et al. Molecular and functional heterogeneity of IL-10-producing CD4+ T cells. *Nat Commun* 2018;9:5457.
- [32] Baessler A, Vignali DAA. T cell exhaustion. *Annu Rev Immunol* 2024;42:179–206.
- [33] Jin S, Plikus MV, Nie Q. CellChat for systematic analysis of cell-cell communication from single-cell transcriptomics. *Nat Protoc* 2025;20:180–219.
- [34] Cepero-Donates Y, Rakotoarivelo V, Mayhue M, et al. Homeostasis of IL-15 dependent lymphocyte subsets in the liver. *Cytokine* 2016;82:95–101.
- [35] Kim H, Hwang JS, Woo CH, et al. TNF-alpha-induced up-regulation of intercellular adhesion molecule-1 is regulated by a Rac-ROS-dependent cascade in human airway epithelial cells. *Exp Mol Med* 2008;40:167–175.
- [36] Hartl J, Ehlken H, Sebode M, et al. Usefulness of biochemical remission and transient elastography in monitoring disease course in autoimmune hepatitis. *J Hepatol* 2018;68:754–763.
- [37] Schulthei   C, Steinmann S, Willscher E, et al. Immune signatures in variant syndromes of primary biliary cholangitis and autoimmune hepatitis. *Hepatol Commun* 2023;7:e0123.
- [38] Chaouali M, Ben Azaiez M, Tezeghdenti A, et al. High levels of proinflammatory cytokines IL-6, IL-8, TNF-A, IL-23, and IFN- in Tunisian patients with type 1 autoimmune hepatitis. *Eur Cytokine Netw* 2020 Dec;3. <https://doi.org/10.1684/ecn.2020.0450>.
- [39] MacParland SA, Liu JC, Ma XZ, et al. Single cell RNA sequencing of human liver reveals distinct intrahepatic macrophage populations. *Nat Commun* 2018;9:4383.
- [40] Jin C, Jiang P, Zhang Z, et al. Single-cell RNA sequencing reveals the pro-inflammatory roles of liver-resident Th1-like cells in primary biliary cholangitis. *Nat Commun* 2024;15:8690.
- [41] Mix H, Weiler-Normann C, Thimme R, et al. Identification of CD4 T-cell epitopes in soluble liver antigen/liver pancreas autoantigen in autoimmune hepatitis. *Gastroenterology* 2008;135:2107–2118.
- [42] Bielekova B, Muraro PA, Golestaneh L, et al. Preferential expansion of autoreactive T lymphocytes from the memory T-cell pool by IL-7. *J Neuroimmunol* 1999;100:115–123.
- [43] Liu K, Catalfamo M, Li Y, et al. IL-15 mimics T cell receptor crosslinking in the induction of cellular proliferation, gene expression, and cytotoxicity in CD8+ memory T cells. *Proc Natl Acad Sci U S A* 2002;99:6192–6197.
- [44] Alves NL, Hooibrink B, Arosa FA, et al. IL-15 induces antigen-independent expansion and differentiation of human naive CD8+ T cells in vitro. *Blood* 2003;102:2541–2546.
- [45] Kim SH, Han SY, Azam T, et al. Interleukin-32: a cytokine and inducer of TNFalpha. *Immunity* 2005;22:131–142.
- [46] Tiegs G, Horst AK. TNF in the liver: targeting a central player in inflammation. *Semin Immunopathol* 2022;44:445–459.
- [47] Lampi S, Janas MK, Donakonda S, et al. Reduced mitochondrial resilience enables non-canonical induction of apoptosis after TNF receptor signaling in virus-infected hepatocytes. *J Hepatol* 2020;73:1347–1359.
- [48] Plagiannakos CG, Hirschfield GM, Lytvyak E, et al. Treatment response and clinical event-free survival in autoimmune hepatitis: a Canadian multicentre cohort study. *J Hepatol* 2024;81:227–237.
- [49] Bj  rnsson HK, Gudbjornsson B, Bj  rnsson ES. Infliximab-induced liver injury: clinical phenotypes, autoimmunity and the role of corticosteroid treatment. *J Hepatol* 2022;76:86–92.
- [50] Weiler-Normann C, Schramm C, Quaas A, et al. Infliximab as a rescue treatment in difficult-to-treat autoimmune hepatitis. *J Hepatol* 2013;58:529–534.
- [51] Efe C, Lytvyak E, E  kazan T, et al. Efficacy and safety of infliximab in patients with autoimmune hepatitis. *Hepatology* 2025;81:1660–1670.
- [52] Lewis JD, Scott FI, Brensinger CM, et al. Increased mortality rates with prolonged corticosteroid therapy when compared with antitumor necrosis factor-  directed therapy for inflammatory bowel disease. *Am J Gastroenterol* 2018;113:405–417.
- [53] Scott FI, Johnson FR, Bewtra M, et al. Improved quality of life with anti-TNF therapy compared with continued corticosteroid utilization in crohn's disease. *Inflamm Bowel Dis* 2019;25:925–936.
- [54] D  az-Gonz  lez   , Schregel I, Carballo L, et al. Isolated IgG elevation in patients with persistently normal transaminases does not affect the outcome of autoimmune hepatitis. *JHEP Rep* 2025;7:101562.

Keywords: Autoimmune hepatitis; Infliximab; Tissue resident memory T cells; Auto-aggressive CD8+ T cells; TNF; Immune cell network; Single-cell sequencing atlas.

Received 13 May 2025; received in revised form 13 February 2026; accepted 26 February 2026; available online 19 March 2026

## Supplemental information

### **Integrative omics and phase IIa clinical trial identify TNF as key node in autoimmune hepatitis**

**Yang Xu, Jan Philipp Weltzsch, Christoph Kilian, Babett Steglich, Christina Weiler-Normann, Michael Dudek, Jonas Fackler, Malte H. Wehmeyer, Joseph Tintelnot, Laura A. Liebig, Silja Steinmann, Alena Laschtowitz, Ludwig J. Horst, Ida Schregel, Marcial Sebode, Johannes Hartl, Christian Casar, Jing Lu, Gerhard Schön, Antonia Zapf, Maria Rosa Bono, Mariana V. Roseblatt, Sarah Nuñez, Justine Castañeda, Sören Alexander Weidemann, Nico Kaiser, Maria Schwerk, Manuela Kolster, Guido Rattay, Hanna Ulrich, Varshi Sivayoganathan, Ning Song, Jenny Krause, Marius Böttcher, Adrian Sagebiel, Jonas Wagner, Christian F. Krebs, Victor G. Puelles, Norbert Hübner, Eva Tolosa, Stefan Bonn, Samuel Huber, Percy A. Knolle, Johannes Herkel, Lorenz Adlung, Christoph Schramm, Nicola Gagliani, and Ansgar Wilhelm Lohse**

# **Integrative omics and phase IIa clinical trial identify TNF as key node in autoimmune hepatitis**

Yang Xu, Jan Philipp Weltzsch, Christoph Kilian, Babett Steglich, Christina Weiler-Normann, Michael Dudek, Jonas Fackler, Malte H. Wehmeyer, Joseph Tintelnot, Laura A. Liebig, Silja Steinmann, Alena Laschtowitz, Ludwig J. Horst, Ida Schregel, Marcial Sebode, Johannes Hartl, Christian Casar, Jing Lu, Gerhard Schön, Antonia Zapf, Maria Rosa Bono, Mariana V. Roseblatt, Sarah Nuñez, Justine Castañeda, Sören Alexander Weidemann, Nico Kaiser, Maria Schwerk, Manuela Kolster, Guido Rattay, Hanna Ulrich, Varshi Sivayoganathan, Ning Song, Jenny Krause, Marius Böttcher, Adrian Sagebiel, Jonas Wagner, Christian F. Krebs, Victor G. Puelles, Norbert Hübner, Eva Tolosa, Stefan Bonn, Samuel Huber, Percy A. Knolle, Johannes Herkel, Lorenz Adlung, Christoph Schramm, Nicola Gagliani, Ansgar Wilhelm Lohse

## Table of contents

Supplementary methods.....	2
Supplementary references.....	10
Supplementary tables.....	11
Supplementary figures.....	25

## Supplementary methods

**See Supplementary CTAT Table 1 (page 13) for details on reagents and software packages**

### Multi-omics workflow

**Bulk RNA purification and Sequencing.** Total RNA was extracted from frozen liver tissue using the NucleoSpin Kit (Macherey-Nagel). Complementary DNA (cDNA) was then transcribed from the total RNA using the High-Capacity cDNA Reverse Transcriptase Kit (Thermo Fisher Scientific). The quality was evaluated using Bioanalyzer (Agilent Technologies) and samples with an RNA integrity number < 7 were excluded from further analysis. mRNA libraries were synthesized using Illumina TruSeq Stranded mRNA Library Preparation assay and sequencing were conducted on a HiSeq 4000 system.

**Quantitative real-time PCR.** Total liver RNA was prepared with the NucleoSpin RNA Kit (Macherey-Nagel) according to the manufacturer's instructions. RNA was reverse-transcribed to cDNA with the High-Capacity cDNA Reverse Transcription Kit (Thermo Fisher Scientific). To determine the relative expression level of each gene of interest, qPCR was performed with TaqMan probes and the KAPA PROBE FAST Universal 2X qPCR Master Mix Kit (Roche). RNA expression of target genes was determined with probes from Thermo Fisher Scientific relative to the expression of hypoxanthine-guanine phosphoribosyltransferase (HPRT) (Hs02800695\_m1).

**Alignment, preprocessing and bioinformatic analysis.** The FASTQ files were assessed using FastQC to ensure a proper sequencing quality. Next, TruSeq2-PE adapter and low quality read trimming was performed with Trimmomatic<sup>1</sup> using the options ILLUMINACLIP:TruSeq2-PE.fa:2:30:10:2:falseSLIDINGWINDOW:4:15. STAR was used to align the read against ensemble 87 reference genome and annotation. Bioinformatic and statistical analysis was performed in R. For the sake of reproducibility, the seed was set to 0. If not mentioned otherwise, we run the methods with the default parameters of the respective R package. We only considered genes being expressed in more than 1/3 of our patients. Subsequently, every gene and sample passed WGCNAs method goodSampleGenes. We further removed all genes, which could not be translated to HGNC symbols by biomaRt. DESeq2<sup>2</sup> median of ratio (method estimateSizeFactors) normalization was used to create a normalized count matrix. Variance stabilizing transformation (method vst(blind = TRUE), library DESeq) was applied to calculate principal components (method prcomp). Based on the geneset HALLMARK\_INFLAMMATORY\_RESPONSE provided by the Molecular Signature Database (Human MSigDB v2024.1.Hs, <https://www.gsea-msigdb.org/>) the inflammation

score (Fig. 1c) was obtained. Important gene dynamics in the process of inflammation in patients with AIH were identified by applying rank-based correlation. Therefore, a gene  $\times$  feature correlation matrix with the correlation coefficient (Spearman's rho ( $r_s$ )) between each gene and the feature as elements ( $a_{ij} = r_{s \text{ R}(\text{gene } i)\text{R}(\text{feature } j)}$ ) was constructed. Rank-based correlation was selected because we aimed to capture strictly monotonic behaviour. Furthermore, mHAI values are measured on an ordinal scale. The method `fgsea` from R package `fgsea` was applied to genes ranked with respect to their respective  $r_s$ . Additionally, parent and grandparent terms/categories and the annotated genes were retrieved using the R package `KEGGREST` to group and subset the overrepresented terms. The KEGG pathway maps "Human Diseases" were excluded from the analysis. The R package `decoupleR` was utilized to evaluate the transcription factor activity. Transcription factor activity was determined by the t-statistic of the coefficients of a univariate linear model (method `run_ulm`) based on our input data ( $|r_s| > 0.6$ ) and the CollecTRI gene regulatory network.<sup>3</sup>

**Human liver single cell suspension.** Fresh liver samples were processed independent of disease status. Human liver tissue was rinsed with 0.9% NaCl, and a single-cell suspension was prepared by mechanical fragmentation followed by enzymatic digestion in 10ml RPMI medium (Gibco) containing 10% FBS (PAN Biotech), 0.1mg/ml collagenase D (Roche), 0.1mg/ml DNase I (Roche), 1mM CaCl<sub>2</sub>, and 1mM MgCl<sub>2</sub>. Digestion was performed on a rotary shaker at 180rpm, 37°C for 30 minutes. The suspension was filtered through a 30 $\mu$ m filter, and residual tissue was mechanically disrupted further. The digestion was halted by adding washing buffer containing 1x PBS (Gibco) with 1% FBS and 2mM EDTA (Sigma-Aldrich), followed by centrifugation. The resulting cell pellets were processed for CITE-seq preparation or flow cytometry analysis.

**Human peripheral blood mononuclear cell (PBMC) isolation.** PBMCs were isolated by diluting blood 1:1 with 1x PBS and layering onto equal amounts of Ficoll (Cytiva), followed by centrifugation at 400  $\times$  g, room temperature for 30 minutes. Cells from the interphase layer were collected, washed, and centrifuged. The cell pellets were subsequently processed for CITE-seq preparation or flow cytometry analysis.

### **CITE-seq and snRNA-seq workflow**

**Antibody staining for CITE-seq.** Antibodies for epitope capture in the sequencing workflow are listed in Supplementary (CTAT) table 1. To capture live cells, fixable viability dye eFluor 506 (Thermo Fisher) was used to stain cells on ice for 10 minutes. To minimize nonspecific antibody binding, cells were incubated with Human FC Block (BD Biosciences) together with fluorochrome conjugated anti-human antibodies (BioLegend) on ice for 10 minutes, including

anti-CD45 (clone HI30) for liver single cell suspensions, and anti-CD3 (clone SK7) for PBMCs. Liver samples were further stained with TotalSeq™-C barcode-labelled anti-human antibodies (BioLegend) on ice for 30 mins. PBMCs were stained with TotalSeq™-C Human Universal Cocktail V 1.0 (BioLegend) on ice for 30 minutes. The cells were then washed thoroughly and subjected to FACS sorting.

**Single cell FACS, library preparation and next generation sequencing.** To enrich immune cells from AIH liver single cell suspension, CD45<sup>+</sup> cells were FACS-sorted. CD3<sup>+</sup> T cells were FACS-sorted from paired PBMCs. FACS was conducted using a FACSAria Fusion (BD Bioscience). CITE-seq was performed using the Chromium Controller (10X Genomics). Single-cell libraries were generated using the Chromium Next GEM Single Cell V(D)J Reagent kit v1.1 (10X Genomics), following the manufacturer's instructions. Quality control was conducted using the BioAnalyzer (Agilent). The libraries were sequenced on an Illumina NovaSeq 6000 system.

**Human liver single nuclear suspension.** Frozen liver samples were processed independent of disease status. Nuclei isolation and library preparation were performed at the Max-Delbrück Center for Molecular Medicine as previously described.<sup>4</sup> The following adjustments were made for liver tissue: The homogenization buffer was modified with 0.3% Triton X-100 in nuclease-free water. After filtering, the homogenate was incubated in the buffer for 3 minutes. Single nuclei were purified by FACS using FACSAria (BD Biosciences). Nuclei purity and integrity were confirmed using a microscope and Countess III FL (Life Technologies), which was also used for nuclei counting.

**Single nuclei high-throughput sequencing.** Nuclei were then processed with the Chromium Controller (10X Genomics), targeting 5000–10000 nuclei per reaction. Gene expression libraries were prepared using the Chromium Next GEM Single Cell 3' Reagent Kits v3.1 (10X Genomics). Quality control was performed on final cDNA using the Bioanalyzer (Agilent) and KAPA Library Quantification kit. Libraries were sequenced on an Illumina HiSeq 4000 or NovaSeq, targeting 30000–50000 reads per nucleus.

**Pre-processing of CITE-seq and snRNA-seq data.** The CellRanger software pipeline (v6.1.1, 10X Genomics) was used to demultiplex cellular barcodes and map reads to the human reference genome (GRCh38-2020-A)<sup>5</sup> using the CellRanger count command. For snRNA-seq data, the include-introns option was applied. CITE-seq antibody and barcode information were incorporated via a feature reference CSV file provided to the CellRanger count command. This process generated feature-barcode matrices containing gene

expression and CITE-seq counts for each cell barcode. The feature-barcode matrices for all samples were further analysed in R using Seurat package. During quality control, cells with fewer than 350 detected features in both CITE-seq and snRNA-seq were excluded. Additionally, cells with more than 5% mitochondrial reads in CITE-seq and more than 1% in snRNA-seq were filtered out as low-quality cells. To remove potential doublets of the same cell type, cells with a feature-count ratio below 0.2 were excluded. Doublets of different cell types were identified and filtered using DoubletFinder, with adjustments to the estimated doublet threshold based on total input cell numbers.

**Sample merge and integration.** To generate the AIH liver atlas, we aggregated ten CITE-seq and six snRNA-seq samples using Seurat's *merge* function. After creating the merged AIH liver Seurat object, RNA assays were normalized using Seurat's *NormalizeData* function, and highly variable genes were identified with the *FindVariableFeatures* function (method = "vst", nfeatures = 2000) across samples. Integration features were selected using the *SelectIntegrationFeatures* function, followed by batch effect correction across patients using Seurat's integration workflow (*FindIntegrationAnchors* and *IntegrateData* function). For the combined analysis of AIH liver and paired blood T cells from patients AIH9, AIH13, and AIH15, we selected T cell clusters identified in the AIH liver atlas and merged them with the corresponding blood CD3<sup>+</sup> samples using the *merge* function. Integration and batch correction were performed using the same approach described above.

**Dimensionality reduction, clustering and cluster annotation.** For each integrated object, the integrated matrix was scaled using the *ScaleData* function with default parameters. Principal component analysis (PCA) was then performed on the scaled data using the *RunPCA* function (npcs = 30), followed by dimensionality reduction with the Uniform Manifold Approximation and Projection (UMAP) method (*RunUMAP* function, dims = 1:30). Using the top 30 principal components, a k-nearest neighbor graph was computed based on Euclidean distances (*FindNeighbors* function). Cell clusters were generated using the *FindClusters* function, adjusting the resolution parameter to the highest value that maintained clear distinctions between adjacent clusters. Next, we normalized scRNA-seq data using Seurat's LogNormalize method and CITE-seq counts using the CLR method. The top differentially expressed genes (DEGs) in each cluster were identified using the *FindAllMarkers* function with parameters min.pct = 0.25 and logfc.threshold = 0.5, employing Wilcoxon rank-sum tests. The *DoHeatmap* function in Seurat was used to visualize the expression of the top marker genes for each cluster. Cluster annotation was performed by matching DEGs with published literature and further validated using EnrichR<sup>6</sup> when necessary. Some clusters (e.g., UD-1) were left undefined due to their heterogeneous gene expression profiles spanning multiple cell types.

UD-2 could be classified as plasmacytoid dendritic cells based on the expression of marker genes such as *PLD4*, *JCHAIN*, and *LILRA4*; however, due to the low number of cells, we opted to annotate them as UD-2. For DEGs, see research data repository under DOI 10.25592/uhhfdm.18135.

**Liver CD4<sup>+</sup> T cells, CD8<sup>+</sup> T cells and hepatocytes clustering.** For the separate analysis of liver CD4<sup>+</sup> T cells, CD8<sup>+</sup> T cells, and hepatocytes, the corresponding clusters identified in the AIH liver atlas were selected and re-integrated by patient. For DEGs, see research data repository under DOI 10.25592/uhhfdm.18135.

Regarding T cells, CD4<sup>+</sup> and CD8<sup>+</sup> T cells were initially re-integrated and re-clustered together to generate a CD3<sup>+</sup> UMAP. Cells were then assigned to the CD4<sup>+</sup> UMAP based on the average *CD4* expression per cluster, while all other cells expressing *CD8A* or belonging to CD8<sup>+</sup> clusters were assigned to the CD8<sup>+</sup> UMAP. CD4<sup>+</sup> and CD8<sup>+</sup> T cells were subsequently re-integrated and re-clustered separately using the previously described method. Detailed cell type annotations were then obtained by examining the top marker genes and CITE-seq expression profiles of the clusters.

For CD4<sup>+</sup> T cell clustering, one donor from CITE-seq and one donor from snRNA-seq were excluded due to low cell numbers (< 80 cells), which affected integration quality. Additionally, since the original cluster 2 of CD4<sup>+</sup> T cells appeared to contain two distinct populations of cells - i.e., one expressing higher level of *IL10* than the other - it was further analysed using Seurat's *FindSubCluster* function and subsequently split into two additional CD4<sup>+</sup> T cell clusters (T<sub>EM-b</sub> and T<sub>EM-e</sub>).

A subset of *CD8A*-expressing cells, originally part of cluster 1 in the CD3<sup>+</sup> UMAP (a CD4<sup>+</sup> cluster), formed a distinct cluster in the CD8<sup>+</sup> UMAP, which was designated as T<sub>CM-b</sub>.

**Processing of TCR-seq data and integration.** TCR-seq data for each sample were processed using Cell Ranger software with the cellranger *vdj* command and the reference genome (vdj\_GRCh38\_alts\_ensembl-5.0.0). The output file *filtered\_contig\_annotations.csv* contained information on TCR- $\alpha$  and TCR- $\beta$  chain CDR3 nucleotide sequences for single cells identified by barcodes. The R package *scRepertoire* was used to combine contig annotation data from different samples into a single list object using the *combineTCR* function. This combined TCR contig list was then integrated with the corresponding Seurat object from CITE-seq data using the *combineExpression* function (*cloneCall* = "gene+nt"). Only cells with both TCR and CITE-seq data were retained for downstream clonotype analysis.

Each cell's clone was defined based on the corresponding amino acid sequence of the CDR3 region. The frequency of each clone (*n*) within each patient was calculated, and the clonotype was categorized by frequency into four groups: single, small, medium, and high.

**Liver and Blood TCR analysis.** To analyse TCR repertoires between the liver and paired blood samples, we generated a UMAP combining liver CD4<sup>+</sup> and CD8<sup>+</sup> T cells alongside blood sample CD3<sup>+</sup> T cells. To balance cell numbers and capture full transcriptional diversity from liver and blood, the UMAP was generated using all liver donors and three paired blood samples. Subsequently, liver cells from the three donors with paired blood samples were used for further TCR analysis.

We compared and quantified clonotypes between either liver CD4<sup>+</sup> or liver CD8<sup>+</sup> T cells, and their paired blood CD3<sup>+</sup> T cells. In particular, we highlighted the clones shared between the liver and blood compartments, as well as liver-specific clones, in the CD4<sup>+</sup> and CD8<sup>+</sup> liver UMAPs.

In the liver TCR analysis of CD4<sup>+</sup> T cells, 14 clones from 3 clonotypes shared between liver and blood were not present in the CD4<sup>+</sup> T cell UMAP, as they clustered within CD8<sup>+</sup> T cell UMAP. Notably, only 3 of the 14 excluded shared clones exhibited a gene signature similar to that of T<sub>RM</sub>1 cells. For the same reason, 6 clones from 3 liver-specific clonotypes were not present in the CD4<sup>+</sup> UMAP and 2 of these 6 clones exhibited a gene signature similar to that of T<sub>RM</sub>1 cells.

**Calculation of gene signature scores.** Signature scores for gene sets were calculated using Seurat's *AddModuleScore* function with default parameters. The residency and migration gene sets for CD4<sup>+</sup> and CD8<sup>+</sup> T cells were derived from published ~~core~~ lists of core genes upregulated in CD69<sup>+</sup> CD4<sup>+</sup> and CD69<sup>+</sup> CD8<sup>+</sup> T cells, respectively (Table S8), whereas migratory gene sets were derived from lists of core genes upregulated in CD69<sup>-</sup> CD4<sup>+</sup> and CD69<sup>-</sup> CD8<sup>+</sup> T cell (Table S9)<sup>7</sup> The a.a. gene set consisted of a core list of upregulated genes identified in a.a. CD8<sup>+</sup> T cells from human NASH liver (Table S10).<sup>8</sup> We used the *lme* function (*nlme* package) to apply a linear mixed-effects model with the patient ID as a random effect. We applied a Dunnett's test post-hoc, comparing each T<sub>EM</sub> cluster to the pool of the two TCM clusters, using the *glht* function (*multcomp* package).

**Interactome Analysis.** The R package CellChat<sup>9</sup> and its associated database were utilized to calculate the interaction strength. Based on the results from our bulk mRNA sequencing analysis, we used a supervised approach to select only the ligands *TNF*, *IFNG*, *FASLG*, *IL7*, and *IL15* from CellChat's database. Additionally, we integrate the *IL15 trans* presentation<sup>10</sup> into the database, specifying the following interaction: (*IL15 + IL15RA*) - (*IL2RG + IL2RB*). The communication probability was determined using the *computeCommunProb* method, with the truncated mean approach and a trim factor set to 0.05. To visualize the interaction network, we used the R package *ggraph*.

**Regression of TNF-dependent adhesive molecules on hepatocytes.** The R package AUCell was used to calculate the TNF pathway score and thresholds in hepatocytes based on the annotated genes of the KEGG TNF Pathway (hsa04668), excluding genes annotated in the KEGG Cell Adhesion Molecules pathway (hsa04514). Given the sparsity of the snRNA-sequencing data, we performed a zero-inflated regression using a hurdle model to estimate the relationship between the calculated TNF score and cell adhesion molecule expression. For this, we used the *zlm* method from the R package MAST, correcting for feature counts and sample identity.

### **Xenium *in situ* spatial analysis workflow**

**Gene panel design.** The Xenium In Situ technology used targeted panels to detect gene expression, including 377 genes from the Xenium Human Multi-Tissue and Cancer Panel (10X Genomics) and an additional 100 custom genes (10X Genomics) selected based on CITE-seq and snRNA-seq data from human AIH liver tissue.

**Xenium data generation.** The Xenium workflow began with sectioning 5µm FFPE tissue onto a Xenium slide, following the Xenium In Situ for FFPE - Tissue Preparation Guide (10X Genomics, CG000578). Deparaffinization and permeabilization were then performed to make the mRNA accessible, using the Xenium In Situ for FFPE - Deparaffinization & Decrosslinking Demonstrated Protocol (10X Genomics, CG000580). The mRNAs were targeted by the 477 probes described earlier, following the Xenium In Situ Gene Expression - Probe Hybridization, Ligation, Amplification & Cell Segmentation User Guide (10X Genomics, CG000749). Subsequently, slides were loaded onto the automated Xenium Analyzer (10X Genomics, GC000584). Regions of interest covering the full tissue sections were selected for imaging and processed using the fully automated, on-instrument analysis pipeline in Xenium Analyzer software (v3.0).

**Pre-processing of Xenium data and integration.** Xenium data was analysed in R, using Seurat and tidyverse packages. Data from the Xenium Onboard Analysis was imported into Seurat for each sample, filtering out cells without any RNA signals. To identify cell types, RNA count tables from all AIH and all control samples were merged separately, normalized using *SCTransform* function and integrated using Harmony (15 iterations, no early stop). UMAP and (shared) nearest-neighbour graphs were calculated using the first 30 harmony-adjusted embeddings. Cells were clustered using the Louvain algorithm at resolution 0.4 and annotated based on marker gene expression. As specified in the legend to Fig.4d, we identified T<sub>RM</sub>1

cells as CD4<sup>+</sup> T cells that express *CD69* and/or *CXCR6* in combination with *TNF* and/or *IFNG*; a.a.CD8<sup>+</sup> T cells were defined within the CD8<sup>+</sup> T cell cluster as CD69<sup>-</sup> CD62L<sup>-</sup> CCR7<sup>-</sup>.

**Spatial cell-cell communication analysis.** CellChat was used to calculate interaction probabilities as described above for the CITE-seq and snRNA-seq data, but additionally using an interaction range of 50 µm for soluble ligands and 10 µm for contact dependent interactions.

**Spatial neighbourhood analysis.** The *get.knnx* function from the FNN package was used to calculate the 5 nearest neighbouring cells around each cell in each sample. For each sample and cell type, neighbours were tallied by cell type and quantified as proportion of total neighbouring cells.

**TNF reacting cell analysis.** The distance to the closest TNF producing cells was calculated for each cell in each sample. For cells within 20 µm of a TNF producing cell, TNF-receptor positive and TNF-receptor negative cells were compared using the *FindMarkers* function, applying a Wilcoxon Rank Sum test followed by Bonferroni correction for multiple hypothesis testing. TNF-receptor positive was defined as the expression of either *TNFRSF1A* or *TNFRSF1B*.

### **Statistical analyses**

Statistical analyses were performed using R and GraphPad Prism. The statistical tests applied to each dataset were described in the corresponding figure legends. Patients from the clinical trial receiving infliximab (n=12) were matched to patients from the R-LIVER registry receiving standard care (SoC, n=24). in a 1:2 ratio using propensity score matching (PSM). Propensity scores were estimated via logistic regression including the baseline covariates age, ALT, mHAI, bilirubin and IgG, while sex and histological evidence of advanced fibrosis/cirrhosis (F3/4) were included as exact matching variables (see Fig. S10b-c for details of the PSM). Given the high collinearity between AST and ALT in the dataset (see Fig. S10a), AST was not included in the Propensity Matching to avoid redundancy-related overfitting of the model. Matching was performed without replacement using the nearest-neighbour method with an ATT (average treatment effect on the treated) estimate. Covariate balance was assessed using standardized mean differences (SMDs), with values <0.2 considered sufficiently balanced. After matching, all covariates achieved this threshold, with the exception of AST (SMD = 0.96); to account for this residual imbalance, AST was hence included as a covariate in subsequent analyses to adjust for residual confounding. Baseline variables of patients in the IFX and the SoC cohort were summarized descriptively, group comparability was assessed using SMDs (Table 1). Group comparisons for AST, ALT, IgG, liver stiffness (LSM) and Body Mass Index

(BMI) were performed by fitting linear mixed-effects models (LMM) to evaluate the effects of group (IFX vs. SoC) and time point (baseline vs month 6) on the respective parameters. To account for subject-level variability, all models included a random intercept for each participant and fixed effects for group, time point, and their interaction. Models were estimated using restricted maximum likelihood and t-tests employed Satterthwaite's approximation for degrees of freedom. Within-group changes from baseline to 6 months were assessed using estimated marginal means (EMMs) derived from the fitted models.

### Supplementary references

- 1 Bolger AM, Lohse M, Usadel B. Trimmomatic: a flexible trimmer for Illumina sequence data. *Bioinformatics*. 2014;30:2114-20.
- 2 Love MI, Huber W, Anders S. Moderated estimation of fold change and dispersion for RNA-seq data with DESeq2. *Genome Biology*. 2014;15:550.
- 3 Müller-Dott S, Tsirvouli E, Vazquez M, et al. Expanding the coverage of regulons from high-confidence prior knowledge for accurate estimation of transcription factor activities. *Nucleic Acids Res*. 2023;51:10934-10949.
- 4 Litviňuková M, Talavera-López C, Maatz H, et al. Cells of the adult human heart. *Nature*. 2020;588:466-472.
- 5 Yates AD, Achuthan P, Akanni W, et al. Ensembl 2020. *Nucleic Acids Res*. 2020;48:D682-D688.
- 6 Kuleshov MV, Jones MR, Rouillard AD, et al. Enrichr: a comprehensive gene set enrichment analysis web server 2016 update. *Nucleic Acids Research*. 2016; gkw377
- 7 Kumar BV, Ma W, Miron M, et al. Human Tissue-Resident Memory T Cells Are Defined by Core Transcriptional and Functional Signatures in Lymphoid and Mucosal Sites. *Cell Rep*. 2017;20:2921-2934.
- 8 Dudek M, Pfister D, Donakonda S, et al. Auto-aggressive CXCR6+ CD8 T cells cause liver immune pathology in NASH. *Nature*. 2021;592:444-449.
- 9 Jin S, Plikus MV, Nie Q. CellChat for systematic analysis of cell-cell communication from single-cell transcriptomics. *Nat Protoc*. 2025;20:180-219.
- 10 Jabri B, Abadie V. IL-15 functions as a danger signal to regulate tissue-resident T cells and tissue destruction. *Nat Rev Immunol*. 2015;15:771-83.

## Supplementary tables

**Table S1**

### Journal of Hepatology CTAT methods

Tables for a “Complete, Transparent, Accurate and Timely account” (CTAT) are now mandatory for all revised submissions. The aim is to enhance the reproducibility of methods.

- Only include the parts relevant to your study
- Refer to the CTAT in the main text as ‘Supplementary CTAT Table’
- Do not add subheadings
- Add as many rows as needed to include all information
- Only include one item per row

**If the CTAT form is not relevant to your study, please outline the reasons why:**

--

#### 1.1 Antibodies

Name	Citation	Supplier	Cat no.	Clone no.
anti-human CD45 PE-Cy7		BioLegend	304016	HI30
anti-human CD3 FITC		BioLegend	344804	SK7
anti-human TCR $\alpha/\beta$ AF488		BioLegend	306712	IP26
anti-human TCR $\gamma/\delta$ PerCP-Cy5.5		BioLegend	331224	BI4
anti-human TCR V $\alpha$ 24-J $\alpha$ 18 BV421		BioLegend	342916	6B11
anti-human CD4 BV605		BioLegend	317438	OKT4
anti-human CD8 $\alpha$ APC-Cy7		BioLegend	300926	HIT8a
anti-human CD8a BV711		BioLegend	301044	RPA-T8
anti-human CD45RO AF700		BioLegend	304218	UCHL1
anti-human CD45RO PE/Cy5		BioLegend	304208	UCHL1
anti-human CD62L BV421		BioLegend	304827	DREG-56
anti-human CD25 BV510		BioLegend	302639	BC96
anti-human CD127 PE-Cy7		BioLegend	351320	A019D5
anti-human CD69 BV785		BioLegend	310932	FN50
anti-human CD69 BV650		BioLegend	310933	FN50
anti-human CXCR6 PE/Dazzle		BioLegend	356016	K041E5
anti-human CD49a AF647		BioLegend	328310	TS2/7
anti-human TIGIT PE		BioLegend	372703	A15153G
anti-human PD-1 BV650		BioLegend	329950	EH12.2H7
anti-human TNF AF488		BioLegend	502917	MaAb11
anti-human IFN- $\gamma$ BV785		BioLegend	502542	4S.B3
anti-human Granzyme A PE-Cy7		BioLegend	507221	CB9
anti-human Granzyme B BV510		BD Biosciences	563388	GB11
anti-human Granzyme K PE		BioLegend	370511	GM26E7
Phospho-STAT5 Monoclonal Antibody, PE		Thermo Fisher	12-9010-42	SRBCZX
TotalSeq <sup>TM</sup> -C Human Universal Cocktail V 1.0		BioLegend	399905	--
TotalSeq <sup>TM</sup> -C0048 anti-human CD45		BioLegend	368545	2D1
TotalSeq <sup>TM</sup> -C0224 anti-human TCR $\alpha/\beta$		BioLegend	306743	IP26
TotalSeq <sup>TM</sup> -C0045 anti-human CD4		BioLegend	344651	SK3

TotalSeq™-C0046 anti-human CD8		BioLegend	344753	SK1
TotalSeq™-C0085 anti-human CD25		BioLegend	302649	BC96
TotalSeq™-C0390 anti-human CD127		BioLegend	351356	A019D5
TotalSeq™-C0146 anti-human CD69		BioLegend	310951	FN50
TotalSeq™-C0145 anti-human CD103		BioLegend	350233	Ber-ACT8
TotalSeq™-C0140 anti-human CXCR3		BioLegend	353747	G025H7
TotalSeq™-C0143 anti-human CCR6		BioLegend	353440	G034E3
TotalSeq™-C0148 anti-human CCR7		BioLegend	353251	G043H7
TotalSeq™-C0169 anti-human TIM-3		BioLegend	345049	F38-2E2
TotalSeq™-C0152 anti-human LAG-3		BioLegend	369335	11C3C65
TotalSeq™-C0371 anti-human CD49b		BioLegend	359317	P1E6-C5
TotalSeq™-C0088 anti-human PD-1		BioLegend	329963	EH12.2H7
TotalSeq™-C0151 anti-human CTLA-4		BioLegend	369621	BNI3
Anti-CD71 antibody		BioLegend	334102	CY1G4
Anti-TNF neutralizing antibody		BioXcell	SIM0001	Adalimumab

## 1.2 Cell lines

Name	Citation	Supplier	Cat no.	Passage no.	Authentication test method
K562		ATCC	CCL-243™		

## 1.3 Organisms

Name	Citation	Supplier	Strain	Sex	Age	Overall n number

## 1.4 Sequence based reagents

Name	Sequence	Supplier
TaqMan probes: TNF IFNG IL12A IL1B HPRT	Hs01113624_g1 Hs00989291_m1 Hs01073447_m1 Hs01555410_m1 Hs02800695_m1	Thermo Fisher Scientific
Chromium Next GEM Single Cell V(D)J Reagent Kits v1.1		10X Genomics
Chromium Next GEM Single Cell 3' Reagent Kits v3.1		10x Genomics
Xenium In Situ Gene Expression Kit		10x Genomics

## 1.5 Biological samples

Description	Source	Identifier
Liver biopsies	human	
Primary blood T cells	human	
Primary hepatocytes	human	

## 1.6 Deposited data

Name of repository	Identifier	Link

--	--	--

## 1.7 Software

Software name	Manufacturer	Version
RStudio	Posit Software, PBC formerly RStudio, PBC Boston, MA, USA	2023.12.1+402 "Ocean Storm"
Biorender	Science Suite Inc.	Version 2025
CellRanger	10X Genomics	6.1.1
Trimmomatic	Usadel Lab (RWTH Aachen University)	0.36
FastQC	Babraham Bioinformatics (Babraham Institute)	0.11.5
STAR	Dobin Lab (Cold Spring Harbor Laboratory)	2.7.3a
R	R Foundation for Statistical Computing	4.3.3
Seurat	Satija Lab <a href="https://github.com/satijalab/seurat">https://github.com/satijalab/seurat</a>	4.3.0 (SCS/SNS) / 5.0.3 (Xenium)
DoubletFinder	Chris McGinnis (UCSF) <a href="https://github.com/chris-mcginnis-ucsf/DoubletFinder">https://github.com/chris-mcginnis-ucsf/DoubletFinder</a>	2.0.3
scRepertoire	Nick Borcharding (Borcharding Lab) <a href="https://github.com/BorchLab/scRepertoire">https://github.com/BorchLab/scRepertoire</a>	1.12.0
CellChat	Suoqin Jin <a href="https://github.com/jinworks/CellChat">https://github.com/jinworks/CellChat</a>	2.1.2
tidyverse	Posit Software <a href="https://cran.r-project.org/web/packages/tidyverse/index.html">https://cran.r-project.org/web/packages/tidyverse/index.html</a>	2.0.0
Harmony	Ilya Korsunsky (Raychaudhuri Lab) <a href="https://github.com/immunogenomics/harmony">https://github.com/immunogenomics/harmony</a>	1.2.0
FNN	Shengqiao Li <a href="https://cran.r-project.org/web/packages/FNN/index.html">https://cran.r-project.org/web/packages/FNN/index.html</a>	1.1.14
nlme	R Core Team <a href="https://cran.r-project.org/web/packages/nlme/index.html">https://cran.r-project.org/web/packages/nlme/index.html</a>	3.1
multcomp	Torsten Hothorn <a href="https://cran.r-project.org/web/packages/multcomp/index.html">https://cran.r-project.org/web/packages/multcomp/index.html</a>	1.4
org.Hs.eg.db	Bioconductor Core Team <a href="https://bioconductor.org/packages/org.Hs.eg.db/">https://bioconductor.org/packages/org.Hs.eg.db/</a>	3.19.1
KEGGREST	Bioconductor Core Team <a href="https://bioconductor.org/packages/KEGGREST/">https://bioconductor.org/packages/KEGGREST/</a>	1.44.1
clusterProfiler	Guangchuang Yu <a href="https://bioconductor.org/packages/clusterProfiler/">https://bioconductor.org/packages/clusterProfiler/</a>	4.12.2
DESeq2	Michael Love <a href="https://bioconductor.org/packages/DESeq2">https://bioconductor.org/packages/DESeq2</a>	1.44.0
vegan	Jari Oksanen / vegandevs <a href="https://cran.r-project.org/package=vegan">https://cran.r-project.org/package=vegan</a>	2.6-8
decoupleR	Pau Badia-i-Mompel (Saez-Rodriguez Lab) <a href="https://github.com/saezlab/decoupleR">https://github.com/saezlab/decoupleR</a>	2.10.0
fgsea	Alexey Sergushichev <a href="https://bioconductor.org/packages/fgsea">https://bioconductor.org/packages/fgsea</a>	1.28.0
dplyr	Posit / Tidyverse Team <a href="https://cran.r-project.org/package=dplyr">https://cran.r-project.org/package=dplyr</a>	1.1.4
ggplot2	Posit / Tidyverse Team <a href="https://cran.r-project.org/package=ggplot2">https://cran.r-project.org/package=ggplot2</a>	3.5.1

ggvoronoi	Robert C. Garrett <a href="https://github.com/garrettc/ggvoronoi">https://github.com/garrettc/ggvoronoi</a>	0.8.6
ggpubr	Alboukadel Kassambara <a href="https://github.com/kassambara/ggpubr/releases">https://github.com/kassambara/ggpubr/releases</a>	0.6.0
ggpmisc	Pedro J. Aphalo <a href="https://github.com/aphalo/ggpmisc">https://github.com/aphalo/ggpmisc</a>	0.6.0
ggrepel	Kamil Slowikowski <a href="https://github.com/slowkow/ggrepel">https://github.com/slowkow/ggrepel</a>	0.9.5
ggraph	Thomas Lin Pedersen <a href="https://github.com/thomasp85/ggraph">https://github.com/thomasp85/ggraph</a>	2.2.1
stringr	Posit / Tidyverse Team <a href="https://github.com/tidyverse/stringr">https://github.com/tidyverse/stringr</a>	1.5.1
reshape2	Hadley Wickham <a href="https://cran.r-project.org/package=reshape2">https://cran.r-project.org/package=reshape2</a>	1.4.4
AUCell	Gert Hulselmans (Aerts Lab) <a href="https://github.com/aertslab/AUCell">https://github.com/aertslab/AUCell</a>	1.26.0
MAST	Andrew McDavid (Gottardo Lab) <a href="https://github.com/RGLab/MAST">https://github.com/RGLab/MAST</a>	1.30.0

### 1.8 Other (e.g. drugs, proteins, vectors etc.)

NucleoSpin RNA Kit	Macherey-Nagel	
High-Capacity cDNA Reverse Transcription Kit	Thermo Fisher	
KAPA PROBE FAST Universal 2X qPCR Master Mix Kit	Roche	
High Sensitivity DNA Kit	Agilent	5067-4626
DPBS	Gibco	14190-094
EDTA	Sigma-Aldrich	03690
Collagenase D	Roche	11088882001
DNase I	Roche	10104159001
Fixable Viability Dye eFluor 506	Thermo Fisher	65-0866-14
Zombie UV Fixable Viability Kit	BioLegend	423108
Alexa Fluor 750 NHS Ester	Thermo Fisher	A20011
Human FC Block	BD Biosciences	564220
Phorbol-12-myristate-13-acetate (PMA)	Sigma-Aldrich	524400
Ionomycin from Streptomyces conglobatus	Sigma-Aldrich	I9657
Brefeldin A Solution (1,000X)	BioLegend	420601
BD Cytotfix/Cytoperm™ Plus	BD Biosciences	555028
Lectin from Phaseolus vulgaris (PHA)	Sigma-Aldrich	L9017
Recombinant human IL-2	Miltenyi Biotec	130-097-746
Recombinant human IL-7	R&D system	207-IL/CF
Recombinant human IL-15	R&D system	247-ILB/CF
Recombinant human IL-15	PeproTech	AF-200-15
Recombinant human TNF	PeproTech	300-01A
Ficoll-Paque PLUS	Cytiva	17144003
PanColl	PAN Biotech	P04-60100
FBS Supreme	PAN Biotech	P30-3031
RPMI Medium 1640, GlutaMAX™	Gibco	61870-010
X-VIVO medium	Lonza	02-060F
Collagen R	Advanced Biomatrix	5026
Williams E medium	Gibco	22551-022
Insulin-transferrin-selenium	Gibco	41400-045
Bovine Serum Albumin	AppliChem	A1391,0500
GlutaMAX	Sigma-Aldrich	G7513

Non-essential amino acids	Gibco	11140-035
Penicillin-Streptomycin	Sigma-Aldrich	P0781
CD8 MicroBeads, human	Miltenyi Biotec	130-045-201
CellTrace CFSE cell proliferation kit	Thermo Fisher	C34554
CellTrace Violet cell proliferation kit	Thermo Fisher	C34557
Dynabeads™ Human T-Activator CD3/CD28 for T Cell Expansion and Activation	Gibco	11161D
ImmunoCult Human CD3/CD28 T Cell Activator	STEMCELL Technologies	10971
LEGENDplex Human CD8/NK Panel	BioLegend	741148
Infliximab (Inflectra®)	Pfizer	Not applicable

**1.9 Please provide the details of the corresponding methods author for the manuscript:**

--

**2.0 Please confirm for randomised controlled trials all versions of the clinical protocol are included in the submission. These will be published online as supplementary information.**

<p>The phase IIa clinical trial (EudraCT No.: 2017-003311-19) followed a proof-of-concept design and was therefore not randomised nor controlled. To ensure maximum transparency, the most recent version of the protocol (V3.0) has been added to the supplementary material provided.</p>
---

**Table S2. Comparison of biochemical markers, liver stiffness and BMI during baseline and after 6 months between patients receiving IFX and the cohort receiving the standard of care (SoC) for 6 months.**

	IFX			SoC		
	Baseline (FA)	Week 24 (FA)	Relative Change	Baseline	Month 6	Relative Change
<b>AST xULN</b>	6.48 (3.32-16.71)	0.71 (0.29-1.66)	-89.0%	16.49 (4.26-28.46)	1.01 (0.42-10.12)	-93.9%
<b>ALT xULN</b>	11.29 (4.4-21.54)	0.83 (0.31-1.97)	-92.7%	13.11 (2.16-24.26)	0.81 (0.34-3.62)	-93.8%
<b>IgG (g/l)</b>	19.4 (14.3-32.1)	16.7 (12.7-25.2)	-13.2%	19.8 (1.8-51.2)	11.7 (1.3-30.9)	-40.9%
<b>gGT (U/l)</b>	116 (41-331)	35 (9-93)	-69.8%	146 (50-422)	36 (11-352)	-75.3%
<b>ALP (U/l)</b>	131 (67-343)	73 (48-150)	-44.3%	130 (59-396)	66 (41-149)	-49.2%
<b>Total Bilirubin (mg/dl)</b>	1.1 (0.5-4.7)	0.6 (0.3-1.4)	-45.5%	1.2 (0.4-3.0)	0.7 (0.3-1.3)	-41.7%
<b>Albumin (g/dl)</b>	35.7 (33.0-41.7) <sup>1</sup>	42.8 (37.9-45.4)	+19.9%	37.0 (25.6-46.1) <sup>3</sup>	41.3 (29.8-45.8) <sup>3</sup>	+11.6%
<b>INR</b>	1.0 (1.0-1.1) <sup>2</sup>	1.0 (0.9-1.1)	±0.0%	1.1 (0.9-1.5)	1.0 (0.9-1.2) <sup>3</sup>	-9.1%
<b>Liver stiffness (kPa)</b>	14.8 (6.9-34.8)	7.1 (5.2-18.8)	-52.0%	10.4 (4.9-35.3) <sup>4</sup>	7.0 (3.5-22.3) <sup>5</sup>	-32.7%
<b>BMI (kg/m<sup>2</sup>)</b>	25.1 (19.2-32.1)	25.5 (19.5-32.4)	+1.6%	23.7 (17.9-33.5) <sup>6</sup>	25.5 (21.2-32.0) <sup>7</sup>	+7.6%

Shown are data of patients with values **both at baseline and at month 6** (IFX [final analysis, FA] cohort n = 9, SoC cohort n = 24, if not specified differently).

Continuous variables = medians (range)

<sup>1</sup> data available for n = 6

<sup>2</sup> data available for n = 7

<sup>3</sup> data available for n = 22

<sup>4</sup> data available for n = 18

<sup>5</sup> data available for n = 13

<sup>6</sup> data available for n = 23

<sup>7</sup> data available for n = 15

**Table S3. Results of the Short Form 36 questionnaire (SF-36) regarding health-related quality of life from patients in the clinical trial.**

Baseline	ID 001	ID 002	ID 003	ID 004	ID 005	ID 006	ID 007	ID 008	ID 009	ID 011	ID 012	ID 013	Median	Mean	SD	IQR25	IQR75	Min	Max
Physical Function	80	80	80	55	85	85	85	70	35	85	80	80	80,0	75,0	14,6	77,5	85,0	35	85
Mental Health	88	60	92	92	84	68	80	56	64	76	80	84	80,0	77,0	11,8	67,0	85,0	56	92
Pain	89	100	100	44	56	89	100	100	78	78	100	89	89,0	85,3	17,8	78,0	100,0	44	100
Change in Health	25	25	50	25	25	25	25	0	0	75	50	25	25,0	29,2	20,0	25,0	31,3	0	75
Role limitation physical	75	50	100	100	50	100	100	0	0	100	100	50	87,5	68,8	37,0	50,0	100,0	0	100
Role limitation emotional	100	67	100	100	100	67	100	0	0	100	100	100	100,0	77,8	36,8	67,0	100,0	0	100
Energy/Vitality	70	25	75	50	45	55	65	0	30	45	70	20	47,5	45,8	22,3	28,8	66,3	0	75
Health Perception	70	50	65	50	90	75	75	0	50	45	80	30	57,5	56,7	23,7	48,8	75,0	0	90
<b>6 Months</b>	<b>ID 001</b>	<b>ID 002</b>	<b>ID 003</b>	<b>ID 004</b>	<b>ID 005</b>	<b>ID 006</b>	<b>ID 007</b>	<b>ID 008</b>	<b>ID 009</b>	<b>ID 011</b>	<b>ID 012</b>	<b>ID 013</b>	<b>Median</b>	<b>Mean</b>	<b>SD</b>	<b>IQR25</b>	<b>IQR75</b>	<b>Min</b>	<b>Max</b>
Physical Function	85	80	80	65	85	85	85			85	85	85	85,0	81,7	6,2	80,0	85,0	65	85
Mental Health	92	68	92	92	80	44	88			88	92	64	88,0	79,1	16,1	68,0	92,0	44	92
Pain	89	100	89	89	100	67				100	100	100	100,0	92,7	10,4	89,0	100,0	67	100
Change in Health	75	75	75	100	25	50				75	50	75	75,0	66,7	20,4	50,0	75,0	25	100
Role limitation physical	100	100	100	100	100	50				100	100	100	100,0	94,4	15,7	100,0	100,0	50	100
Role limitation emotional	100	100	100	100	67	0				100	100	33	100,0	77,8	35,2	67,0	100,0	0	100
Energy/Vitality	75	60	75	75	60	35				60	75	60	60,0	63,9	12,4	60,0	75,0	35	75
Health Perception	85	75	70	65	65	55				70	75	70	70,0	70,0	7,8	65,0	75,0	55	85
<b>Differences (A<sub>6</sub> results vs. Baseline)</b>	<b>ID 001</b>	<b>ID 002</b>	<b>ID 003</b>	<b>ID 004</b>	<b>ID 005</b>	<b>ID 006</b>	<b>ID 007</b>	<b>ID 008</b>	<b>ID 009</b>	<b>ID 011</b>	<b>ID 012</b>	<b>ID 013</b>	<b>Median</b>	<b>Mean</b>	<b>SD</b>	<b>IQR25</b>	<b>IQR75</b>	<b>Min</b>	<b>Max</b>
Physical Function	5	0	0	10	0	0	0			0	5	5	0,0	2,8	3,4	0,0	5,0	0	10
Mental Health	4	8	0	0	12	-36				12	12	-20	4,0	-0,9	15,6	0,0	12,0	-36	12
Pain	0	0	-11	45	11	-33				22	0	11	0,0	5,0	20,4	0,0	11,0	-33	45
Change in Health	50	50	25	75	0	25				0	0	50	25,0	30,6	25,8	0,0	50,0	0	75
Role limitation physical	25	50	0	0	0	-50				0	0	50	0,0	8,3	28,9	0,0	25,0	-50	50
Role limitation emotional	0	33	0	0	0	-100				0	0	-67	0,0	-14,9	38,8	0,0	0,0	-100	33
Energy/Vitality	5	35	0	25	5	-30				15	5	40	5,0	11,1	19,8	5,0	25,0	-30	40
Health Perception	15	25	5	15	-10	-20				25	-5	40	15,0	10,0	18,1	-5,0	25,0	-20	40

Follow-up data is missing for n = 3 patients who were not eligible for endpoint analysis due to early treatment discontinuation.

**Table S4. Clinical characteristics of bulk mRNA-seq cohorts.**

	Autoimmune hepatitis	Primary biliary cholangitis	p
	N=16	N=11	
<b>Basic characteristics</b>			
Age - median (range)	51 (25 - 70)	53.5 (40 - 82)	0.256*
Sex Female – no (%)	10 (62.5%)	9 (81.8%)	0.404**
<b>Histological features</b>			
mHAI Score			
Median (range) (missing)	9 (4-14) (0)	4 (1-8) (0)	0.002*
<6 – no (%)	5 (31.2)	8 (72.7)	
6-9 – no (%)	3 (29.8)	3 (27.3)	
10-18 – no (%)	8 (50.0)	0 (0)	
Fibrosis score			
Median (range) (missing)	2 (0-4) (0)	2 (0-4) (0)	0.841*
<= 3 – no (%)	12 (75.0)	8 (72.7)	
>3 – no (%)	4 (25.0)	3 (27.3)	
<b>Laboratory features</b>			
Mean ± SD (missing)			
Hemoglobin – g/dl	13.22 ± 1.56 (0)	13.11 ± 2.08 (1)	0.792*
Platelets – bn/l	250.81 ± 51.15 (0)	259.5 ± 48.18 (1)	0.897*
Creatinine – mg/dl	0.82 ± 0.12 (2)	0.9 ± 0.18 (5)	0.455*
ALT [xULN]	15.05 ± 13 (2)	3.38 ± 2.3 (3)	0.008*
AST [xULN]	12.88 ± 9.62 (2)	3.37 ± 2.2 (3)	0.024*
GGT – U/l	264.14 ± 149.74 (2)	361.88 ± 177.17 (3)	0.413*
AP – U/l	184.93 ± 48.18 (2)	301.57 ± 216.46 (4)	0.247*
IGG – g/dl	21.98 ± 7.26 (3)	16.1 ± 8.61 (4)	0.074*
INR	1.12 ± 0.16 (1)	0.99 ± 0.03 (3)	0.065*
			* Mann-Whitney U test
			** Fishers exact test

**Table S5. Clinical characteristics of CITE-seq and snRNA-seq cohorts.**

	CITE-seq	snRNA-seq
	N=10	N=6
<b>Basic characteristics</b>		
Age - median (range)	48 (30 - 62)	48 (22 - 63)
Sex Female – no (%)	7 (70.0%)	6 (100%)
<b>Histological features</b>		
mHAI Score		
Median (range) (missing)	5.75 (3-11) (0)	7.0 (3-13) (0)
<6 – no (%)	5 (50.0)	2 (33.3)
6-9 – no (%)	4 (40.0)	2 (33.3)
10-18 – no (%)	1 (10.0)	2 (33.3)
Fibrosis score		
Median (range) (missing)	1.25 (0-4) (0)	0 (0-4) (0)
<= 3 – no (%)	8 (80.0)	5 (83.3)
>3 – no (%)	2 (20.0)	1 (16.7)
<b>Laboratory features</b>		
Mean ± SD (missing)		
Hemoglobin – g/dl	12.55 ± 1.13 (0)	12.9 ± 0.84 (0)
Platelets – bn/l	236.5 ± 145.19 (0)	304.0 ± 53.38 (0)
Creatinine – mg/dl	0.75 ± 0.17 (4)	0.86 ± 0.17 (2)
ALT [xULN]	10.02 ± 8.03 (0)	15.33 ± 17.40 (0)
AST [xULN]	3.97 ± 4.61 (0)	10.18 ± 16.59 (0)
GGT – U/l	112.0 ± 120.84 (0)	180.5 ± 115.7 (0)
ALP – U/l	95.00 ± 29.29 (0)	154.0 ± 56.93 (2)
IGG – g/dl	17.64 ± 4.95 (4)	20.33 ± 12.77 (4)
INR	1.0 ± 0.11 (1)	1.1 ± 0.36 (1)

**Table S6. Clinical characteristics of FACS cohorts.**

	AIH	Control
	N=11	N=6
<b>Basic characteristics</b>		
Age - median (range)	54 (22 - 77)	52.5 (35 - 67)
Sex Female – no (%)	7 (63.64%)	6 (100%)
<b>Histological features</b>		
mHAI Score		
Median (range) (missing)	9.0 (3-16) (0)	--
<6 – no (%)	1 (9.09)	
6-9 – no (%)	5 (45.45)	
10-18 – no (%)	5 (45.45)	
Fibrosis score		
Median (range) (missing)	1.0 (0-4) (0)	0.5 (0-1) (2)
<= 3 – no (%)	10 (90.91)	4 (100)
>3 – no (%)	1 (9.09)	0 (0)
<b>Laboratory features</b>		
Mean ± SD (missing)		
Hemoglobin – g/dl	13.6 ± 1.62 (0)	--
Platelets – bn/l	179.0 ± 78.83 (0)	--
Creatinine – mg/dl	0.82 ± 0.16 (0)	--
ALT [xULN]	9.10 ± 6.94 (0)	1.19 ± 4.38 (0)
AST [xULN]	5.77 ± 5.69 (0)	0.66 ± 3.26 (0)
GGT – U/l	141.0 ± 94.04 (0)	47.5 ± 32.92 (0)
ALP – U/l	102.0 ± 75.64 (0)	--
IGG – g/dl	22.71 ± 9.10 (0)	--
INR	1.0 ± 0.11 (0)	--

**Table S7. Clinical characteristics of spatial *in situ* RNA expression cohorts.**

	AIH	Control
	N=6	N=3
<b>Basic characteristics</b>		
Age - median (range)	38.5 (28 - 73)	39 (35 - 49)
Sex Female – no (%)	5 (83.3%)	0 (0%)
<b>Histological features</b>		
mHAI Score		
Median (range) (missing)	11.5 (10-13) (0)	0 (0-1) (0)
<6 – no (%)	0 (0)	3 (100)
6-9 – no (%)	0 (0)	0 (0)
10-18 – no (%)	6 (100)	0 (0)
Fibrosis score		
Median (range) (missing)	1.5 (0-4) (0)	0 (0-0) (0)
<= 3 – no (%)	4 (66.7)	3 (100)
>3 – no (%)	2 (33.3)	0 (0)
<b>Laboratory features</b>		
Mean ± SD (missing)		
Hemoglobin – g/dl	13.35 ± 0.76 (0)	16.3 ± 0.6 (0)
Platelets – bn/l	166.5 ± 117.61 (0)	204.0 ± 82.53 (0)
Creatinine – mg/dl	0.70 ± 0.47 (0)	1.03 ± NA (2)
ALT [xULN]	24.71 ± 17.41 (0)	1.24 ± 0.25 (0)
AST [xULN]	23.0 ± 17.16 (0)	0.84 ± 0.25 (0)
GGT – U/l	135.5 ± 67.7 (0)	119.0 ± 44.84 (0)
ALP – U/l	165.5 ± 79.58 (0)	71.0 ± 20.82 (0)
IGG – g/dl	15.49 ± 7.22 (0)	11.8 ± 0.42 (1)
INR	1.2 ± 0.33 (0)	1.05 ± 0.07 (1)

**Table S8. Gene list for residency score.**

<b>CD4+ T cells</b>	<b>CD8+ T cells</b>
CD69	CD69
CA10	CA10
IL17F	IL17A
IL2	CXCL13
CDHR1	SCUBE1
IL21	HASPIN
IL10	ITGA1
IL23R	CXCR6
CXCL13	ATP8B4
CXCR6	CSF1
KCNK5	ITGAE
ITGA1	CPNE7
JAG2	IL10
SRGAP3	SPRY1
TOX2	MCAM
CH25H	RGS1
NEK10	KCNQ3
TMEM200A	DAB2IP
MYO1B	TRPM2
PLXDC1	KCNK5
IKZF3	IL23R
GFOD1	PELO
CRTAM	COL5A1
DUSP6	IRF4
RGS1	FSD1
TP53I11	IL17RE
GFI1	ADAM12
IFNG	CRTAM
SLC7A5	ARHGAP18
GCNT4	CCR1
	JAML
	ICOS
	TMIGD2
	TP53INP1
	BMF
	CD9
	RIMS3
	DUSP6
	CCR6
	GZMB
	ZNF683

**Table S9. Gene list for migratory score.**

CD4+ T cells	CD8+ T cells
RIPOR2	PXN
STK38	FLNA
GRASP	CYB561
KLF3	CD300A
SAMD3	TSPAN32
GABBR1	RASA3
FRY	ADGRG5
ARHGEF11	TGFBR3
VIPR1	SAMD3
BAIAP3	PELI2
MFGE8	C11orf21
SBK1	RASGRP2
HAPLN3	SYNE1
TTC16	GK5
CX3CR1	SSX2IP
USP46	STK38
PLXNA4	FGR
NSG1	SSBP3
DSEL	CFH
CNTNAP1	ADAMTS10
VSIG1	MTSS1
RGMB	KLF3
TTYH2	KLF2
EPHA4	SVIL
TNFRSF11A	CACNA2D2
MUC1	RIPOR2
CR1	SBK1
E2F2	PATL2
KLF2	TMCC3
EDA	KIR2DS4
KRT73	HPCAL4
ZNF462	VCL
RAP1GAP2	TTC16
S1PR1	PDZD4
NPDC1	DCHS1
KLF3-AS1	EBF4
ISM1	OSBPL5
TSPAN18	FZD4
KCTD15	GNLY
KRT72	NHSL2
SEMA5A	TSPAN18
WNT7A	ME3
SOX13	MSX2P1
FUT7	ZNF711
PTGDS	NSG1
PI16	FCGR3A
SEMA3G	GPA33
SYT4	COL6A2
	CXCR2
	TTYH2
	AGPAT4
	TKTL1
	SELP
	LILRB1
	ITGAM
	LOXL4
	KLF3-AS1
	TFCP2L1
	C1orf21
	SLCO4C1
	NUAK1
	PALLD
	DNAI2
	SOX13
	S1PR1
	SELL
	PLEKHG3
	ADGRG1
	SPTB
	ZNF365
	PCDH1
	NPDC1
	KRT73
	KRT72
	ASCL2
	TAF1
	SGCD
	LAIR2
	EFHC2
	RAP1GAP2
	NME8
	PODN
	SH3RF2
	KIF19
	PTGDS
	EPHX4
	PRSS23
	KIR3DX1
	CX3CR1
	SLC1A7
	FGFBP2
	LRFN2
	DGKK

**Table S10. Gene list for a.a. score.**

RUNX3
JUN
RGS1
CD8A
DUSP2
NR4A2
PDCD1
CXCR6
TIGIT
ZBTB38
GZMK
GZMA
CD74
FYN
IFNGR1
TOX
GABARAPL1
IFNG
ALOX5AP
CCL5
IKZF3
CST7
GZMM
ZFP36

Supplementary figures

Supplementary Fig. 1

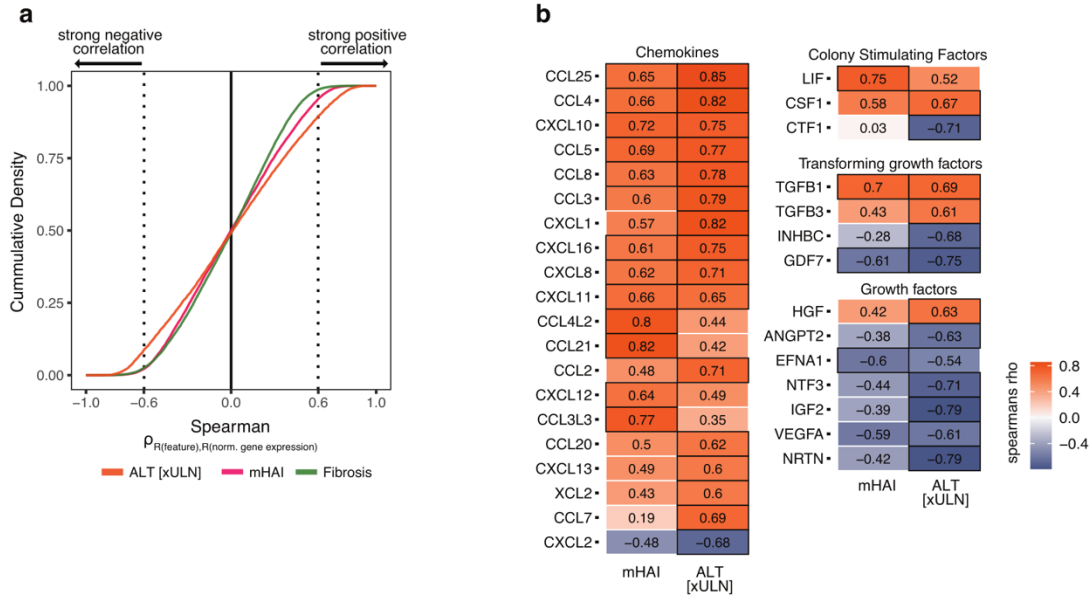


**Fig. S1. Gene - feature correlation of patients with AIH identified by bulk mRNA sequencing. (a)** Distribution of  $r_s$  values across all genes and the features ALT, mHAI, Fibrosis Score in patients with AIH depicted by cumulative density.  $r_s \geq 0.6$  or  $< -0.6$  defined as strong correlation. **(b)** Heatmap of strongly correlating chemokines, colony stimulating factors, transforming growth factors and growth factors.

Supplementary Fig. 2

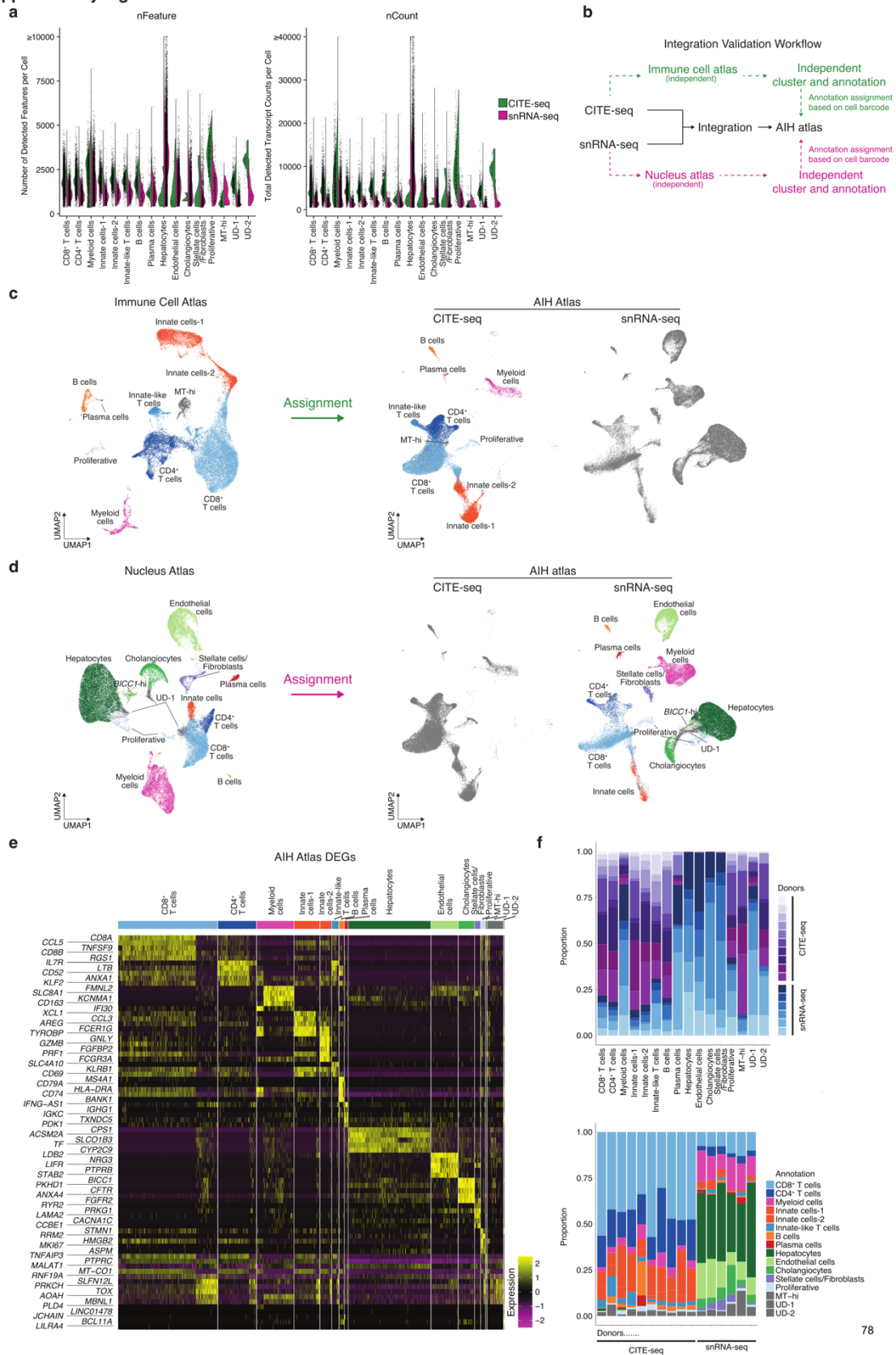


**Fig. S2. CITE-seq and snRNA-seq integration validation and cluster annotation.** (a) Violin plots for quality control: library size (nFeature) and total transcript counts (nCount) by cell type and sequencing approach. Values of nFeature exceeding 10,000 were capped at 10,000 on

the y-axis for visualization, and values of nCount exceeding 40,000 were capped at 40,000 on the y-axis for visualization. **(b)** Schematic representation of the validation strategy for integrating CITE-seq and snRNA-seq datasets. **(c)** Left: Cell type annotation of the immune cell atlas performed independently (CITE-seq, n=10). Right: Annotation transfer to the AIH atlas using barcode matching. **(d)** Left: Cell type annotation of the nucleus atlas performed independently (snRNA-seq, n=6) (UD: Un-defined). Right: Annotation transfer to the AIH atlas using barcode matching. **(e)** Heatmap of scaled expression values of the top 5 DEGs per cell type in CITE-seq and snRNA-seq integrated AIH atlas. UD-1 and UD-2 are not explicitly labelled in Fig. 2c, but are represented in grey (UD: Un-defined). **(f)** Top: Distribution of samples/datasets per cell type; Bottom: Distribution of cell type per samples/datasets.

Supplementary Fig. 3

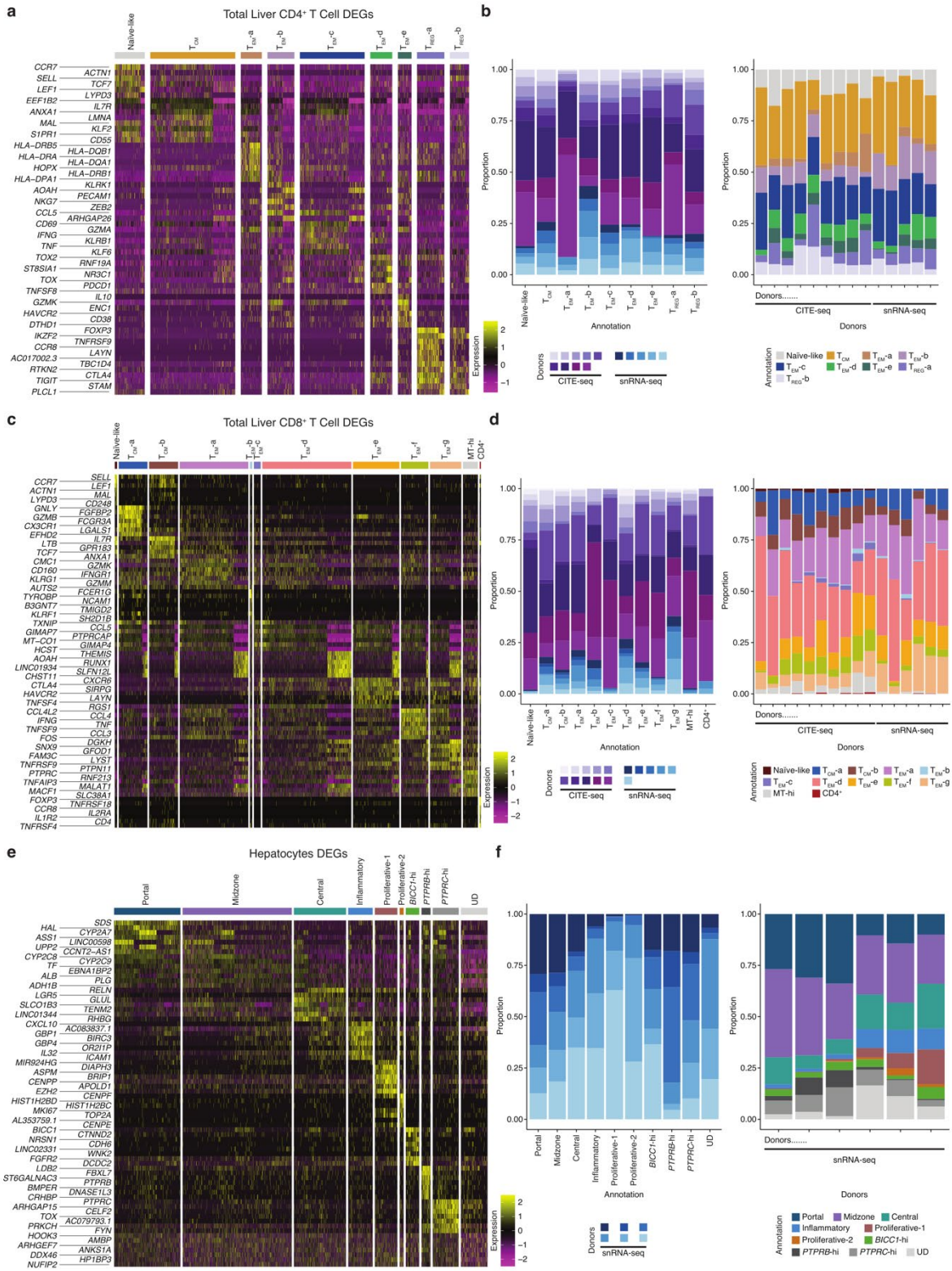


**Fig. S3. Zoom-in analysis of CD4<sup>+</sup> T cells, CD8<sup>+</sup> T cells, and Hepatocytes from the AIH atlas: subcluster specific differential expression genes and sample contribution. (a, c, e) Heatmap of scaled expression values of the top 7 DEGs per CD4<sup>+</sup> T cells (a) CD8<sup>+</sup> T cells**

(c) and Hepatocytes (e) subtypes. RPL and RPS genes are not displayed. (RPL: Ribosomal Protein L; RPS: Ribosomal Protein S) (**b**, **d**, **f**) Left: Contribution of each sample to the subtypes. Right: Contribution of subtypes to each sample.

**Supplementary Fig. 4**

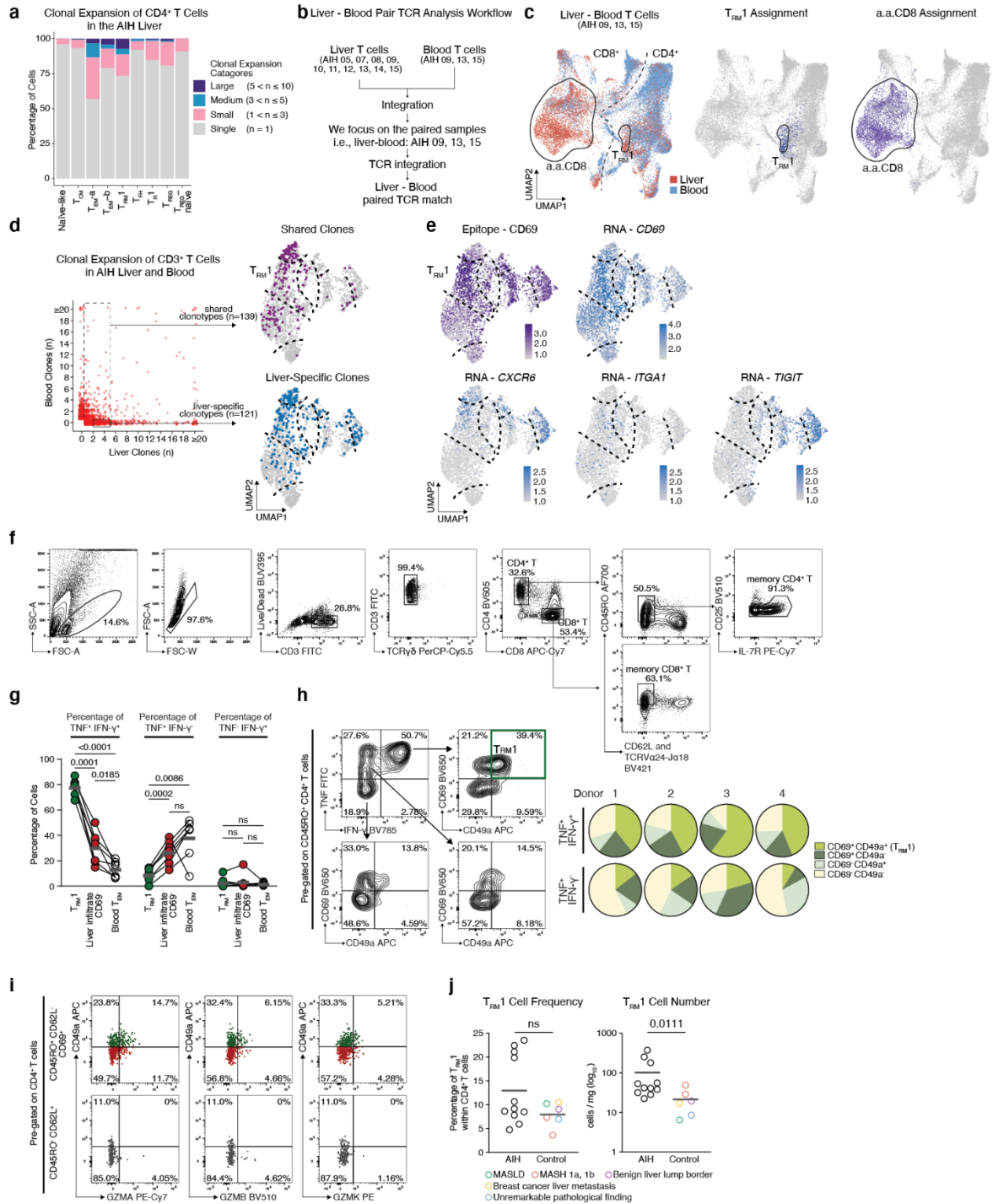


**Fig. S4. Proinflammatory profile of T<sub>RM1</sub> cells.** (a) Bar chart depicting clonal expansion percentages within each liver CD4<sup>+</sup> T cell cluster. (b) Schematic representation of the TCR analysis strategy. (c) Left: UMAP of liver and paired blood T cells, coloured by organ source. Right: T<sub>RM1</sub> cells (corresponding to Fig. 2d, T<sub>EM-c</sub>) and a.a.CD8<sup>+</sup> T cells (corresponding to Fig. 2e, T<sub>EM-a</sub> to -g) are shown after annotation transfer of T<sub>RM1</sub> and a.a.CD8<sup>+</sup> T cells from Fig. 2d (T<sub>EM-c</sub>) and Fig. 2e (T<sub>EM-a</sub> to -g) to this liver - paired blood T cell UMAP using barcode matching. (d) Left: Clonal expansion of CD3<sup>+</sup> T cells, in the livers and paired blood (liver CITE-seq: n = 3; paired blood CITE-seq: n = 3). The X-axis and Y-axis represent liver and blood

clones, respectively, with clone counts  $\geq 20$  truncated to 20 for visualization. Right: UMAP of CD4<sup>+</sup> T cells highlighting clones shared between the liver and blood with frequencies of  $1 \leq n \leq 5$  (top) and liver-specific clones with frequencies of  $2 \leq n \leq 5$  (bottom). (e) UMAP of the expression of marker epitope and genes used for T<sub>RM1</sub> identification. (f) Flow cytometry gating strategy for the identification of T<sub>RM1</sub> and a.a.CD8<sup>+</sup> T cells by surface staining. Auto-fluorescence events were excluded between the third and fourth dot plots by combining multiple fluorescence channels. (g) Frequencies of three distinct TNF and IFN- $\gamma$  expression combinations across the indicated CD4<sup>+</sup> populations in 7 AIH donors. The gating strategies for the indicated populations is shown in Fig.3f left. TNF and IFN- $\gamma$  detection were performed after in vitro stimulation. Each dot represents a single donor, with frequencies of different populations from the same donor connected by lines. Grey lines represent mean values. Significant differences are determined by RM one-way ANOVA, Tukey's multiple comparisons test. (h) Representative flow cytometry plots (left) and pie chart quantifications (right) depicting the contribution of indicated cell populations across different TNF and IFN- $\gamma$  expression profiles. CD45RO<sup>+</sup> CD4<sup>+</sup> T cells were pre-gated on TCR $\alpha\beta$ <sup>+</sup> TCRV $\alpha$ 24-J $\alpha$ 18<sup>-</sup> live, singlet lymphocytes. (i) Flow cytometry plots illustrating the expression patterns of selected granzymes in the indicated CD4<sup>+</sup> populations (n = 1). CD4<sup>+</sup> T cells were pre-gated on TCR $\alpha\beta$ <sup>+</sup>, live, singlet lymphocytes. Auto-fluorescence events were excluded by combining multiple fluorescence channels. Granzymes were detected by intracellular staining without prior in vitro stimulation. (j) Frequencies (left) of T<sub>RM1</sub> cells within total CD4<sup>+</sup> T cells are shown to illustrate the basis for calculating absolute T<sub>RM1</sub> cell numbers (right), which were normalized per gram of liver tissue in patients with AIH (n=11) and controls (n=6), as measured by flow cytometry. The gating strategy for T<sub>RM1</sub> cells is shown in Fig. S4f followed by Fig. 3e. Weight normalized T<sub>RM1</sub> cell numbers were further log<sub>10</sub> transformed for statistical analysis, while the y-axis displays the original untransformed values. Each dot represents a single donor, and the bar represents the mean. Statistical differences are determined by unpaired t-test. Panels a - e were based on the AIH atlas, whereas panels f - j were based on the FACS dataset.

Supplementary Fig. 5

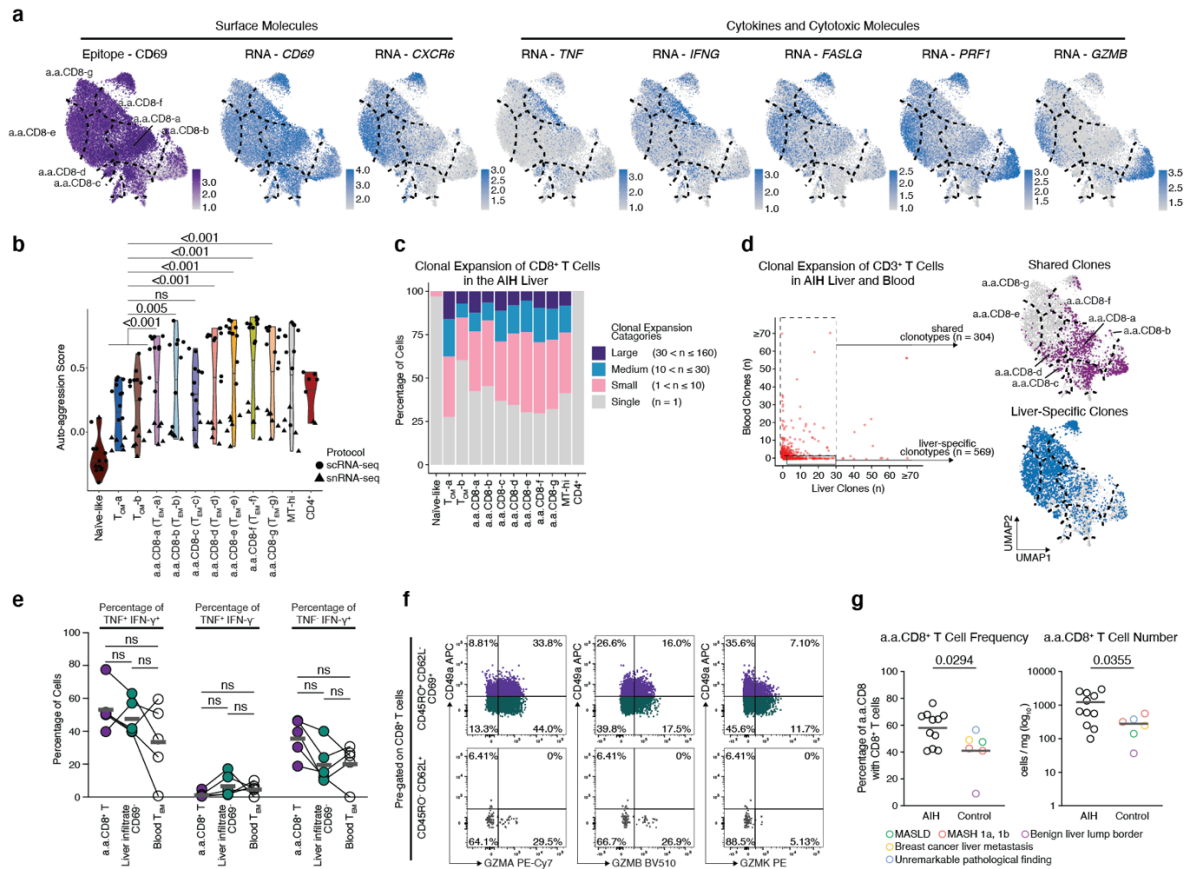


**Fig. S5. Cytotoxic profile of a.a.CD8<sup>+</sup> T cells.** (a) UMAP showing the expression of marker epitope and genes characteristic of liver a.a.CD8<sup>+</sup> T cells. (b) a.a. scores for all CD8<sup>+</sup> T cell subclusters are shown as the average per sample. P values were determined on the cluster- and sample- averaged scores using a mixed linear effects model with Dunnett's test post hoc. Two T<sub>CM</sub> clusters were merged for statistical analysis but are displayed as separate clusters for visualization. (c) Bar chart depicting clonal expansion percentages within each liver CD8<sup>+</sup> T cell clusters. (d) Left: Clonal expansion of CD3<sup>+</sup> T cells, in the livers and paired blood (liver CITE-seq: n = 3; paired blood CITE-seq: n = 3). The X-axis and Y-axis represent liver and blood clones, respectively, with clone counts ≥ 70 truncated to 70 for visualization. Right: UMAP of CD8<sup>+</sup> T cells highlighting clones shared between the liver and blood with frequencies of 1 ≤ n ≤ 30 (top) and liver-specific clones with frequencies of 2 ≤ n ≤ 30 (bottom). (e) Frequencies of distinct TNF and IFN-γ expression patterns across the indicated CD8<sup>+</sup> populations in 5 AIH donors. The gating strategies for the indicated CD8<sup>+</sup> populations are shown in Fig.3I left. TNF and IFN-γ detection were performed after in vitro stimulation. Each dot represents a single donor, with frequencies of different populations from the same donor connected by lines. Grey lines represent mean values. Statistical differences are determined by RM one-way ANOVA, Tukey's multiple comparisons test. (f) Flow cytometry plots illustrating the expression patterns of selected granzymes in the indicated CD8<sup>+</sup> populations (n = 1). CD8<sup>+</sup> T cells were pre-gated on TCRαβ<sup>+</sup>, live, singlet lymphocytes. Auto-fluorescence events were

excluded by combining multiple fluorescence channels. Granzymes were detected by intracellular staining without prior in vitro stimulation. **(g)** Frequencies (left) of a.a.CD8<sup>+</sup> T cells within total CD8<sup>+</sup> T cells are shown to illustrate the basis for calculating absolute a.a.CD8<sup>+</sup> T cell numbers (right), which were normalized per gram of liver tissue in patients with AIH (n=11) and controls (n=6), as measured by flow cytometry. The gating strategy for a.a.CD8<sup>+</sup> T cells is shown in Fig. S4f followed by Fig.3k. Weight normalized a.a.CD8<sup>+</sup> T cell numbers were further log<sub>10</sub> transformed for statistical analysis, while the y-axis displays the original untransformed values. Each dot represents a single donor, and the bar represents the mean. Statistical differences are determined by unpaired t-test. Panels a - d were based on the AIH atlas, whereas panel e - g were based on the FACS dataset.

Extended Data Fig. 6

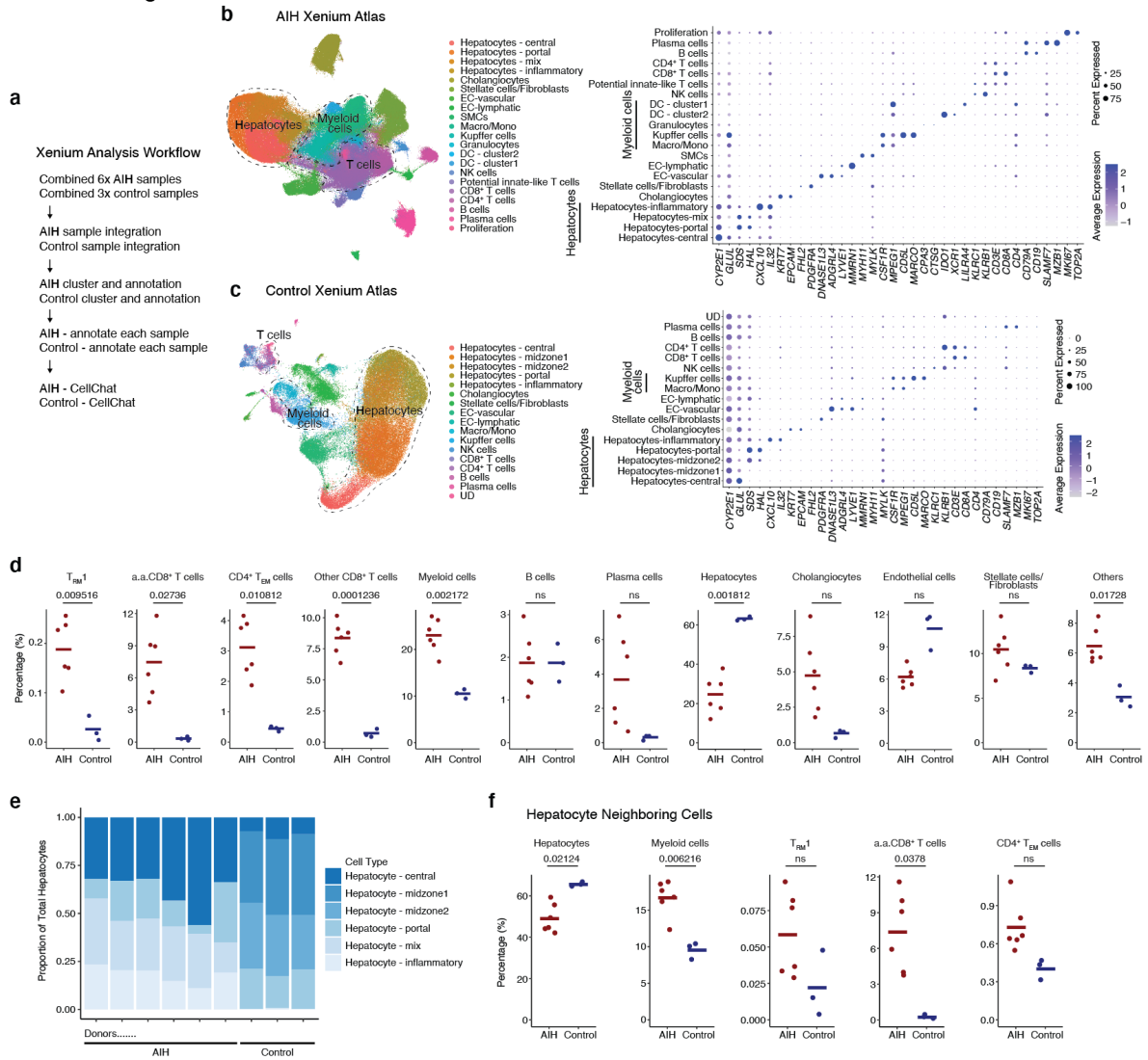


**Fig. S6. Comparison of the spatial frequency and distribution of cells in AIH and control liver samples, based on spatial in situ RNA expression dataset. (a)** Schematic representation of spatial in situ RNA expression analysis workflow. **(b)** Left: UMAP of integrated spatial in situ RNA expression data of AIH patients (n = 6). Right: Dot plots showing expression of marker genes in indicated cell types. (NK cells: natural killer cells; DC: dendritic cells; SMC: smooth muscle cells) **(c)** Left: UMAP of integrated spatial in situ RNA expression data of control samples (n = 3). Right: Dot plots showing expression of marker genes in indicated cell types. **(d)** Percentage of indicated clusters within total cells per biopsy in AIH and control. Each dot represents a single donor, and the bar indicating the mean. Significant differences were determined using a t-test with Bonferroni correction for multiple comparisons. **(e)** Proportions of hepatocyte populations in AIH and control samples. **(f)** Quantification of hepatocytes neighbouring cells. Each dot represents a single donor, and the bar indicating the mean. Significant differences are indicated by t-test with Bonferroni correction for multiple hypothesis testing.

Supplementary Fig. 7

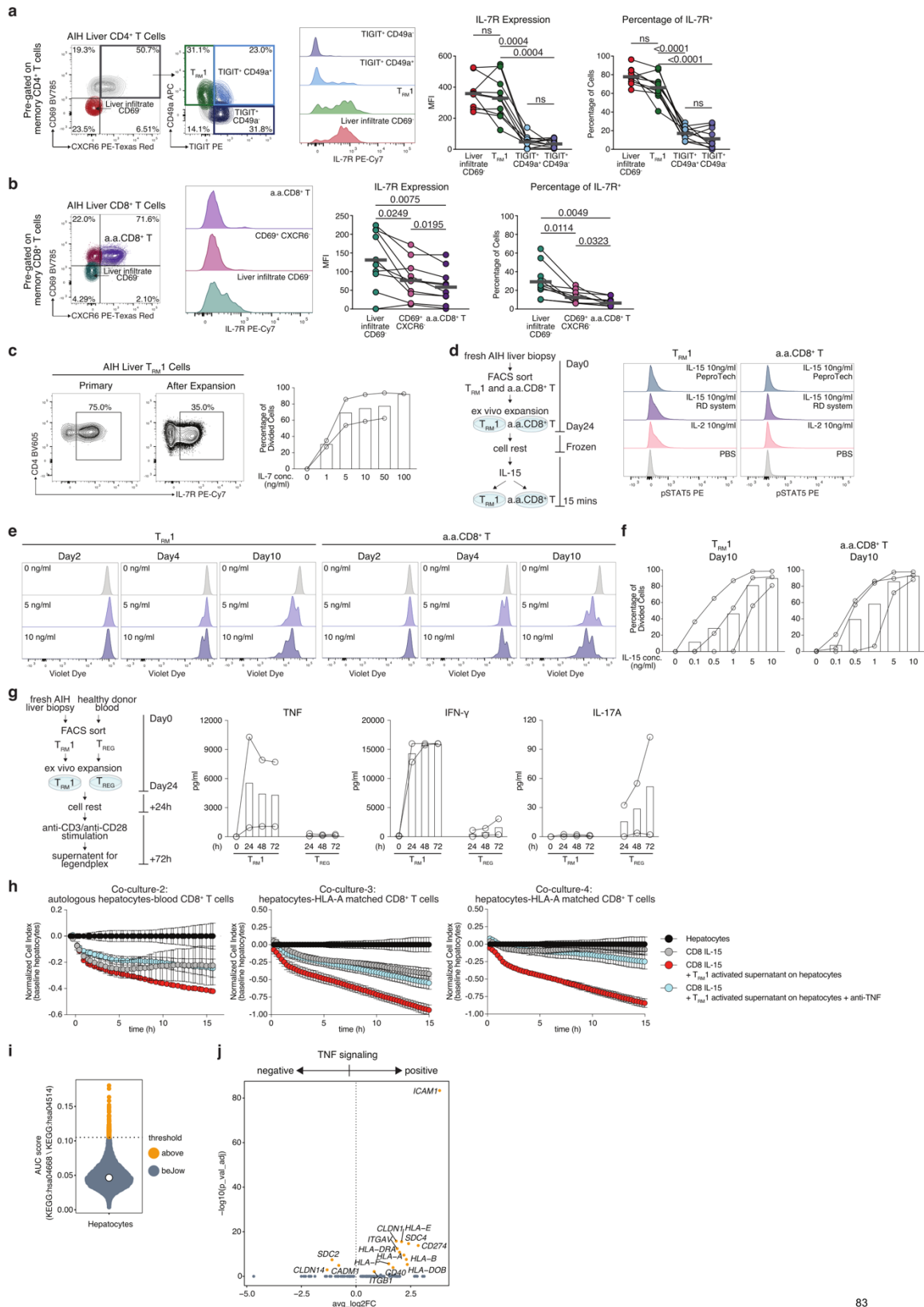


**Fig. S7. In vitro validation of IL-7, IL-15 and TNF effects on liver T cells. (a-b) Left:** Representative flow cytometry plots illustrating the gating strategy for the indicated CD4<sup>+</sup> (a) and CD8<sup>+</sup> (b) T cell populations from patients with AIH; gating for memory CD4<sup>+</sup> and CD8<sup>+</sup> T

cells is shown in Fig. S4f. Middle: Representative histograms showing the MFI of IL-7R across the indicated liver CD4<sup>+</sup> (a) and CD8<sup>+</sup> (b) T cell populations in 10 AIH donors. Each dot represents a single donor, and MFI/frequency of different populations from the same donor is connected by lines. Grey lines represent mean values. Significant differences are determined by RM one-way ANOVA, Tukey's multiple comparisons test. (c) Left: Representative flow cytometry plot showing IL-7R expression in T<sub>RM</sub>1 cells isolated from AIH liver before and after ex vivo clonal expansion. Right: Bar plot illustrating the proliferation effect of IL-7 on T<sub>RM</sub>1 cells at indicated doses (AIH patients n = 2). Each dot represents a single donor, with cells treated with different IL-7 concentration from the same donor connected by lines. Bars indicate the mean. (d) Left: Schematic representation of IL-15R activation detection strategy. Right: Histogram showing the MFI distribution of STAT5 phosphorylation (pSTAT5) across AIH liver derived T<sub>RM</sub>1 and a.a.CD8<sup>+</sup> T cells under the specified conditions (n=1). This analysis aims to detect the phosphorylation of STAT5, a downstream component of IL-15 signalling pathway, to indirectly validate IL-15R activation. (e) CellTrace Violet histograms showing proliferation of AIH liver derived T<sub>RM</sub>1 and CD8<sup>+</sup> T cells under indicated conditions (n=1). Due to the multiple roles of IL-15 on T cells, this analysis aims to determine if the proliferative effect of IL-15 is time dependent. The results show that the proliferative effect begins only after day 4 of ex vivo exposure. (f) Bar plot illustrating the proliferation effect of IL-15 on AIH liver derived T<sub>RM</sub>1 and a.a.CD8<sup>+</sup> T cells at different doses (n = 3) over 10 days. Each dot represents a single donor, with cells treated with different IL-15 concentration from the same donor connected by lines. Bars indicate the mean. (g) Left: Schematic representation of the validation strategy for the cytokine profile of AIH liver-derived T<sub>RM</sub>1 cells following ex vivo clonal expansion. Healthy donor blood-derived T<sub>REG</sub>-like cells were included as control. CD25<sup>+</sup> IL7R<sup>-</sup> CD45RO<sup>+</sup> CD62L<sup>-</sup> CD4<sup>+</sup> TCRαβ<sup>+</sup> live, singlet lymphocytes were defined as T<sub>REG</sub>-like cells in the FACS-sorting gating strategy. Right: bar plots illustrating the selected cytokine profiles of T<sub>RM</sub>1 and T<sub>REG</sub>-like cells following anti-CD3/anti-CD28 stimulation at the indicated time points. Supernatants were analysed using the LegendPlex assay as the readout. (T<sub>RM</sub>1 from AIH livers, n = 2; T<sub>REG</sub>-like cells from healthy donor blood, n = 2). Each dot represents the mean of duplicate measurements, with data from the same donor at different time points connected by lines. Bars indicate the mean. (h) Co-culture-2: Real-time cell impedance analysis over 15h showing auto-aggressive activity of autologous blood CD8<sup>+</sup> T cells against primary human hepatocytes under the indicated conditions. Hepatocytes were co-cultured with CD8<sup>+</sup> T cells (grey), or pre-treated with supernatant from anti-CD3/anti-CD28 activated T<sub>RM</sub>1 cells in the absence (red) or presence of anti-TNF (blue). Baseline hepatocytes are shown in black. Primary hepatocytes and autologous blood CD8<sup>+</sup> T cells were obtained from one healthy donor distinct from the donor used in Fig.5f. T<sub>RM</sub>1 cells were isolated from the liver of the same AIH donor used in Fig.5f. Co-culture-3 and -4: Primary hepatocytes were derived from a third healthy donor co-

cultured with blood CD8<sup>+</sup> T cells from two HLA-A matched donors, respectively. T<sub>RM</sub>1 cells were isolated from the liver of one AIH donor distinct from the donor used in co-culture-1 and -2. Auto-aggression was assessed by hepatocyte viability and quantified using xCELLigence. Each dot represents the mean of triplicates for the indicated condition at the specified time point, with bars indicating the SD. (i) Hepatocyte TNF signalling score, based on the AIH atlas. The distribution threshold of the AUC values were marked and cells above and below were coloured with orange and grey, respectively. (j) Volcano plot of hepatocyte cell adhesion genes differentially expressed between cells above and below the TNF signalling score threshold of Fig. S7i.

Supplementary Fig. 8

a

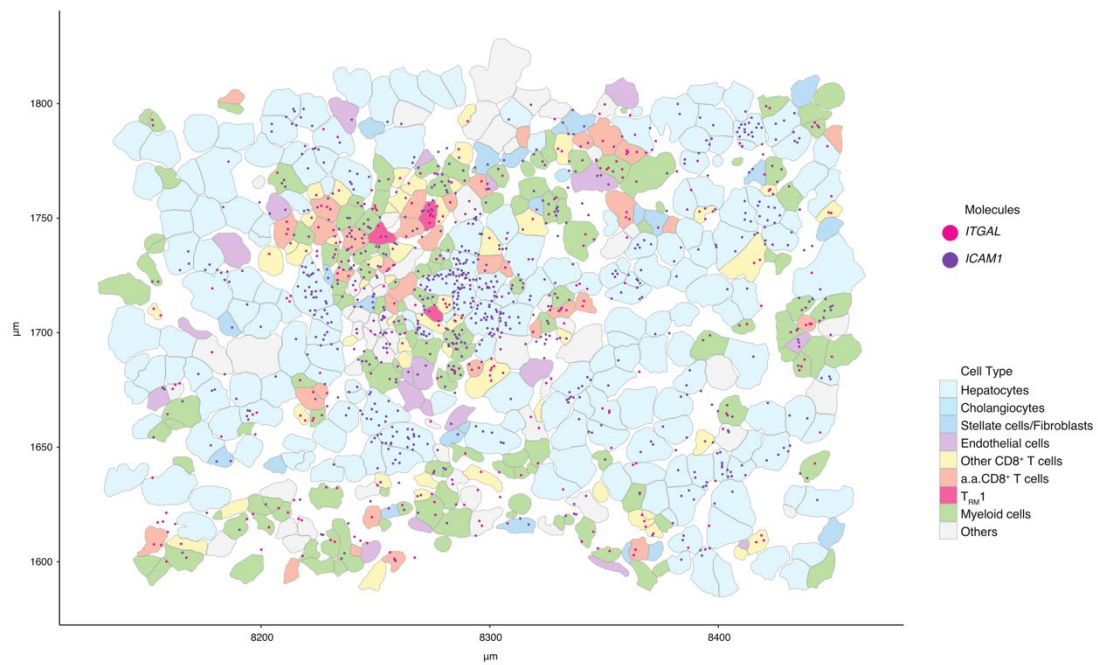
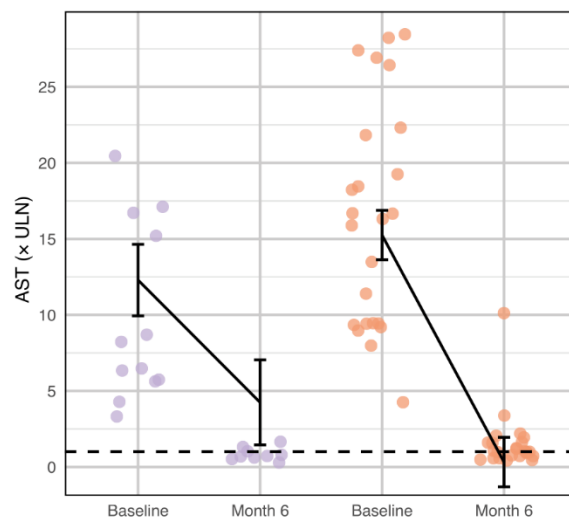


**Fig. S8. Spatial distribution of cells showing *ICAM1* and *ITGAL* expression pattern at interphase hepatitis. (a)** Spatial distribution of cells coloured by cell type, with *ICAM1* and *ITGAL* RNA expression overlaid.

Supplementary Figure 9

a



b

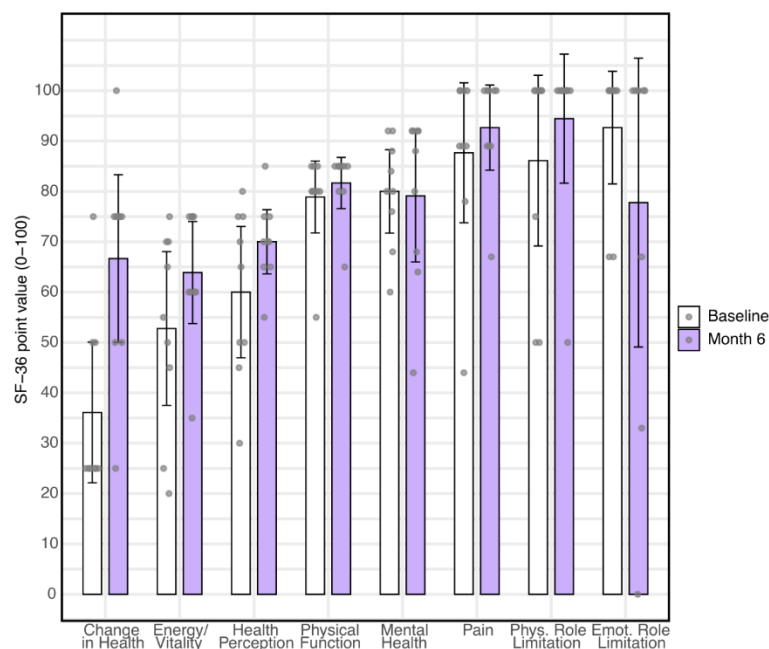


**Fig. S9. Additional outcome measurements of the AIH-MAB trial.** (a) Comparison of AST (times upper limit of normal, xULN) between baseline and month 6, separated by treatment (IFX [individual patients depicted by orange circles], n=12 vs. PSM-matched cohort, receiving standard care [SoC, purple circles], n=24). Black lines and error bars indicate respective estimated marginal means (EMMs) and their respective 95% confidence intervals (CI) of the linear mixed-effects model analyses. (b) Health-related Quality of life (HRQoL)

measurements of n=9 patients in the trial as shown per category of the Short Form 36 (SF-36) questionnaire between baseline and month 6 (point values from 0-100, 100 points indicate absence of HRQoL impairments). Dots represent individual patients, bars represent means, error bars depict respective  $\pm$  95% confidence intervals.

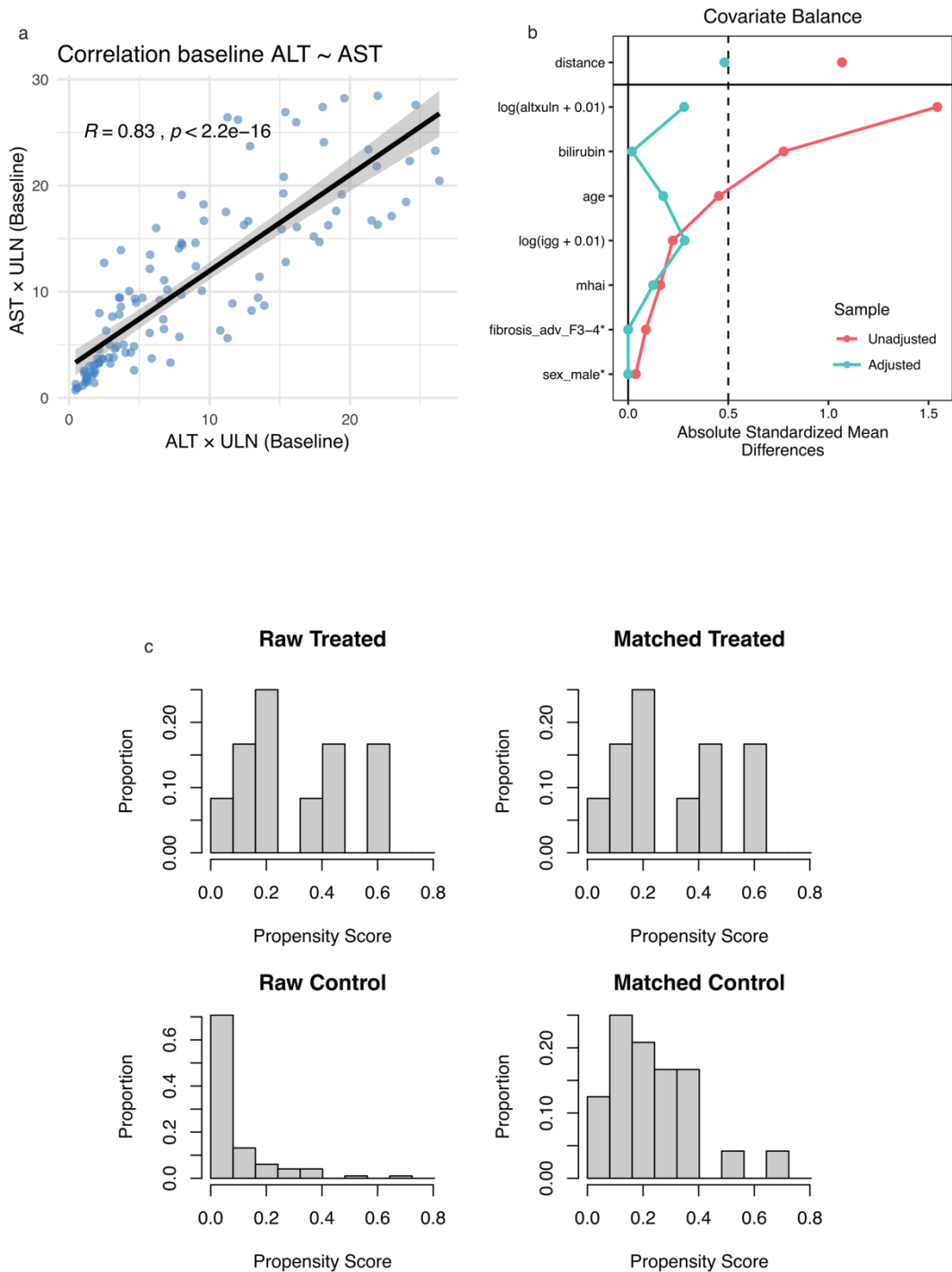


**Fig. S10. Baseline correlation and propensity score matching diagnostics** for the comparison of the clinical trial cohort and the standard of care cohort from the prospective RLIVER registry. (a) Pearson Correlation between baseline ALT and AST values. Scatterplot showing the strong linear association between baseline ALT and AST expressed as multiples of the upper limit of normal ( $\times$ ULN). (b) Covariate balance before and after propensity score matching. Absolute standardized mean differences (SMDs) for each covariate are displayed before (unadjusted, pink line) and after matching (adjusted, blue line). (c) Propensity score

distributions before and after matching. Histograms showing the distribution of propensity scores for treated (IFX) and control (SoC) individuals before (left panels) and after (right panels) 1:2 nearest-neighbor matching with exact matching on sex and fibrosis stage. Matching achieved overlap between groups, supporting adequate comparability of baseline covariates.